ÖAW ÖSTERREICHISCHE AKADEMIE DER WISSENSCHAFTEN

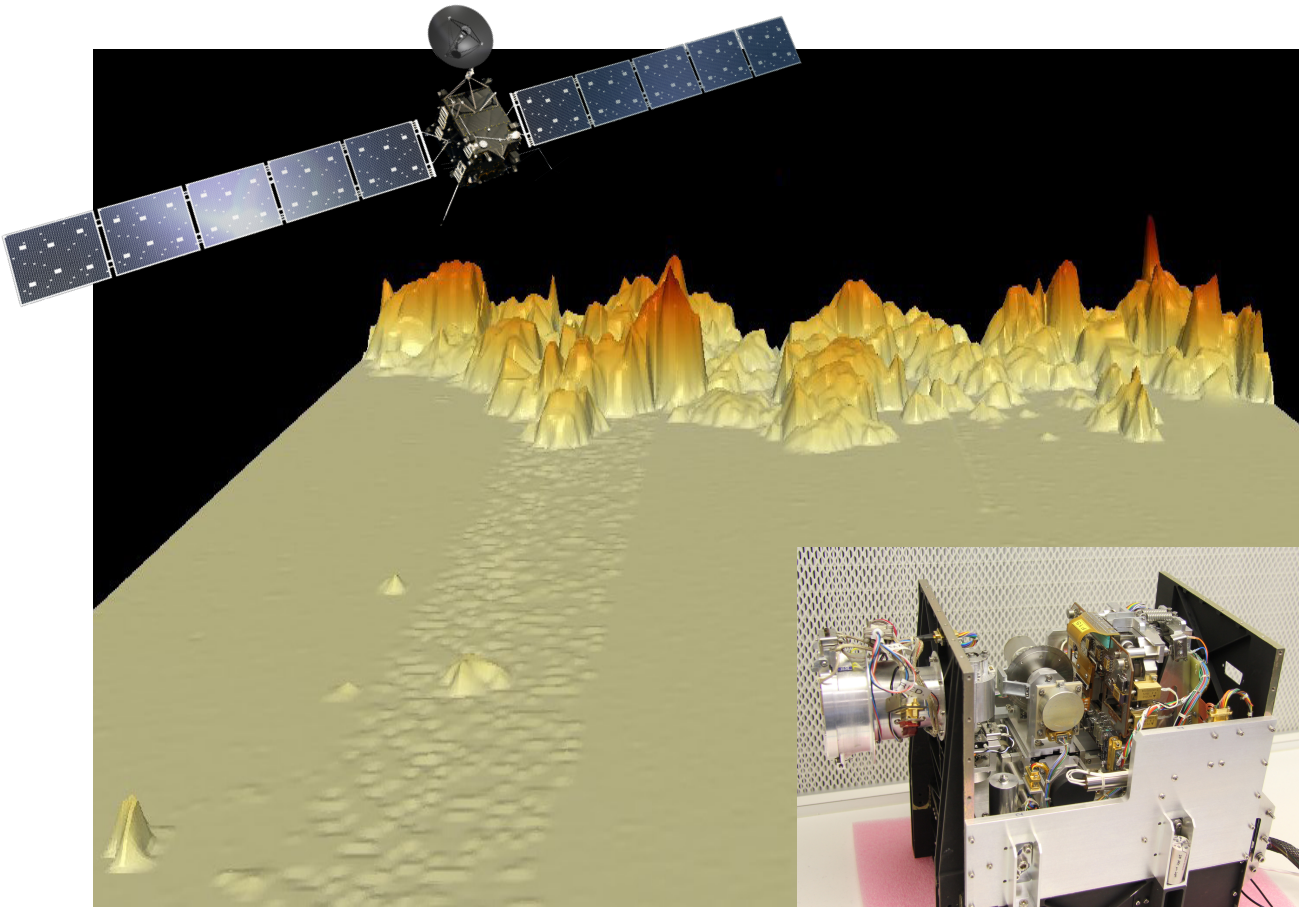

ANNUAL REPORT 2016

IWF INSTITUT FÜR WELTRAUMFORSCHUNG

ÖSTERREICHISCHE AKADEMIE DER WISSENSCHAFTEN

ANNUAL REPORT 2016

IWF INSTITUT FÜR WELTRAUMFORSCHUNG

COVER IMAGE

Topographic image of a dust particle collected and analyzed by the atomic force microscope *MIDAS* (insert) aboard ESA's *Rosetta* mission (Credit: ESA/Rosetta/IWF for the MIDAS team IWF/ESA/LATMOS/Universiteit Leiden/Universität Wien).

TABLE OF CONTENTS

INTRODUCTION

The Space Research Institute (Institut für Weltraumforschung, IWF) in Graz focuses on the physics of (exo-) planets and space plasmas. With about 100 staff members from 20 nations it is one of the largest institutes of the Austrian Academy of Sciences (Österreichische Akademie der Wissenschaften, ÖAW).

IWF develops and builds space-qualified instruments and analyzes and interprets the data returned by them. Its core expertise is in building magnetometers and on-board computers, as well as in satellite laser ranging, which is performed at a station operated by IWF at the Lustbühel Observatory. In terms of science, the institute concentrates on dynamical processes in space plasma physics, on the upper atmospheres of planets and exoplanets, and on the gravity fields of the Earth and the Moon.

IWF cooperates closely with space agencies all over the world and with numerous other national and international research institutions. A particularly intense cooperation exists with the European Space Agency (ESA).

The institute is currently involved in eighteen active and future international space missions; among these:

- *BepiColombo* will be launched in 2018 to investigate planet Mercury, using two orbiters, one specialized in magnetospheric studies and one in remote sensing.
- ESA's first Small-class mission *CHEOPS (CHaracterizing ExOPlanets Satellite)* will classify exoplanets in detail. Its launch is expected in 2018.
- The *China Seismo-Electromagnetic Satellite (CSES)* will be launched in 2017 to study the Earth's ionosphere.
- The *Chinese Mars Mission* is planned for launch in 2020.
- *Cluster*, ESA's four-spacecraft mission, is still providing unique data leading to a new understanding of space plasmas.
- *GEO-KOMPSAT-2A* is a Korean satellite for space weather investigations due for launch in 2018.
- ESA's *JUpiter ICy moons Explorer (JUICE)* will observe the giant gaseous planet Jupiter and three of its largest moons, Ganymede, Callisto, and Europa. It is planned for launch in 2022.
- *MMS* uses four identically equipped spacecraft to explore the acceleration processes that govern the dynamics of the Earth's magnetosphere.

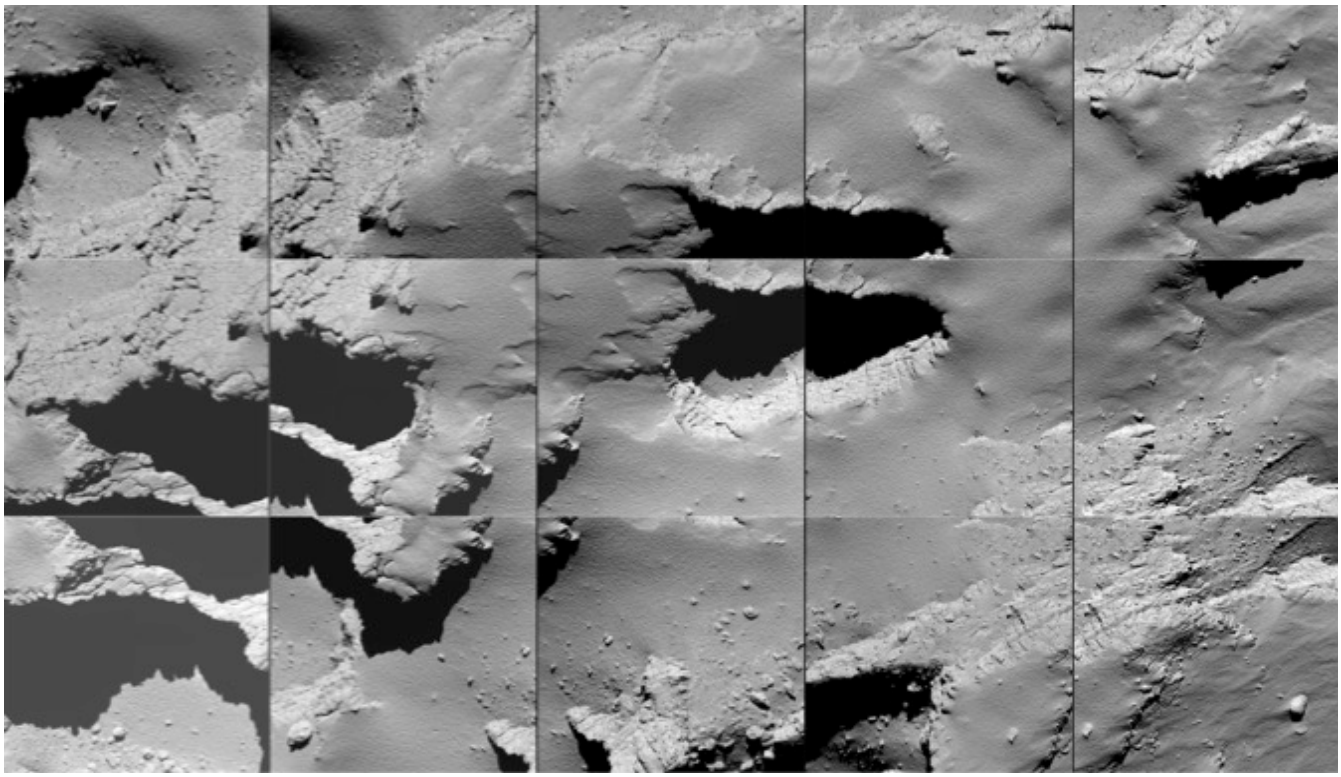

Fig. 1: Sequence of images captured by Rosetta during its descent to the surface of comet 67P/CG on 30 September 2016 (Credit: ESA/Rosetta/MPS for OSIRIS Team MPS/UPD/LAM/IAA/SSO/INTA/UPM/DASP/IDA).

- ESA's third Medium-class science mission *PLATO* is a space-based observatory to search for planets orbiting alien stars. It is planned for launch by 2024.
- *Rosetta* finished its mission in September 2016 by landing on the comet (Fig. 1).
- *Solar Orbiter* is to study along an innovative trajectory solar and heliospheric phenomena, planned for launch in 2019.
- *THEMIS* has been reduced to a near-Earth three-spacecraft mission. The two other spacecraft are now orbiting the Moon in the *ARTEMIS* mission.

HIGHLIGHTS IN 2016

- On 30 September 2016, ESA's historic *Rosetta* mission concluded with the controlled impact onto the comet it had been investigating for more than two years. IWF published a "Nature" study on cometary dust and its implication for the creation of the early solar system.
- Already one year after its launch, the *MMS* team reported in "Science" its first detection of the electron diffusion region. IWF contributed to nearly 50 refereed articles.
- In the "Monthly Notices of the Royal Astronomical Society" an international team led by IWF reported, that haze and clouds high up in the atmospheres of some hot and light exoplanets might make them appear bigger than they really are.
- In "Nature Physics" IWF reported about observations of the Earth's vibrating magnetic field and its relation to the northern lights.

THE YEAR 2016 IN NUMBERS

Members of the institute published 185 papers in refereed international journals, of which 49 were first author publications. During the same period, articles with authors from the institute were cited 4014 times in the international literature. In addition, 91 talks and 49 posters have been presented at international conferences by IWF members, including 6 by special invitation from the conveners. Last but not least, institute members were involved in the organization of 6 international meetings or workshops.

IWF STRUCTURE AND FUNDING

IWF was, as a heritage since foundation, structured into three departments. Nowadays, the institute has been restructured into four research fields covering eight research groups (Fig. 2). Wolfgang Baumjohann serves as Director, Werner Magnes as Deputy Director.

The bulk of financial support is provided by ÖAW. Significant support is also given by other national institutions, in particular the Austrian Research Promotion Agency (Österreichische Forschungsförderungsgesellschaft, FFG) and the Austrian Science Fund (Fonds zur Förderung der wissenschaftlichen Forschung, FWF). Furthermore, European institutions like ESA and the European Union contribute substantially.

Fig. 2: IWF research fields and groups with their respective leaders.

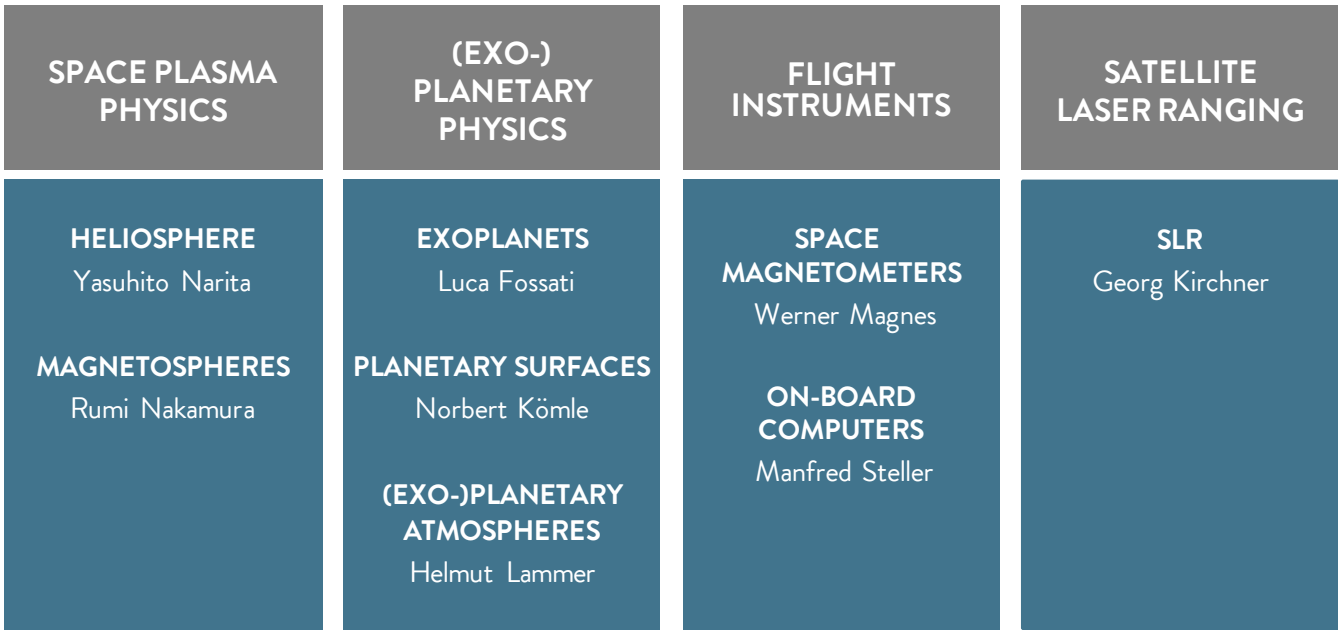

EARTH & MOON

For the last decades, gravimetric and geometric space geodesy techniques have constituted an integral part in Earth and planetary sciences. In order to improve the knowledge about the environment, state and evolution of the Earth and the Earth's only natural satellite, the Moon, IWF is engaged in terrestrial and lunar gravity field research, crustal dynamics, and Satellite Laser Ranging (SLR) to Earth-orbiting spacecraft and space debris objects.

GRAVITY FIELD

Gravity field research includes the analysis of data collected by Earth- and Moon-orbiting spacecraft.

GRACE

Temporal variations of the gravity field derived from the *Gravity Recovery and Climate Experiment (GRACE)* satellite mission have become one of the most valuable source of information for Earth system studies. In the context of global climate change, this information is of utmost importance from a scientific but also socio-economic perspective (cf. the latest assessment report of the Intergovernmental Panel on Climate Change, IPCC). On regional to local scales, however, the potential of *GRACE* has not been fully exploited yet. Although the vast majority of Earth's glacial ice is contained in Antarctica and Greenland, alpine glacier shrinkage has been identified as one of the most dominant contributors to global sea level rise in recent years.

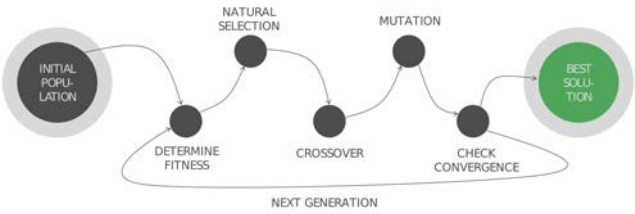

Fig. 3: The concept of global optimization by means of Genetic Algorithms.

Motivated by the fact that the quantification of these deglaciation effects is typically based on sparse in-situ measurements, IWF together with the working group of Theoretical Geodesy and Satellite Geodesy at TU Graz have developed a tailored analysis strategy to assess mass balances of alpine glacier systems from space-borne gravimetric data. The method is based on regional adaption (concerning both data and modeling) and involves the use of localized basis functions (point masses) and parameter estimation by means of Genetic Algorithms. Inspired by the evolutionary idea of natural selection, this heuristic search algorithm aims to detect the global minimum/maximum of an optimization problem without any a priori knowledge (Fig. 3).

In order to test the viability of this inference technique, a series of closed-loop simulations has been carried out for several alpine glacier systems including the Alps, Himalaya and Patagonia. Mass balance information of the selected glaciers was provided by the experts at the World Glacier Monitoring Service (WGMS) in Zurich. Two different variants of the point-mass modeling (PMM) approach have been investigated: (i) PMM with predefined and fixed positions and (ii) PMM with unknown locations of the surface mass changes.

Approach (i) yields a linear functional model in which only the magnitudes of the point-masses are considered unknown. A highly non-linear optimization problem needs to be solved for approach (ii), since both the magnitudes and the coordinates of the point-masses are introduced as unknown parameters. As demonstrated by the example of the Central Asia region in Fig. 4, both deglaciation magnitudes and geometries could be recovered very well using approach (ii).

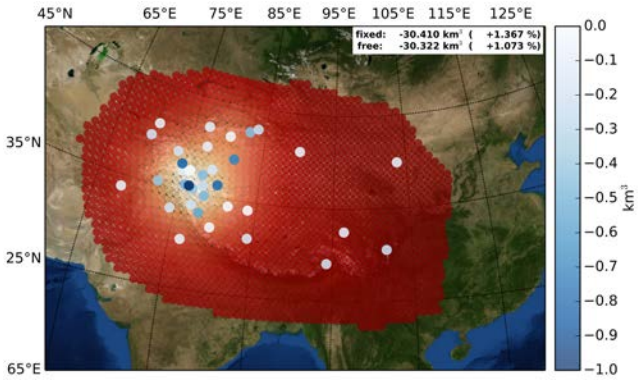

Fig. 4: Point-mass modeling (PMM) applied to the Central Asia region: Simulated gravity signal in space (red dots) and glacier volume changes (blue dots) obtained by the free-positioned PMM.

GRAIL

The twin satellite mission *Gravity Recovery And Interior Laboratory (GRAIL)* orbited the Moon in nearly circular tandem orbits from March to December 2012. The inter-satellite range variations were observed, as the distance between the two probes changed slightly due to different gravity induced perturbations. The range variations were recorded by means of Ka-band range-rate observations (KBRR) between the spacecraft. Hence, it is possible to obtain their relative velocity change very precisely, which can subsequently be translated into gravity field variations. The measurement technique is adopted from *GRACE* and is ideally suited to reveal the lunar gravity field (even at the far-side) with unprecedented accuracy.

The *GRAIL* mission was placed in near polar orbit and comprised a primary and an extended mission phase, with a duration of approximately three month each. Consequently at least six full mapping cycles (lunar sidereal period) were completed. During the complete mission both satellites were linked to stations of the Deep Space Network on Earth via S-Band radiometric tracking. This allowed for determining the absolute position of the two probes, which is a prerequisite to exploit the inter-satellite Ka-band observations.

Following a batch least squares differential adjustment process, the initial value problem is solved using variational equations in conjunction with numerical integration techniques. A completely in-house developed software package is used in order to determine the orbits of *GRAIL-A* and *GRAIL-B*. Fig. 5 shows a comparison to the official orbit product GNI1B (NASA, JPL), for *GRAIL-A* in cross-track, along-track and radial direction, respectively. The GNI1B orbit product can be regarded as a sort of reference, because it implicitly includes also the inter-satellite observations, whereas the determined orbit of *GRAIL-A* is based on DSN range-rates in S-band only.

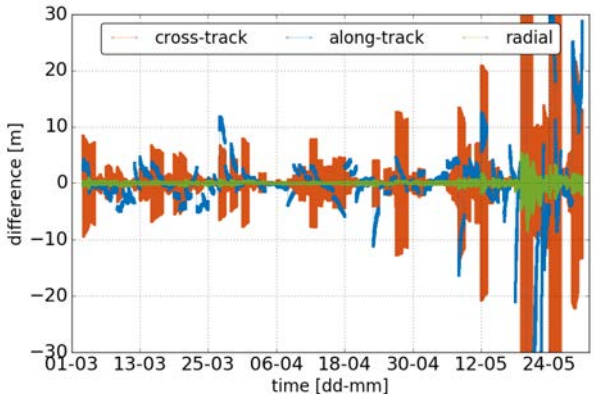

Fig. 5: Orbit comparison to GNI1B for *GRAIL-A* in cross-track (orange), along-track (blue) and radial (green) direction, respectively.

Concerning the recovery of the lunar gravity field a short-arc integral approach is applied to exploit the inter-satellite KBRR observations. For the latest release, particular attention is paid to the incorporation of observations recorded during the extended mission phase. This time period was characterized by a substantially lower orbit than during the primary mission (in some places <10 km) and an even higher temporal data resolution (Δt=2s). Both factors led to a significantly increase of the computational expense and required the IWF in-house High Performance Computer architecture to solve this task.

Fig. 6 shows percentage differences, in terms of free air gravity anomalies, between the state of the art lunar gravity model (GRGM0900C) published by the Centre of Space Research (CSR) and the latest IWF solution (GrazLGM300cx). It should be noted that, for reason of comparison both solutions GRGM0900C and GrazLGM300cx are adjusted to the same spatial resolution (degree and order 300). It is gratifying to see, that both solutions match pretty well and that the applied short-arc approach provides similar results.

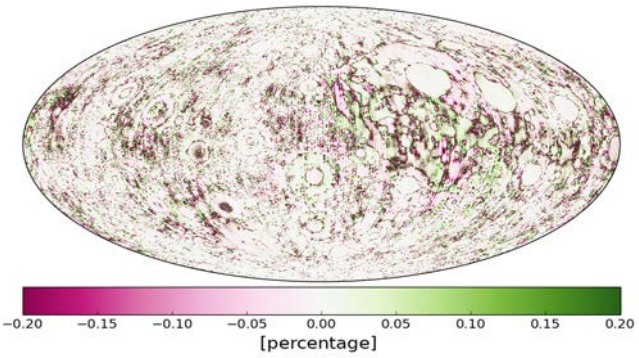

Fig. 6: Percentage difference between GRGM0900C and GrazLGM300cx in terms of free air gravity anomalies (both solved to degree and order 300).

INTERNATIONAL GEODETIC NETWORK

OLG Data Center is one of two regional Global Navigation Satellite System (GNSS) data centers for Europe and has been run successfully administrating the GNSS data in the old and new data formats. The transition period has been prolonged internationally for additional two years. The OLG Analysis Center contributes its products for densification within and around Europe at a weekly base. This increases the knowledge about tectonic patterns, not only during earthquakes, but generally of tectonic faults. Because one network is focused on Greece, the most active part of Europe (Fig. 7), the major movements around earthquakes can be observed.

In April 2016, the Coordinating Office (CO) of GGOS (Global Geodetic Observing Systems) was transferred to Graz. GGOS is an institution directly under the IAG (International Association of Geodesy), the highest scientific geodetic institution. The CO has the duty to keep in touch with all services (VLBI, Laser, GNSS, DORIS, and Sea Level), the geodetic scientific community, but also with neighboring disciplines, like geophysics and hydrology. One large part is the outreach to explain how global geodetic measurements of highest precision can contribute to mitigate problems, like earthquakes and tsunamis, global warming and sea level rising as well as dangers from space (especially solar impacts).

Fig. 7: Active horizontal movements at the tectonic boundary zone Greece.

SATELLITE LASER RANGING

In addition to routinely tracking more than 150 targets, which are equipped with laser retro-reflectors, space debris laser ranging is getting an increasing amount of attention. A laser transmit unit and a detection package were installed on an astronomical telescope to demonstrate a simple and innovative SLR station concept.

SP-DART on an Astronomical Telescope: The SP-DART (Single-Photon Detection, Alignment and Reference Tool) developed in Graz works as a tiny mobile SLR station. It consists of a transmitting module (15 µJ / 1 ns / 2 kHz laser) and a detection package (laptop, FPGA-based control unit, Riga event timer, GNSS unit, meteorological instruments), but without mount/receiving telescope. Using such an SP-DART, an experiment was carried out in Sandl, Upper Austria, with a 70 cm astronomical telescope owned by ASA (Astrosysteme Austria, Fig. 8).

Fig. 8: The SP-DART system was mounted on the 70 cm ASA astronomical telescope in Sandl.

The transmitting module was mounted on the telescope, and two additional detectors were aligned for laser ranging and light curve measurements individually. The mount / telescope system was remote-controlled from Switzerland. After a short setup time of a few hours various low earth orbit (LEO) satellites were successfully tracked. Testing the limits of the tiny 15 µJ laser, returns from several GNSS satellites as well as from the geostationary (GEO) *Compass-I5* satellite were received. Overall, during two observation nights 17 different targets were tracked with maximum return rates ranging from >30 % for LEO satellites to 0.2 % for *Compass-I5* (Tab. 1).

Table 1: Summary of all successful passes measured with the SP-DART in Sandl.

	# Passes	Max return rate
GEO	1	0.2 %
GNSS	6	2.6 %
Lageos	3	12.5 %
LEO	7	>30 %

Furthermore, simultaneously to laser ranging, light curves of periodically spinning defunct satellites were recorded by using a second single photon detector. The detector operates in a non-gated mode and records reflected sunlight with wavelengths larger than 532 nm (Fig. 9). The additional CCD camera (Watec) is used to align the transmit and receive axis.

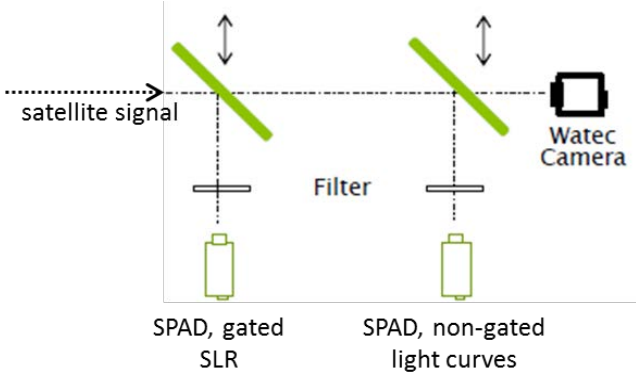

Fig. 9: Optical setup recording light curves of defunct rotating satellites by utilizing reflected sunlight.

Two typical light curves, shown in Fig. 10, of the defunct *Glonass* satellite COSMOS 1988 show one complete rotational cycle (phase, x-axis) of the satellite taking 8.8 seconds for completion. The y-axis represents the normalized reflected intensity detected by the single-photon avalanche diode (SPAD). The four-way symmetry of the box-wing satellite can be clearly detected.

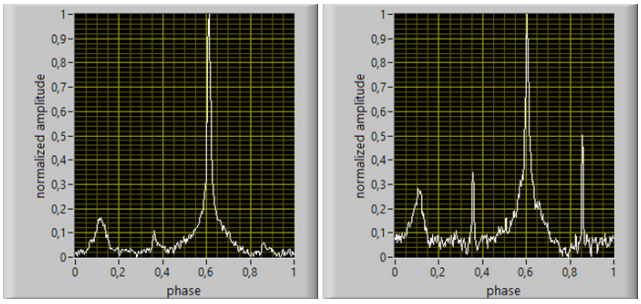

Fig. 10: Light curves of the defunct *Glonass* satellite COSMOS 1988 rotating with a period of 8.8 seconds.

Space Debris Data Information System (SDDIS): A common thread to all efforts towards space situational awareness is the precise knowledge of the location of objects orbiting Earth. Space debris represents the overwhelming majority of man-made objects. About 20 percent of the cataloged debris consists of large objects like upper stages or defunct satellites, which are potential targets for laser ranging.

SDDIS provides a platform in order to realize observation campaigns to these objects. The exchange of tracking data, the calibration of sensors and the predicted orbits provided by SDDIS are available for almost a year now. In order to show the benefit of laser based orbit predictions, the validation of two observation campaigns in 2016 is presented in Fig. 11. The figure shows residuals of the observed laser ranges and the predicted orbits of *Envisat* and *Topex/Poseidon*. The performance is most of the time below 50 meters after three days of prediction. This level of prediction accuracy enables even non-dedicated debris laser ranging stations to track defunct satellites. Further steps are on its way to establish a network to track space debris by means of laser ranging and benefit from these complementary and highly precise observations.

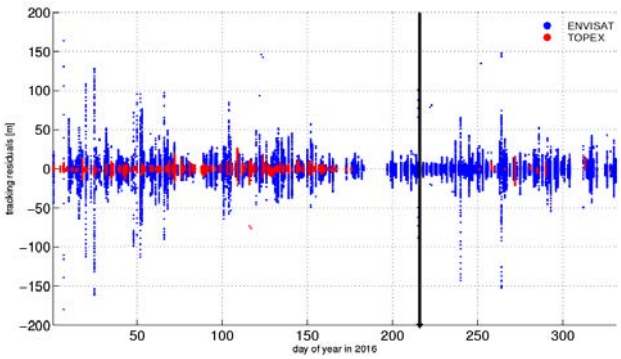

Fig. 11: Laser tracking residuals to orbit predictions of *Envisat* (blue) and *Topex/Poseidon* (red) in 2016. The prediction period corresponds to three days. The official end of the observation campaign to *Topex/Poseidon* is shown in black.

Multistatic / Two Color Debris Ranging: A space debris laser ranging experiment was carried out connecting three different stations, while using two different laser wavelengths (532 and 1064 nm). Graz SLR station sent photons using its green high power (20 W / 100 Hz) space debris laser. Simultaneously Wettzell SLR station sent photons using its infrared space debris laser to the same space debris target. After diffuse reflection on the space debris target the photons were spread across Europe. Graz green photons were detected by Graz itself and by Wettzell SLR station. At the same time Graz, Wettzell, and Stuttgart detected Wettzell's infrared photons (Fig. 12).

In two observation campaigns more than 200 passes of 35 different objects were observed by the three stations with success rates up to 70%.

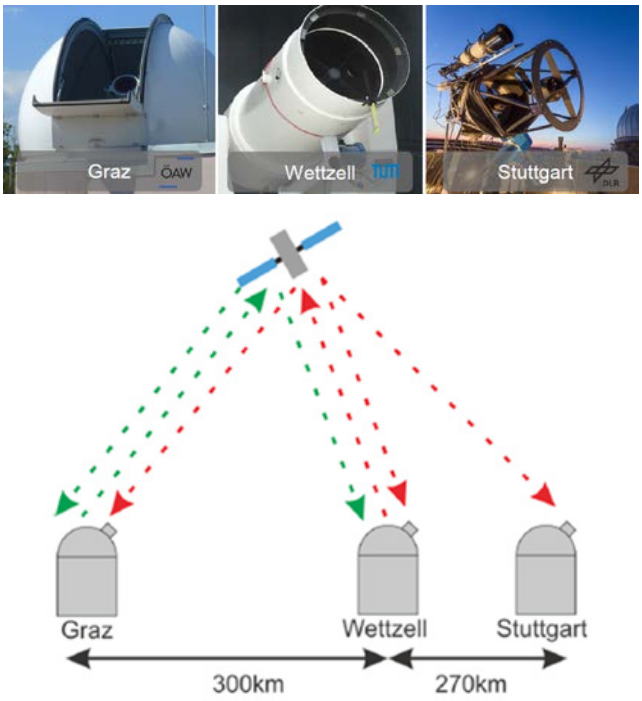

Fig. 12: The setup of the multistatic two color space debris ranging experiment, including the SLR stations of Graz, Wettzell, and Stuttgart.

Stare & Chase: "Stare & Chase" is a method to track and range to space debris targets of which no a priori orbit information is available by optically determining the pointing direction to these targets. An analogue astronomy camera is equipped with an off-the-shelf 50 mm objective monitoring a field of view of approximately 7° of the sky. The camera system is piggyback mounted on an SLR telescope and roughly aligned with the optical axis. The telescope is then moved to an arbitrary position "staring" into the sky and displaying stars up to 9th order magnitude. From the stellar background the equatorial pointing direction of the camera center is determined with an accuracy of approx. 15 arc seconds, utilizing a plate solving algorithm.

Once a sunlit space debris object passes through the field of view its equatorial coordinates and the current time are stored. From the pointing information a CPF (Consolidated Prediction Format) orbit prediction file is generated and used to immediately track the satellite within the same pass. The process from the first detection of the satellite until successful tracking can be completed within less than two minutes.

As soon as tracking is established, the SLR system starts "chasing" the target with a high power (20 W / 100 Hz) space debris laser. Space debris laser ranging to several cooperative and uncooperative (without retro-reflectors) targets was successfully achieved using the "Stare & Chase" predictions.

NEAR-EARTH SPACE

Near-Earth space enables the study of fundamental space plasma processes based on in-situ measurements of the charged particles together with electric and magnetic fields. IWF has been participating in the hardware activities of numerous missions, which are now operating, being built or in the planning phase. Data taken from these missions have been extensively analyzed at IWF by applying different methods and by theoretical modeling to compare with the observations. The obtained knowledge contributes to a better understanding of several processes in space plasma and is applicable to our solar system and beyond.

CLUSTER

The *Cluster* spacecraft have been providing data since 2001 for studying small-scale structures of the Earth's magnetosphere and its environment as the first four spacecraft mission in space. The mission is currently planned to be extended to December 2018. IWF is PI/Co-I on five instruments and has maintained the *Austrian Cluster Data Center*. In addition to data analysis, IWF contributed to data archiving activities at the *Cluster Science Archives (CSA)* by producing supporting data products such as science event lists.

THEMIS/ARTEMIS

NASA's *THEMIS* mission, launched in 2007, consisted of five identical satellites flying through different regions of the magnetosphere. In autumn 2010 the two outer spacecraft became *ARTEMIS* and began to orbit the moon, while the other three *THEMIS* spacecraft remained in their orbit. As Co-I of the magnetometer, IWF is participating in processing and analyzing data.

MMS

NASA's *MMS (Magnetospheric MultiScale)* mission, launched in 2015, explores the dynamics of the Earth's magnetosphere and its underlying energy transfer processes. Four identically equipped spacecraft carry out measurements with high temporal and spatial resolution. *MMS* investigates the small-scale basic plasma processes, which transport, accelerate and energize plasmas in thin boundary and current layers. The *MMS* orbit of the first two years is dedicated to study dayside magnetopause reconnection. The apogee is then raised to encounter near-Earth magnetotail reconnection in mid 2017. A proposal for an extension of further five years is under preparation. IWF, which is the biggest non-US participant in *MMS*, has taken the lead for the spacecraft potential control of the satellites *(ASPOC)* and is participating in the electron drift instrument *(EDI)* and the digital fluxgate magnetometer *(DFG)*. In addition to the operation activities of these instruments and scientific data analysis, IWF is contributing to develop new methods of inflight calibration and an algorithm to produce new science data products.

Active Spacecraft Potential Control (ASPOC): *ASPOC* neutralizes the spacecraft charge by releasing positive charge produced by an indium ion source and thereby controls the spacecraft potential. *ASPOC* enables accurate measurements also in sparse plasma environments essential to study properties of reconnection, which is the main scientific goal of *MMS*. *ASPOC* is successfully participating in the two science phase activities by operating in constant current mode simultaneously for all spacecraft. Since summer 2016, several new operation schemes have been implemented by applying different levels of the emitter currents for each spacecraft to obtain environmental plasma information. These modes are: a staggered mode, where only one spacecraft is emitting ion current in a successive way and a current sweep mode, where the ion current levels are changed stepwise. All the *ASPOC* level 1/2 science data products are available from the Science Data Center in Colorado.

Digital FluxGate Magnetometer (DFG): *DFG* is based on a triaxial fluxgate sensor developed by the University of California, Los Angeles, and a front-end Application Specific Integrated Circuit (ASIC) for magnetic field sensors, which has been developed by IWF in cooperation with the Fraunhofer Institute for Integrated Circuits.

During the entire year 2016, all four *DFG* magnetometers operated flawlessly. All twelve calibration parameters were monitored together with US colleagues on a regular basis and no specific anomalies and drifts have been observed.

Electron Drift Instrument (EDI): *EDI* measures electric fields perpendicular to the ambient magnetic field by emitting and detecting coded beams of electrons. IWF contributed to *EDI* with the *Gun Detector Electronics (GDE)* and the electron gun. The *GDE* was developed by Austrian industry in close cooperation with IWF, while the electron gun was entirely developed at the institute. The operation is successfully ongoing by reducing the stress to the sensitive high voltage optocoupler, thus optimizing the instrument life time. The 500 eV energy mode has become the preferred operation mode. The 1 keV beam energy is used only when it is required due to the plasma condition.

Spin-Axis Offset Calibration and Combined Data Product: In the beginning of 2016 all processing tools required for the spin-axis offset calibration have been optimized for a routine calibration on a weekly basis. Precision could be improved to 0.1 nT through an advanced correction of the *EDI* time-of-flight offsets. The team at IWF has been continuously processing the spin-axis offsets of all eight fluxgate magnetometers (AFG and DFG on all four *MMS* observatories) during the science phase 1A and the subsequent intermediate phase 1X (passage through the Earth's magnetotail). The spin-axis offset determination has evidenced a high long-term stability.

One of the top-level scientific goals of *MMS* is to analyze electron diffusion regions and thin current sheets, which are visible in the magnetic field data within a frequency range from 0.5 Hz to more than 20 Hz. On their own the search coil and fluxgate magnetometers are not able to provide the best possible signal-to-noise ratio over this frequency range. It is therefore beneficial to combine data sets from both instruments for advanced scientific analysis. In 2016, it was required to refine the models of the transfer functions and to create a suitable algorithm for a universal merging of the data that is independent from specific science events. The data flow diagram of the merging process is depicted in Fig. 13.

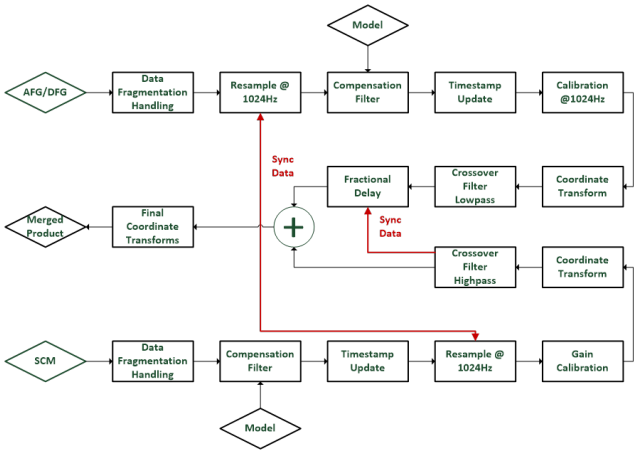

Fig. 13: Data flow diagram of the merging process.

Density Derivation Using ASPOC and Probe Potential: *ASPOC* typically reduces the spacecraft potential to a few volts for all four spacecraft. On several occasions during the commissioning phase of the mission, however, the *ASPOC* instruments were operating only on one spacecraft at a time. Taking advantage of such intervals, photoelectron curves were derived to perform reconstructions of the uncontrolled spacecraft potential and estimate the electron plasma density during those periods.

An example of the derived density is shown in Fig. 14. Comparison of the plasma density estimates with measurements from the plasma detector is in good agreement for this example. For *ASPOC* currents up to 30 μA, spacecraft potential reconstructions are largely viable. The methods allow derivation of relative density variations and recognition of boundary crossings in the magnetosphere.

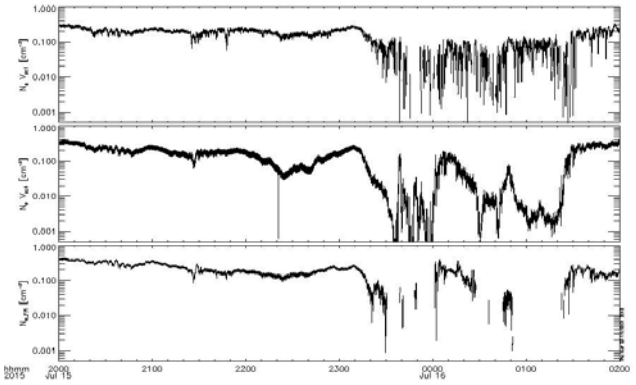

Fig. 14: Plasma density variations based on estimates using the spacecraft potential measurements of the spacecraft under active control, *MMS1* (first panel); estimates using the spacecraft potential measurements of the spacecraft with no active control, *MMS4* (second panel); and electron data from the plasma instrument of *MMS1* (third panel).

Determination of Magnetometer Spin-Axis Offsets from Mirror Mode Observations: A novel and complementary technique to obtain the spin-axis offset has been developed: the mirror mode method. It is based on the assumption that mirror mode fluctuations are nearly compressible such that the maximum variance direction is aligned to the mean magnetic field. Mirror mode fluctuations are typically found in the Earth's magnetosheath region. It has been estimated that about 20 hours of magnetosheath measurements may be sufficient to obtain high-accuracy spin-axis offsets with uncertainties on the order of a few tenths of a nanotesla, if offset stability can be assumed. This method is a complementary method to the conventional ways using Alfvénic fluctuations in the solar wind. While the method is planned to be used for upcoming missions in the Earth's as well as in planetary/cometary environments, *MMS* provides an excellent opportunity to develop and validate this new innovative method.

CSES

The *China Seismo-Electromagnetic Satellite (CSES)* mission is scheduled for launch in August 2017. It will be the first Chinese platform for the investigation of natural electromagnetic phenomena with major emphasis on earthquake monitoring from a Sun synchronous, polar, Low Earth Orbit.

Coupled Dark State Magnetometer (CDSM): The *CSES* magnetometer consists of two sensors and is developed in cooperation between the National Space Science Center (NSSC) of the Chinese Academy of Sciences, the Institute of Experimental Physics (IEP) of the Graz University of Technology, and IWF. NSSC is responsible for the dual sensor fluxgate magnetometer, the instrument processor and the power supply unit, while IWF and IEP participate with the newly developed absolute scalar magnetometer, called *Coupled Dark State Magnetometer (CDSM)*. In 2016, the *CDSM* Flight Model was developed and the flight acceptance tests have been started (see flight sensor in Fig. 15).

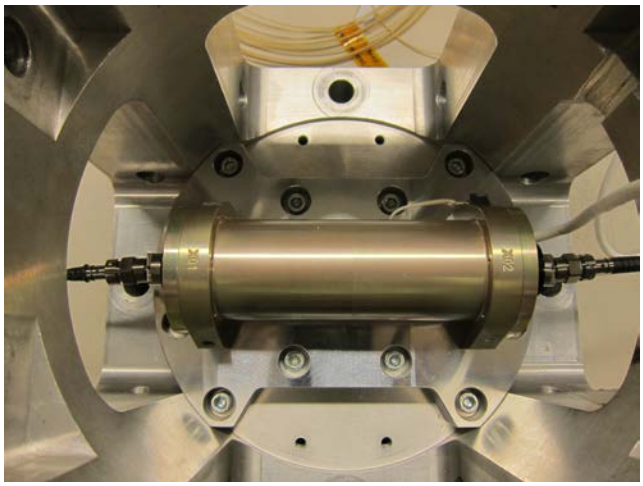

Fig. 15: *CDSM* flight sensor in the vibration test setup.

GEO-KOMPSAT-2A

The prototyping of a *Service Oriented Spacecraft MAGnetometer (SOSMAG)*, which has been developed for ESA's Space Situational Awareness program, was finished in 2016. *SOSMAG* will serve as a ready-to-use space weather monitoring system to be mounted on a variety of different spacecraft built without a magnetic cleanliness program. Up to two high resolution boom-mounted fluxgate-magnetometers, the Digital Processing Unit (DPU), and the boom are provided by Magson GmbH and the Technical University of Braunschweig. For detection and characterization of magnetic disturbers on the spacecraft, two magnetometers based on the anisotropic magnetoresistive (AMR) effect were developed in a joint effort by Imperial College London and IWF.

Based on the prototype, the overall *SOSMAG* design has been further adapted and retested in 2016, so that *SOSMAG* can be used for space weather research aboard the South Korean *GEO-KOMPSAT-2A* mission as part of the *Korean Space Environment Monitor (KSEM)* instrument suit (Fig. 16). It will be launched into a geostationary orbit in May 2018.

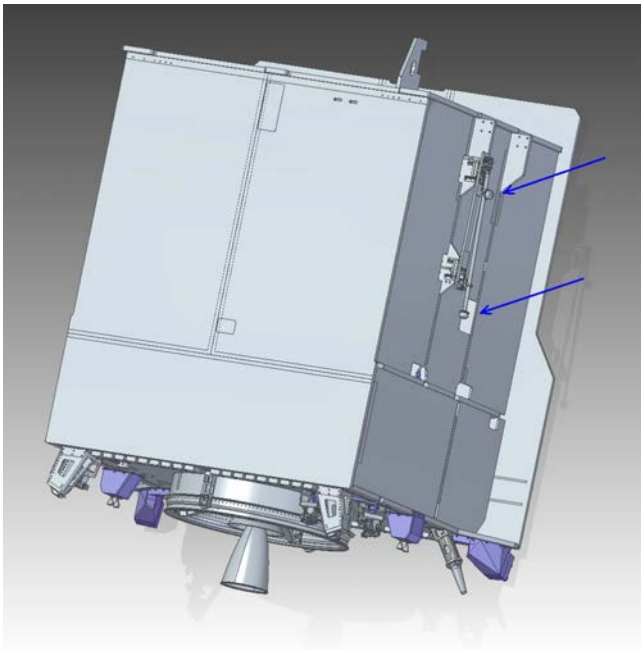

Fig. 16: Drawing of the *GEO-KOMPSAT-2A* spacecraft with *SOSMAG* boom and boom-mounted fluxgate sensors (Credit: KARI).

PHYSICS

Various data from ongoing missions are analyzed and theoretical models are developed to describe physical processes in near-Earth space. The studies deal with interactions between solar wind and magnetosphere, internal disturbances in the magnetosphere such as plasma flows and waves, and plasma instabilities including magnetic reconnection.

Current Sheet Statistics in the Magnetosheath: Both numerical simulations and in-situ observations indicate that the terrestrial magnetosheath downstream of a quasi-parallel bow shock is populated by various interacting multi-scale structures, such as vortices, plasma jets, large-amplitude magnetic structures, shocklets, current sheets, etc. On the basis of simulations it has been proposed that in such a turbulent environment thin current sheets can be generated by interacting magnetic structures or/and flow shears, however, comparisons to observations were missing.

On the basis of multi-point *Cluster* observations the occurrence frequency of magnetic field discontinuities and the associated proton-scale current sheets were investigated. It was found that the strongest thin discontinuities occupy the tail of a non-Gaussian probability distribution associated with extreme values of magnetic field gradients (Fig. 17). About a hundred of strong discontinuities were observed by *Cluster* within a one-hour time interval. Turbulence-generated thin current sheets exhibit similar statistical distributions in numerical simulations. This indicates, that turbulent interactions may play a key role in generating thin current sheets in the quasi-parallel magnetosheath.

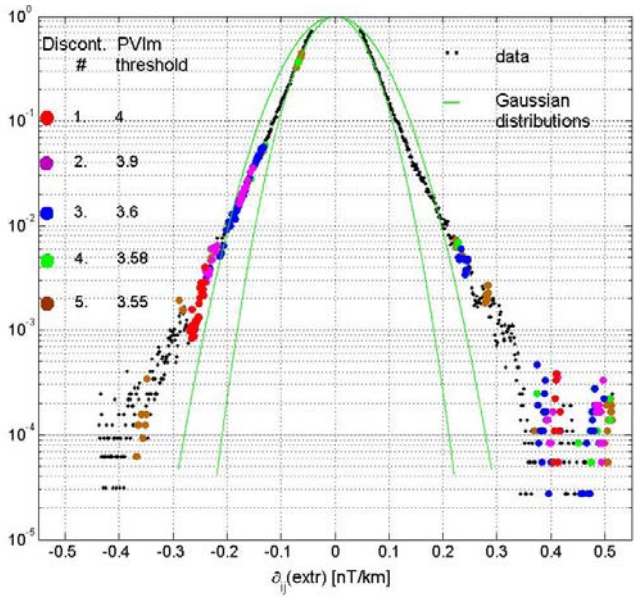

Fig. 17: Probability density function calculated from extreme values of magnetic field partial derivatives. The first five strongest discontinuities are color-coded. Black points show the data, and green lines correspond to Gaussian distributions.

Steepening of Waves at the Dusk Side Magnetopause: Surface waves at the magnetopause flanks typically feature steeper, i.e., more inclined leading (anti-sunward facing) than trailing (sunward facing) edges. This is expected for waves generated or amplified by the Kelvin-Helmholtz Instability (KHI). Very rarely, during strongly northward interplanetary magnetic field (IMF) conditions, anomalous/inverse steepening has been observed. The small-scale tetrahedral configuration of the *MMS* spacecraft and the high time resolution of their measurements make it possible to routinely ascertain magnetopause boundary inclinations on passage of surface waves with high accuracy by four-spacecraft timing analysis. At the dusk flank magnetopause, 77%/23% of the analyzed wave intervals exhibit regular/inverse steepening, respectively. Inverse steepening happens during northward IMF conditions (green circle in Fig. 18), as previously reported and, in addition, during intervals of dominant equatorial IMF (between the blue lines and below the red line in Fig. 18). Inverse steepening observed under the latter conditions may be due to the absence of KHI, if seed waves feature inverse steepening already, or due to instabilities arising from the alignment of flow and magnetic fields in the magnetosheath.

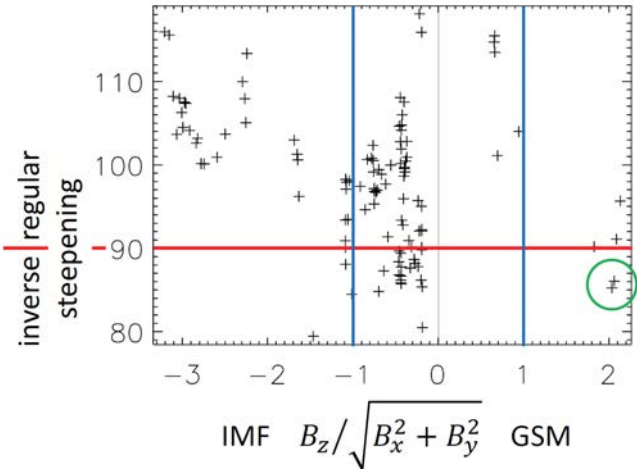

Fig. 18: Inclination angles of the magnetopause with respect to a reference normal, averaged over groups of boundary crossings, plotted against the relative value of the IMF z-component with respect to the equatorial IMF strength. Inclination angles larger/smaller than 90° (over/under the red line) indicate regular/inverse magnetopause wave steepening.

Dipolarization Fronts (DFs): When oppositely directed lobe magnetic field lines reconnect, the relaxation of the magnetic tension of the stretched field lines converts the stored magnetic energy into plasma kinetic energy. This creates so-called Bursty Bulk Flows (BBFs), which are short-duration high-velocity plasma flows predominantly towards the Earth. BBFs are often accompanied by asymmetric bipolar variations of the northward magnetic field component (B_z) which are referred to as dipolarization fronts (DFs). Using data from *MMS* at radial distances of 12 R_E and *Cluster* up to 19 R_E, characteristics of DFs are compared between the inner and outer magnetotail region. Multi-point observations of DFs allow to estimate their velocity and propagation direction. As expected, most of the observed DFs are earthward propagating, but about 25% of DFs are tailward propagating (Fig. 19). The results of the DFs measurements at two tail locations suggest that the tailward propagating events are the result of DFs bouncing off the near Earth dipole-dominated plasma sheet. Another finding from this comparative study shows that a larger fraction of the DFs move faster closer toward Earth than further down the tail (Fig. 19). This indicates highly variable flux transport rates in the near-Earth dipole-dominated plasma sheet. Furthermore, it is found that larger DF velocities correspond to higher values of B_z directly ahead of the DFs. This behavior is observed by both *Cluster* and *MMS*, despite their very different locations. This suggests that the higher B_z originates from a local snowplow-like phenomenon, resulting from a higher DF velocity and thus a higher magnetic flux pileup ahead of the DF.

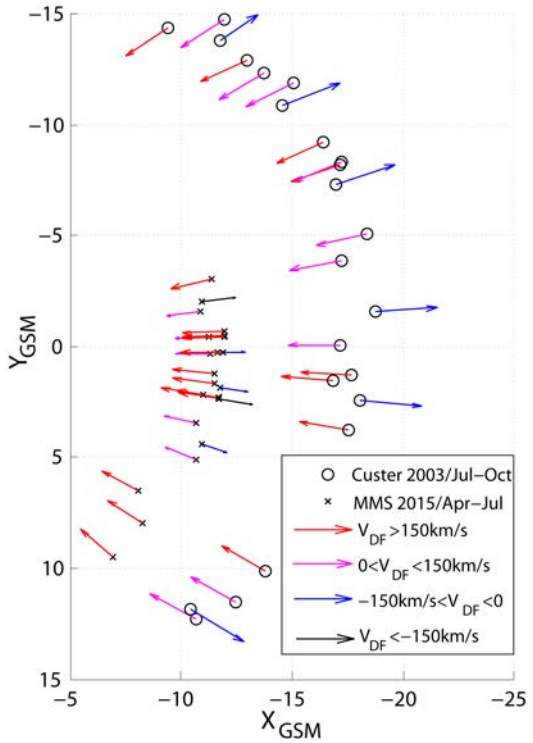

Fig. 19: XY-position (position in equatorial plane) of *MMS* (stars) and *Cluster* (dots) during the DF observations. The colored arrows indicate the earthward and tailward DF propagation directions and velocities.

Magnetotail Energy Dissipation During an Auroral Substorm: Violent releases of space plasma energy from the Earth's magnetotail during substorms produce strong electric currents and bright aurora. But what modulates these currents and aurora and controls dissipation of the energy released in the ionosphere? Data from the *THEMIS* fleet of satellites and ground-based imagers and magnetometers are analyzed to answer this question (Fig. 20). It is shown that plasma energy dissipation is controlled by field-aligned currents (FACs) produced and modulated during magnetotail topology change and oscillatory braking of fast plasma jets at 10–14 Earth radii in the nightside magnetosphere. FACs appear in regions where plasma sheet pressure and flux tube volume gradients are non-collinear. Faster tailward expansion of magnetotail dipolarization and subsequent slower inner plasma sheet restretching during substorm expansion and recovery phases cause faster poleward than slower equatorward movement of the substorm aurora. Anharmonic radial plasma oscillations build up displaced current filaments and are responsible for discrete longitudinal auroral arcs that move equatorward at a velocity of about 1 km/s.

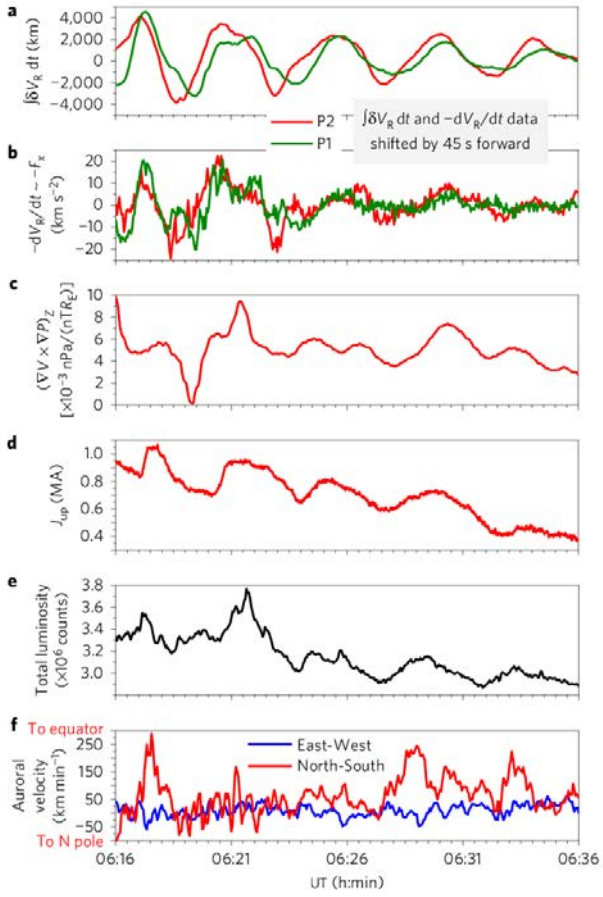

Fig. 20: *THEMIS* and ground observations of a substorm. (a) Time-integrated oscillations of radial ion velocity at spacecraft P1 (red) and P2 (green). (b) Time derivative of radial oscillations at P1 (red) and P2 (green). (c) Measure of collinearity between plasma sheet pressure and flux tube volume. (d) Total upward current at Rankin Inlet geomagnetic station. (e) Total auroral luminosity. (f) Meridional (red) and longitudinal (blue) auroral velocity components.

Ion-Scale Field-Aligned Current Sheets in the Plasma Sheet Boundary Layer (PSBL): The PSBL, between the hot plasma sheet and the tenuous lobe, is a dynamic region in the magnetotail where counter-streaming ions are often observed. The encounter of the PSBL during geomagnetic active times is due to the thinning or expansion of the plasma sheet as a consequence of evolution of the near-Earth magnetotail reconnection process.

The four *MMS* spacecraft, separated at a distance of about few hundred km (Fig. 21 a-b), enabled the study of the dynamics of the PSBL. Multiple layers of magnetic field-aligned electric currents (vertical lines in Fig. 21 c-f) were found, associated with plasma sheet expansion during the period of an intense substorm. It is found that these short-lived earthward (downward) intense field-aligned current sheets with thicknesses of a few tens of kilometers, well below the ion scale, are flowing along flux tubes moving equatorward/earthward. They coincide with upward field-aligned electron beams with energies of a few hundred eV. These electrons are most likely due to acceleration associated with a reconnection jet or high-energy ion beam-produced disturbances. The observations highlight coupling of multiscale processes in the PSBL as a consequence of magnetotail reconnection.

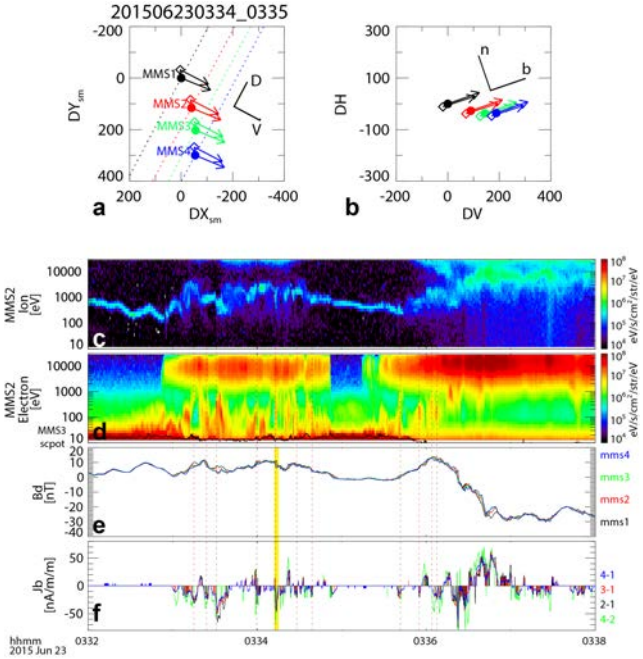

Fig. 21: (a-b) *MMS* four spacecraft configuration with magnetic field depicted as arrows. Energy spectra of (c) ions and (d) electrons from *MMS2*. (e) Eastward magnetic field component (Bd). (f) Field-aligned current density estimated from pairs of *MMS* spacecraft. The red dotted lines indicate the small-scale downward field-aligned currents accompanied by the low-energy electron signatures. The yellow vertical line indicates the 03:34:12 UT event studied in more detail.

Three-Dimensional Evolution of Plasma Jet Fronts Generated by Magnetic Reconnection: Magnetic reconnection, which is one of the most important energy transfer processes in space and laboratory plasmas, rapidly releases magnetic energy and produces fast plasma jets. As reconnection develops, the front layers of the jets are severely compressed and the jet's plasma is coupled with the background plasma, which excites different plasma waves/instabilities.

A large-scale, three-dimensional fully kinetic particle-in-cell simulation of magnetic reconnection is performed (Fig. 22) to investigate the three-dimensional development of reconnection jet fronts treating simultaneously the following three instabilities: the lower-hybrid drift instability (LHDI), the ballooning/interchange instability (BICI), and the ion-ion kink instability (IIKI). Although these three important instabilities have been analyzed independently in previous studies, sufficiently large system size of the simulation permitted to see the coupling between these three instabilities in the fully kinetic regime for the first time. As the front layer of the reconnection jets develop, the LHDI and the BICI become dominant over the IIKI. The rapid growth of the LHDI enhances the BICI growth and results in the formation of finger-like structures at the front layer. Interestingly, the small-scale finger-like structures produced by these instabilities are similar to recent high-resolution field observations of the dipolarization fronts (DFs) in the near-Earth magnetotail by *THEMIS* and *Cluster* spacecraft, and pose important questions for an upcoming full high-resolution observation of reconnection jets by the *MMS* mission.

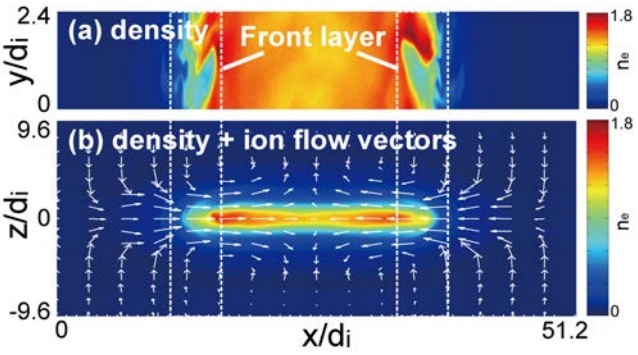

Fig. 22: Density contours in the X-Y (a) and X-Z (b) planes of the 3D fully kinetic simulations. White arrows in Fig. b show the ion flow vectors. The jet front layers become turbulent by the three-dimensional evolution of plasma kinetic instabilities.

SOLAR SYSTEM

IWF is engaged in many missions, experiments and corresponding data analysis addressing solar system phenomena. The physics of the Sun and the solar wind, its interaction with solar system bodies, and various kinds of planetary atmosphere/surface interactions are under investigation.

SUN & SOLAR WIND

The Sun's electromagnetic radiation, magnetic activity, and the solar wind are strong drivers for various processes in the solar system.

SOLAR ORBITER

Solar Orbiter is a future ESA space mission to investigate the Sun, scheduled for launch in 2019. Flying a novel trajectory, with partial Sun-spacecraft corotation, the mission plans to investigate in-situ plasma properties of the near solar heliosphere and to observe the Sun's magnetized atmosphere and polar regions. IWF builds the digital processing unit (DPU) for the *Radio and Plasma Waves (RPW)* instrument aboard *Solar Orbiter* and has calibrated the *RPW* antennas, using numerical analysis and anechoic chamber measurements. Furthermore, the institute contributes to the magnetometer.

Radio and Plasma Waves (RPW): *RPW* will measure the magnetic and electric fields at high time resolution and will determine the characteristics of magnetic and electrostatic waves in the solar wind from almost DC to 20 MHz. Besides the 5 m long antennas and the AC magnetic field sensors, the instrument consists of four analyzers: the thermal noise and high frequency receiver; the time domain sampler; the low frequency receiver; and the bias unit for the antennas. The control of all analyzers and the communication will be performed by the DPU, developed by IWF.

In 2016 the institute delivered the second flight model and finally also the spare model. All tests up to now have been successful completed. The tests at box level, the DPU integrated with the power supply and the analyzers, are still ongoing. The test campaign shall be finished in March 2017. For the assembly of the DPU, CNES has requested a solder qualification for three package types. Finally, the test results for all three package types have been accepted. At the end of 2016 the activities for the *RPW* DPU were completed.

PHYSICS

Charged Dust Grains in the Heliosphere: Non-gravitational forces cause unstable motions of micrometer-sized dust grains in the solar system. The solar wind drag and the Poynting-Robertson effect make the grains fall spirally towards the Sun on secular time scales. However, the interplanetary magnetic field can counteract the inward drift motion of the dust, depending on the electric charge, the particle mass, the optical properties for given orbital elements, and the solar wind speed.

A theoretical relation was found on the condition for the stabilization of dust orbits. For spherical particles with the same mass, the stabilization occurs at specific values of the electrostatic potential at the dust surface. The orbital drift strongly depends on the actual value of the charge-to-mass ratio of the dust grains, but the inward drift can be balanced in the presence of the interplanetary magnetic field with a non-zero northward component.

The stabilizing effect due to the magnetic field is demonstrated in Fig. 23. Dust grains located at 1 AU (Astronomical Unit, distance Earth-Sun) can be stabilized to their initial distance from the sun when the magnetic field balances the forces acting on the orbital motion (middle curve). Otherwise the dust grains may fall gradually onto the Sun for a smaller surface potential (lower curve) or get pushed away from the Sun for a larger potential (upper curve). Dust grains are removed from the system or can spread both in the radial and latitudinal directions with respect to the Sun.

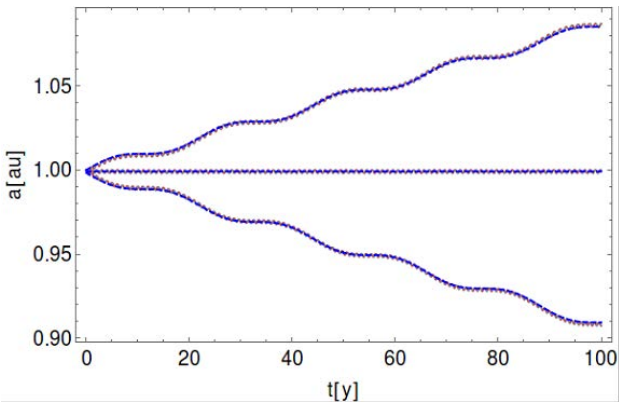

Fig. 23: Distance (semi-major axis a) versus time. Outward drift (upper curve), stabilization (middle curve), inward drift (lower curve).

ElEvoHI - A Novel CME Prediction Tool Based on Heliospheric Images: A new CME forecasting utility, ElEvoHI, is introduced, which assumes an elliptically shaped CME front, that adjusts, through drag, to the background solar wind speed during its propagation. Included within ElEvoHI is the newly presented conversion method, ElCon, which converts the time-elongation profile of the CME obtained from heliospheric imagery into a time–distance profile assuming an elliptical CME geometry. The resultant time–distance profile is used as input into the sub-sequent stage of ElEvoHI, the DBM fit. As a last stage of ElEvoHI, all of the resulting parameters are input in the ElEvo model, which then predicts arrival times and speeds.

The efficacy of the new ElEvoHI procedure was assessed by forecasting the arrival times and speeds of 21 Earth directed, previously analyzed CMEs. ElEvoHI predictions of arrival times and speeds were compared to the output of other single-spacecraft HI-based methods.

It was found that ElEvoHI performs some-what better at forecasting the CME arrival time than usual HI prediction methods (Fig. 24). A substantial improvement is shown in forecasting the arrival speed, which has a direct impact on the accuracy of predicting the intensity of geomagnetic storms at Earth.

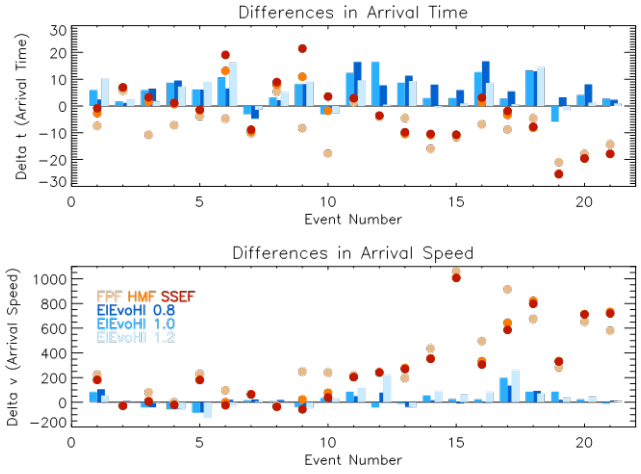

Fig. 24: Comparison of ElEvoHI predictions to previous methods using HI observations. The upper panel shows the differences between the predicted and in situ arrival time, and the lower panel illustrates the equivalent plot for the arrival speed. Especially the improvement of predicting the arrival speed during solar maximum (Events 10 - 20) is remarkable.

MERCURY

Mercury is now in the center of attention because of the upcoming ESA/JAXA *BepiColombo* mission. The planet has a weak intrinsic magnetic field and a mini-magnetosphere, which strongly interacts with the solar wind.

BEPICOLOMBO

Two spacecraft, to be launched in 2018, will simultaneously explore Mercury and its environment: the Japanese *Magnetospheric (MMO)* and ESA's *Planetary Orbiter (MPO*, Fig. 25). IWF plays a major role in developing the magnetometers for this mission: it is leading the magnetometer investigation aboard the *MMO (MERMAG-M)* and is responsible for the overall technical management of the *MPO* magnetometer *(MERMAG-P)*. For *MPO*, IWF also leads the development of the *Planetary Ion CAMera (PICAM)*, an ion mass spectrometer with imaging capability, which is part of the *SERENA* instrument suite, to explore the composition, structure, and dynamics of the exo-/ionosphere.

During 2016, the instrument teams at IWF supported system level testing of both *MMO* and *MPO* spacecraft remotely from the institute as well as on-site at the European Space Research and Technology Centre in Noordwijk. It included e.g. the system validation test in March. In addition, IWF updated the firmware of the *MPO* magnetometer and the *MPO* magnetometer team successfully passed the Flight Spare acceptance review.

Planetary Ion CAMera (PICAM): For *PICAM* 2016 brought another exchange of the actual Flight Model (FM). It turned out that the refurbished Qualification Model, now called FM-02 and originally meant to be the flight spare, outperforms the FM-01 by far. ESA supported the application for the exchange, accordingly the FM-02 was integrated into the spacecraft in June 2016. Refurbishment work on the FM-01 has been started thereafter and will lead to the Flight Spare acceptance review in May 2017.

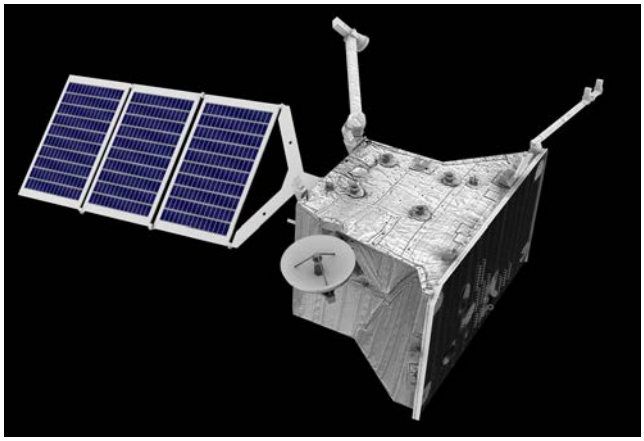

Fig. 25: Artist's impression of ESA's *MPO* spacecraft with the two boom-mounted magnetic field sensors in the top right corner (Credit: ESA).

VENUS & MARS

Two terrestrial planets are located just inside, Venus at 0.7 AU, and outside, Mars at 1.5 AU, the Earth's orbit around the Sun. Venus has a radius slightly smaller than Earth and is differentiated; it does, however, not exhibit an internal magnetic field. Mars has a radius about half as big as that of the Earth, is also differentiated, but only exhibits remnant surface magnetization of a now defunct internal dynamo. Venus is characterized by a very dense, whereas Mars has a very tenuous atmosphere. Both planets generate a so-called induced magnetosphere by their interaction with the solar wind.

INSIGHT

The launch of NASA's Mars mission *InSight*, to which IWF contributes by participating in *HP³ (Heat Flow and Physical Properties Probe)*, had to be postponed by two years to spring 2018. *HP³* consists of a cylindrical body with a built-in hammering mechanism, which will drive the probe at least 3 m into the ground, where it is planned to measure the interior heat flux of Mars as well as the thermal and mechanical properties of the Martian soil.

Numerical models describing the penetration of this mole into the Martian soil have been developed and tested. Fig. 26 shows two representative results. The upper panel illustrates how the stress in a granular material is built up and relaxed within the soil particles, while the lower panel shows the Mole's penetration depth as a function of time in comparison with a measured penetration curve in sand.

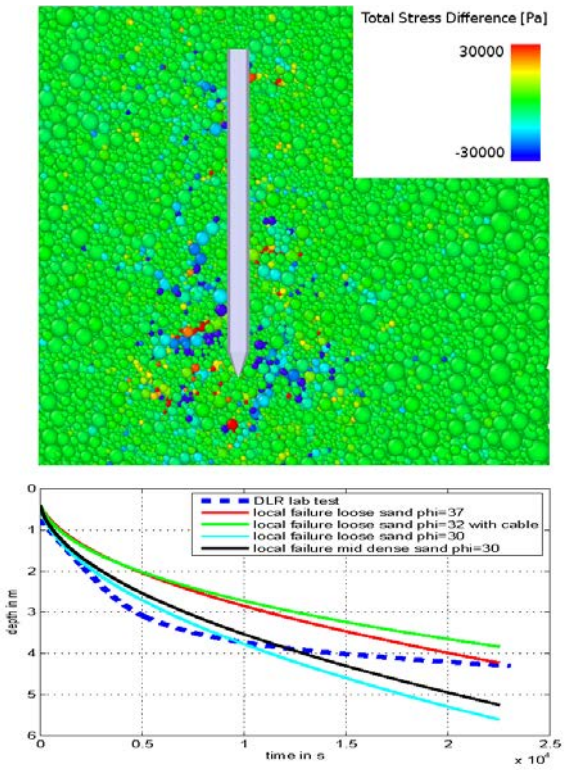

Fig. 26: Penetration characteristics of the *HP³* mole aboard *InSight*.

EXOMARS

In support of planned investigations in the frame of ESA's *ExoMars* mission a series of laboratory tests was performed using a cryo-vacuum chamber, which simulates approximately Mars surface conditions. Hereby, it was studied in detail under which conditions the granular material, which covers a large part of the Martian surface, tends to form cemented crusts under the influence of moisture, which could potentially affect the functionality of the used sampling mechanisms.

CHINESE MARS MISSION

China plans a Mars orbiter, lander, and rover mission to be launched in 2020 (Fig. 27). The main mission will conduct a comprehensive remote sensing of the Red Planet, as well as a surface landing. IWF will contribute a magnetometer.

Fig. 27: China's Mars 2020 lander and (below) the rover (Credit: Xinhua).

PHYSICS

Mirror-Mode Waves in Venus's Magnetosheath: The observational rate of mirror mode (MM) waves in Venus's magnetosheath for solar maximum conditions is studied and compared with previous results for solar minimum conditions. It is found that the number of MM events is approximately 14% higher for solar maximum than for minimum. A possible cause is the increase in solar UV radiation, ionizing more neutrals from Venus's exosphere and the outward displacement of the bow shock during solar maximum. Also, the solar wind properties differ for solar minimum/maximum. The maximum observational rate, however, over Venus's magnetosheath remains almost the same, with only differences in the distribution along the flow line (see Fig. 28). This may be caused by the interplay of a decreasing solar wind density and a slightly higher solar wind velocity for this solar maximum. The distribution of strengths of the MM waves is shown to be exponentially falling off, with (almost) the same coefficient for solar maximum/minimum. The plasma conditions in Venus's magnetosheath are different. For solar minimum, MM waves created directly behind the bow shock will decay, whereas for solar maximum all created MMs can grow.

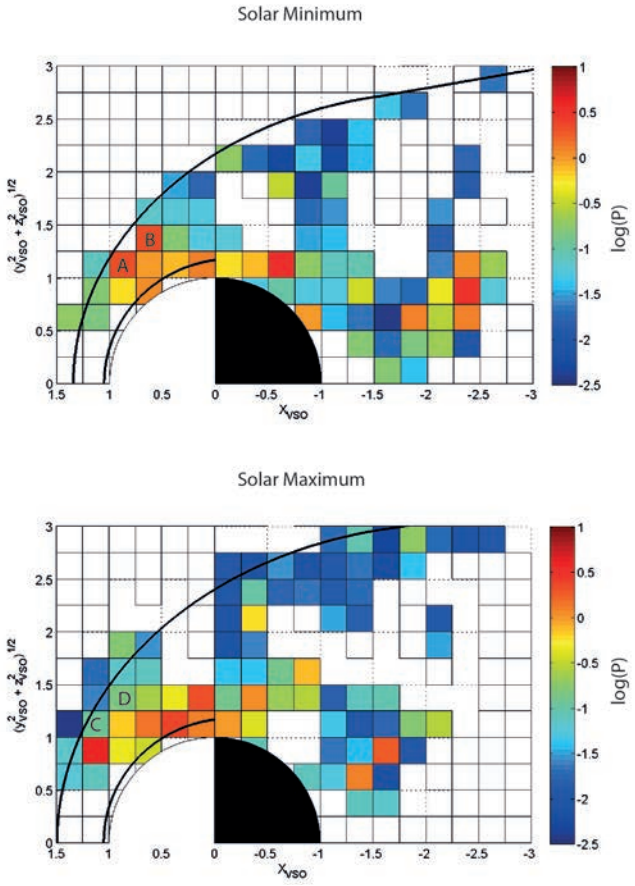

Fig. 28: Comparison of the observational rate P of MM waves in Venus's magnetosheath for solar minimum (top) and solar maximum (bottom). The two thick black curves in each panel show the location of the model ionosphere and model bow shock.

ENA and EUV-Driven Escape from Early Venus: By assuming that the young Sun was an average active young G-type star, the water loss from a hydrogen dominated thermosphere due to the absorption of the solar EUV flux and the precipitation of solar wind produced Energetic Neutral Atoms (ENAs) was studied. The production of ENAs and their interaction with the hydrodynamically extended upper atmosphere, including collision-related feedback processes, have been calculated by means of Monte Carlo models. As can be seen in Fig. 29, ENAs that collide in the upper atmosphere deposit their energy and heat in the surrounding atmosphere mostly above the main EUV energy deposition layer. Contrary to previous suggestions, it was shown that precipitating ENAs modify the thermal structure of the upper atmosphere, but the enhancement of the thermal escape rates caused by these ENAs is negligible.

The results also suggest that most of the initial CO_2 inventory cannot be removed by EUV fluxes less than 100 times the present solar value, while hydrogen originating from H_2O may escape efficiently. The remaining oxygen may be stored in a magmatic surface. A further improvement of this hypothesis could be obtained by collecting precise data of noble gases in the atmosphere of Venus and by knowledge of the water content and oxidation state of Venus's surface rocks.

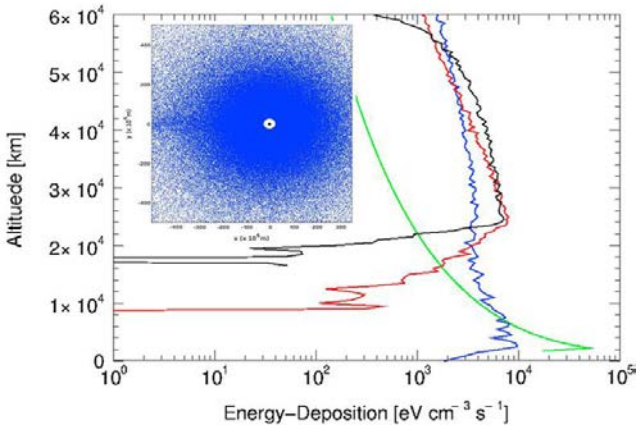

Fig. 29: The insert shows the solar wind induced ENA-cloud (blue dots) around early Venus (white circle). The green line shows the EUV energy deposition rate of the young Sun and the blue, red, and black lines correspond to the ENA energy deposition in early Venus upper atmosphere according to different collision cross sections.

Weak and Quiet Magnetic Fields seen in the Venus's Atmosphere: Toward the end of the *Venus Express* mission, an aerobraking campaign took the spacecraft below the north-polar-region ionosphere into the very weakly electrically conducting atmosphere. It was found that the magnetic field there was much smaller than the ionospheric field and quiet as shown in Fig. 30. These observations confirm that Venus has no significant global intrinsic field. Furthermore, the temporal fluctuations available to undertake electromagnetic sounding of the crust are also weak, making standard techniques, such as might be attempted on a future lander, difficult and likely futile. These results most probably extend as well to the sounding of Mars.

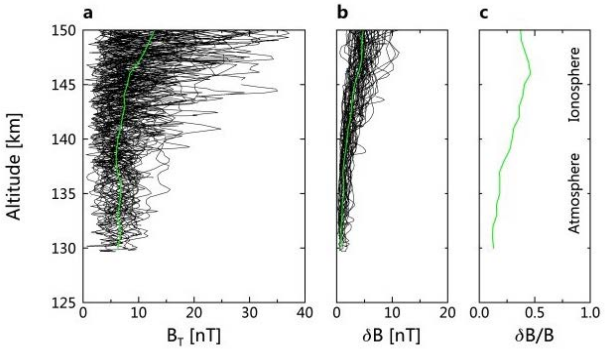

Fig. 30: Altitude profiles of magnetic field strength (panel a) and fluctuation amplitude (panel b). 66 profiles from 33 passes during 6 June to 12 July 2014, when the *Venus Express* periapsis altitude was below 150 km, are displayed. The field strength data shown in left panel is 1 second resolution and the magnetic field fluctuation δB is indicated as the standard deviation of the field in 12 second bin. The green lines in panels (a) and (b) are medians. The line in panel (c) is the ratio of these medians.

JUPITER & SATURN

Jupiter and Saturn are the two largest planets in our solar system. Both planets rotate rapidly and are strongly magnetized, leading to rotationally dominated magnetospheres. There are strong internal plasma sources, like Io at Jupiter or Enceladus at Saturn, and both gas giants are strong sources of radio emissions.

JUNO

The *Juno* spacecraft (Fig. 31) was launched in 2011 and entered a polar orbit around Jupiter in early July 2016. Its main scientific goal is to measure Jupiter's composition, gravity and magnetic field, and to investigate its polar magnetosphere. For the latter task the *Juno Waves* instrument, whose antenna system was calibrated at IWF, is very important.

Fig. 31: Artist's concept of the *Juno* spacecraft orbiting Jupiter (Credit: NASA/JPL-Caltech).

JUICE

ESA's first Large-class mission *JUpiter ICy moons Explorer (JUICE)* is planned for launch in 2022 and arrival at Jupiter in 2030. *JUICE* will spend at least three years making detailed observations of the gas giant Jupiter and three of its largest moons, Ganymede, Callisto, and Europa. IWF is taking part as Co-I for three different selected instrument packages.

Jupiter MAGnetometer (J-MAG): IWF supplies an atomic scalar sensor for *J-MAG*, which is developed in collaboration with TU Graz. In 2016, the Laboratory Model was manufactured and tested as well as the Instrument Preliminary Design Review conducted by ESA was successfully passed.

Particle Environment Package (PEP): *PEP* is a plasma package with sensors to characterize the plasma environment of the Jovian system and the composition of the exospheres of Callisto, Ganymede, and Europa. IWF participates in the *PEP* consortium on Co-I basis in the scientific studies related to the plasma interaction and exosphere formation of the Jovian satellites.

Radio and Plasma Wave Investigation (RPWI): IWF is also responsible for the antenna calibration of the *RPWI* instrument. The antenna system will consist of three dipoles mounted on a long magnetometer boom. Detailed numerical simulations to find the dipole orientations with the best reception properties have started.

CASSINI

The *Cassini* mission is in its second to last year before it will plunge into Saturn's atmosphere in September 2017. During 2016 multiple flybys at Saturn's largest moon Titan were used to raise *Cassini's* orbital inclination above 60°, and the so-called ring-grazing orbits started in November. Until April 2017 these orbits are directing the spacecraft through the unexplored region close to the F-ring every seven days. IWF participates in *Cassini* with the *Radio and Plasma Wave Science (RPWS)* instrument.

PHYSICS

Beaming Cone of Jovian Decameter Emission: The *SWAVES* experiment aboard the *Solar TErrestrial RElations Observatory (STEREO)* is mainly dedicated to measuring solar radio emission, but also provides unique stereoscopic observations of the Jovian radio emission in a frequency range from a few kHz up to 16 MHz. Stereoscopic observations by the *SWAVES* instrument have been used with the aim of estimating the instantaneous wall thickness of an emission cone of Jovian decametric radio emission (DAM). Altogether, 139 dynamic radio spectra, in particular 91 Io- and 48 non-Io-related DAM have been analyzed using 2D cross-correlation between two radio spectra simultaneously recorded by the *STEREO-A* and *STEREO-B* spacecraft. The averaged width of the emission cone wall for Io-DAM as well as for non-Io DAM is about 1.1° ± 0.2°. These results are in agreement with previous findings, which were based on a limited number of observations.

Varying Periodicity of Saturn Kilometric Radiation (SKR): SKR is a strong auroral radio emission in the frequency range from a few kHz to 1.2 MHz. SKR has sources in both hemispheres, which can be separated by wave polarization and which rotate with different periods as can be seen in Fig. 32. Before Saturn equinox (August 2009) the rotation rate of SKR north was ~815°/day (period of 10.6 h), and the rotation rate of SKR south was ~800°/day (period of 10.8 h).

The periods of SKR north and south converged during 2009 and coalesced in spring 2010 and repeatedly showed similar periods and phases for some years after equinox. In late 2014 it turned out that SKR south is faster than SKR north, which could be related to seasonal changes of the winds in Saturn's upper atmosphere. It is thought that the varying periodicity of SKR is caused by rotating field-aligned current systems, which are anchored in the northern and southern auroral regions in Saturn's upper atmosphere.

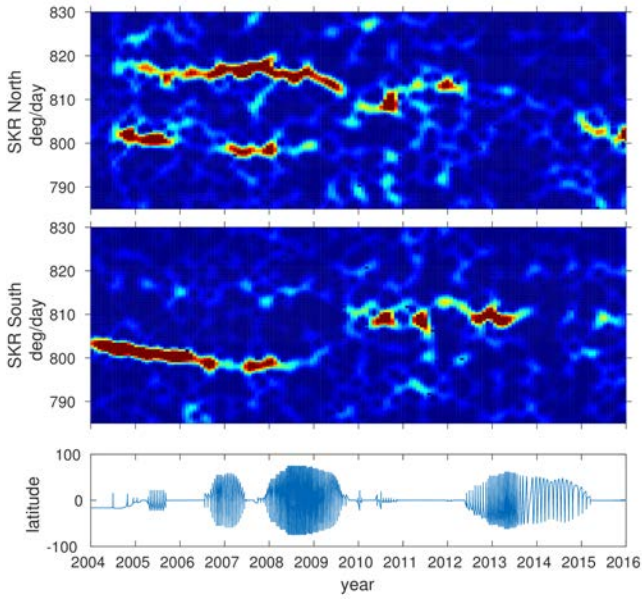

Fig. 32: Lomb-Scargle modulation spectrogram of SKR north (top) and SKR south (middle) as a function of time from 2004 until the end of 2015. Red color indicates strong modulation, whereas blue color means no modulation. The bottom panel shows the latitude of *Cassini*.

COMETS & DUST

Comets and interplanetary dust are the remainders of the building blocks the solar system was formed, although dust can also be created by collisions of e.g. asteroids. *Rosetta's* successful mission at comet 67P/Churyumov-Gerasimenko (67P/CG) gave new life to the study of comets and is the starting point for new future missions to asteroids and comets.

ROSETTA

Rosetta arrived at comet 67P/CG in August 2014 and has since followed the comet along its orbit past perihelion. The nominal mission was extended until September 2016 and ended with a controlled crash of the orbiter onto the Ma'at region on 67P/CG. IWF is participating in five instruments, on PI basis for the *Micro-Imaging Dust Analysis System (MIDAS)* and Co-I basis for the *Rosetta Plasma Consortium (RPC)*, the *Rosetta Lander Magnetometer and Plasma Monitor (ROMAP)*, the *Multi-Purpose Sensor (MUPUS)*, and the *Cometary Secondary Ion Mass Spectrometer (COSIMA)*.

Micro-Imaging Dust Analysis System (MIDAS): The *MIDAS* instrument aboard *Rosetta* was the first Atomic Force Microscope (AFM) designed and built to operate in space. Launched in 2004, *Rosetta* needed a ten year cruise phase to intercept comet 67P/CG on its passage through the inner solar system. After arrival in August 2014 *MIDAS* set to work exposing targets to collect dust from the coma of the comet and scanning them with the microscope. An AFM works by moving a very sharp tip over the target and detecting subtle interactions when the tip is close to the sample surface. This allows *MIDAS* to build a detailed 3D map of dust grains down to a resolution of nanometers.

PHYSICS

MIDAS' First Detection of Dust: Flyby measurements at other comets hinted at a size distribution of dust containing very many small particles. The first scientific surprise came soon after arrival. After weeks of repeated exposures and scans, not a single particle was found. When *MIDAS* eventually detected its first particle, it was far larger than expected, and almost too large to analyze. A new strategy was quickly devised to locate and scan these particles.

By early 2015 *MIDAS* had collected sufficient particles to make a detailed study. All particles studied were found to be aggregates, even for the smallest dust, and they appeared at distinct sizes, suggesting a hierarchical structure. This is important for understanding dust release mechanisms at the surface of the comet, and for linking the observed dust to formation processes in the early solar nebula. In addition, the grains making up these dust particles had an elongation similar to that seen in interstellar dust, suggesting a common origin or formation mechanism. Fig. 33 a-c shows the structure of three dust particles: A and C, which are 5 µm, the size of a red blood cell, and D, which is the size of a bacterium.

Particles comprising many grains were chosen for a detailed structural analysis. Most were made of densely packed sub-units, but one was extremely porous. Its structure (Fig. 33 d) was found to be a statistical fractal and was used as a fingerprint for its growth process. The measured fractal dimension is characteristic for dust agglomerates predicted to have formed in the early solar system.

One interpretation is that *MIDAS* collected a pristine fractal particle stored in comet 67P/CG billions of years ago. This discovery was supported by the detection of a population of similar fractal dust particles by the dust analysis instrument *GIADA*. As theory and experiments predict compaction of the majority of the fractals in the early solar nebula, the detection of a minority of fractal and majority of compact dust particles is consistent. The similar size distribution and shape of the grains of both the fractal and a representative compact particle suggests a similar origin but different evolution, leading to structural differences. Furthermore, the survival of highly fragile fractal particles provides constraints on cometary formation and evolution.

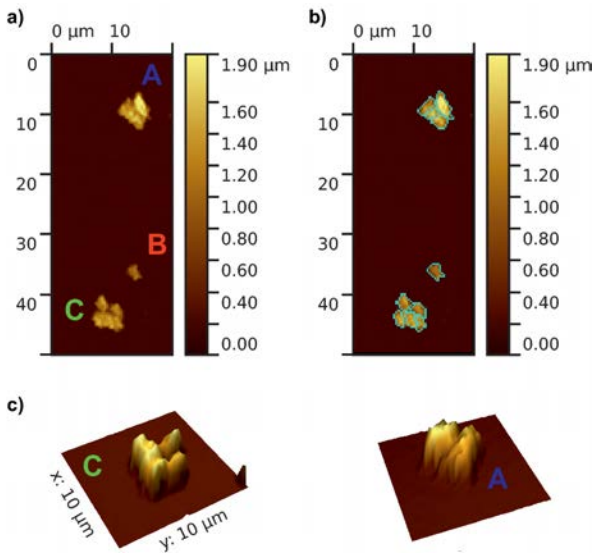

Fig. 33: AFM topographic images of four particles (A, B, C, and D) and their sub-units; a) shows a 20 µm × 50 µm overview image with a pixel resolution of 312 nm and the color scale represents the height; b) as in a, but with particle B and the sub-units of particles A and C outlined in cyan; c) shows 10 µm × 10 µm three-dimensional (rotated) images of particles C and A with two-times height exaggeration to aid visualization; d) shows a 3D AFM topographic image of a fluffy, fractal particle showing a very high porosity structure, with the sub-units (grains) marked in cyan.

Gravity Field Modeling of Comets and Asteroids: Knowledge of a celestial body's gravity field is of crucial importance for navigational and geophysical purposes. The mathematical description of the gravity field typically involves spherical harmonics - a type of special functions representing the solution to Laplace's equation in spherical coordinates. Comets and asteroids, however, are only weakly gravitating and in general non-spherical in shape. The applicability of spherical harmonics and the more sophisticated spheroidal and ellipsoidal harmonics has been investigated for the purpose of gravity field modeling in a large-scale study for some 400 asteroids and comets, including comet 67P/CG (see Fig. 34). While ellipsoidal harmonics proved to be the most effective parametrization in terms of convergence behavior, spheroidal harmonics turned out to be an attractive alternative due to simple and straightforward mathematics.

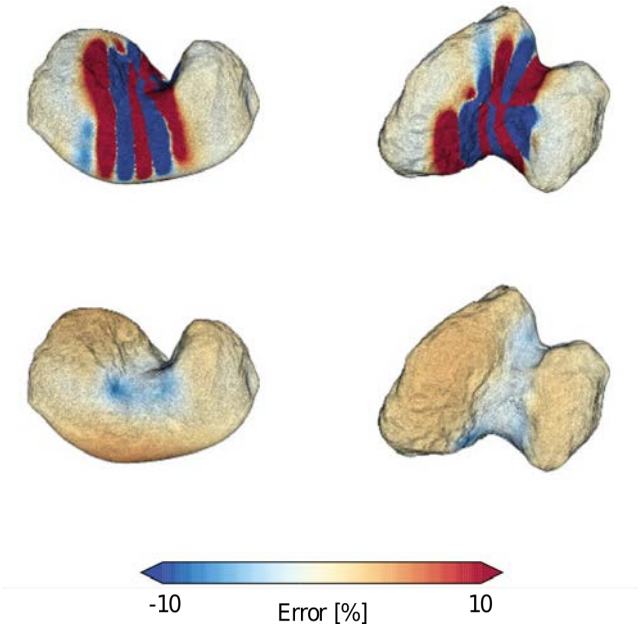

Fig. 34: Error patterns of spherical (above) end ellipsoidal (below) harmonic gravity field models for comet 67P/CG.

Mirror-Mode Waves at Comet 67P/CG: Data from all *Rosetta Plasma Consortium* instruments and from the *ROSINA-COPS* instrument are used to study the interaction of the solar wind with the outgassing cometary nucleus of 67P/CG. During 6 and 7 June 2015, the interaction was first dominated by an increase in the solar wind dynamic pressure, caused by a higher solar wind ion density. This pressure compressed the draped magnetic field around the comet, and the increase in solar wind electrons enhanced the ionization of the outflow gas through collisions. The new ions are picked up by the solar wind magnetic field, and create a ring/ringbeam distribution, which, in a high-β plasma, is unstable for mirror mode wave generation. Two different kinds of mirror modes are observed: one of small size generated by locally ionized water and one of large size generated by ionization and pick-up farther away from the comet. Also, there seems to be a development in the mirror-mode waves over time, as shown in Fig. 35, where the frequency changes and an, as yet unexplained, bi-modal situation appears (red interval).

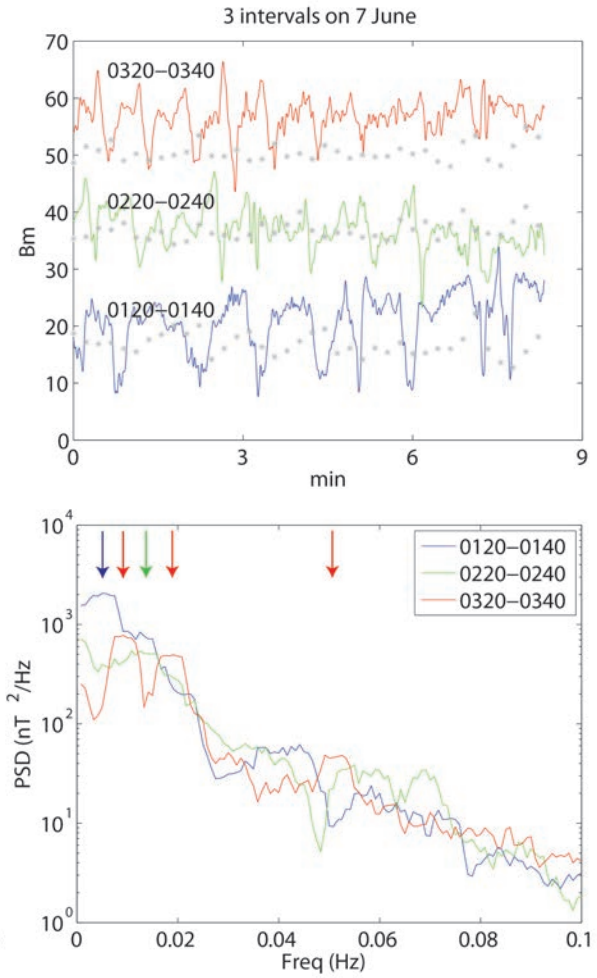

Fig. 35: Upper panel: three 20 min intervals of the magnetic field strength Bm data, shifted to enhance visibility; blue 01:20-01:40 UT, green 02:20-20:40 UT, red 03:20-03:40 UT. The gray stars show the LAP P1 current, which is proportional to the local electron density. Lower panel: the Fourier power spectra for the three intervals. The colored arrows at the top mark the peaks in the spectra.

EXOPLANETARY SYSTEMS

The field of exoplanet research (i.e. investigation of planets orbiting stars other than the Sun) has developed strongly, in the past decade. Since the discovery of 51 Peg b, the first detected exoplanet orbiting a Sun-like star, more than 3000 exoplanets, most of which in planetary systems, are now known. Improved instrumentation and analysis techniques have led to the finding of smaller and lighter planets, down to Earth-size, Earth-mass planets, some of which orbiting in the habitable zone of the cooler stars. However, super-Earths are now prime targets for atmospheric characterization, mostly because of their larger radii, which indicate the presence of a volatile-rich atmosphere and facilitate observations and analyses.

The two main exoplanet missions IWF is involved are *CHEOPS* and *PLATO*. The former will precisely measure the radii of already known planets to greatly improve their inferred density and hence provide a first characterization. The latter will instead look for planets in large portions of the sky, with the primary aim to find Earth-like planets in the habitable zone of Sun-like stars.

IWF concentrates on the study and characterization of planetary atmospheres using both theory and observations, focusing particularly on the analysis of exoplanet atmospheric escape and mass loss processes. Further research is conducted to study star-planet interactions and carry out atmospheric characterization through the collection and analysis of ground- and space-based observations.

Fig. 36: Members of the *CHEOPS* Instrument Team from Bern, Vienna, IWF Graz (3rd and 4th f.l.), and DLR Berlin, in the ESA EMC anechoic test chamber (Credit: ESA/C. Carreau).

CHEOPS

CHEOPS (CHaracterising ExOPlanet Satellite), to be launched in 2018, will study extrasolar planets and observe planetary systems at an unprecedented photometric precision. The main science goals are to find transits of small planets, known to exist from radial-velocity surveys, measure precise radii for a large sample of planets to study the nature of Neptune- to Earth-sized planets, and obtain precise observations of transiting giant planets to study their atmospheric properties. IWF is responsible for the *Back-End-Electronics (BEE)*, one of the two on-board computers, which controls the data flow and the thermal stability of the telescope structure.

IWF manufactured and assembled the Qualification Model. In cooperation with RUAG Space Austria the environmental tests at *BEE* level have been successfully completed. IWF also performed and supported tests at instrument level. *BEE* has gone through the EMC tests at ESA. A second EMC test with the entire electrical system, mounted on a spacecraft dummy, has been performed in cooperation with University of Bern (Fig. 36). Communication tests with the *BEE* Engineering Model and the spacecraft electronics have been performed at Airbus Spain.

PLATO

PLATO (PLAnetary Transits and Oscillations of stars) is ESA's third Medium-class mission, led by DLR. Its objective is to find and study a large number of extrasolar planetary systems, with emphasis on the properties of terrestrial planets in the habitable zone around solar-like stars. *PLATO* has also been designed to investigate seismic activity in stars, enabling the precise characterization of the planet host star, including its age. IWF contributes to the development of the Instrument Controller Unit (ICU) with the development of the *Router and Data Compression Unit (RDCU)*. Launch is expected in 2024.

PLATO consists of 24 telescopes for nominal and two telescopes for fast observations. Each telescope has its dedicated front-end-electronics, reading and digitizing the CCD content. Six nominal and two fast DPUs collect the data from the front-end-electronics and extract the areas of interest. The *RDCU* is a key element in the data processing chain, providing the communication between the DPUs and the ICU. The second task of the *RDCU* is the lossless compression of the science data. For performance reasons, the compression algorithm is implemented in an FPGA. The development of the *RDCU* prototype has been started. A first version of VHDL code has been developed and tested, supporting the communication with the compressor via SpaceWire standard.

PHYSICS

The Ground-Based FORS2 Transmission Spectrum of the Hot Saturn-Mass Exoplanet WASP-49b: The study of transiting planets has become one of the main approaches to characterize exoplanets. Transmission spectroscopy is sensitive to the absorption features imprinted by the planetary atmosphere on the stellar light that passes through it during transit. In this configuration the planetary day-night terminator region is probed. WASP-49b is a hot Saturn-mass planet orbiting a mid G-type star every 2.78 days. Because of its very low density and short orbital period, WASP-49b is a favorable target for transmission spectroscopy. Three transits of WASP-49b have been observed with the FORS2 instrument installed at the VLT/UT1 telescope at the ESO Paranal site to look for the signature of K and H_2O in the planet's atmosphere. The three FORS2 light curves present strong correlated noise features, which are due to rotating flat-field structures introduced by the inhomogeneity of the linear atmospheric dispersion corrector's transparency. This issue has been overcome for the first time using a "common noise model" approach, the efficiency of which is evidenced by reaching consistent results from three independent transit observations. The three individual synthetic transmission spectra agree well among each other and are characterized by a lack of atmospheric features. From the highly precise obtained transmission spectrum (see Fig. 37), the presence of a thick cloud layer at an atmospheric pressure of 1 mbar or less was inferred.

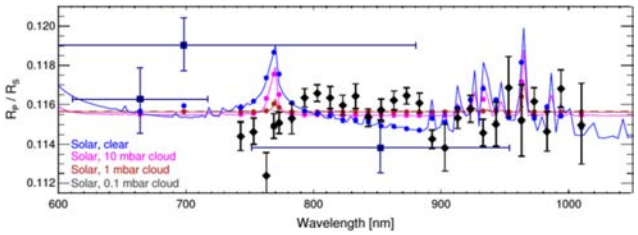

Fig. 37: Transmission spectrum of WASP-49b as observed with FORS2, EulerCam (broadband) and TRAPPIST (broadband) compared to models of a solar-composition atmosphere (blue), a solar-composition atmosphere with a cloud deck at 10 mbar pressure (magenta), and a solar-composition atmosphere with a cloud deck at 1 mbar pressure (dark red). A flat spectrum obtained from a solar-composition atmosphere with a cloud deck at 0.1 mbar pressure is shown as a gray dashed line. The filled circles show the models binned to the observed spectral resolution.

Aeronomical Constraints to the Minimum Mass and Maximum Radius of Hot, Low-Mass Planets and their Application to the Sub-Neptune CoRoT-24b: The last five years have seen an increasing number of detections of close-in, low-density planets. The formation, evolution, and even the existence of such planets are difficult to understand because their atmospheres should be characterized by exceptionally strong escape. Under the assumption of a clear atmosphere, the long-term stability of an atmosphere can be studied by comparing escape rates derived from the energy-limited formula and from a hydrodynamic atmospheric code. Modeling of 5 and 10 M_{Earth} planets with various equilibrium temperatures (T_{eq}) orbiting early G-, K-, and M-type stars indicates that planets, for which Λ (the value of the Jeans escape parameter calculated at the observed planetary radius and mass, for the planet's equilibrium temperature, and considering atomic hydrogen as atmospheric constituent) is smaller than 15-35, depending on the system parameters, lie in the "boil-off" regime, where the escape is driven by the atmospheric thermal energy and low planetary gravity. In particular, the atmosphere of hot (T_{eq}>1000 K), low-mass (<5 M_{Earth}) planets with Λ<15-35 shrinks to smaller radii so that their Λ evolves out of the boil-off regime, in less than about 500 Myr. This provides a strong constraint on the planetary minimum mass/maximum radius, and can be used, for example, to predict the presence of aerosols and/or constrain planetary masses. This result is applied to the sub-Neptune planet CoRoT-24b, which has a measured Λ smaller than 12 (see Fig. 38). Detailed modeling of this planet led to the unphysical conclusion that the atmosphere could last no longer than 100 Myr, though the CoRoT-24 system is several Gyr old. This result indicates that for CoRoT-24b the 100 mbar pressure level, where the photospheric radius is commonly considered to be, lies much below the observed radius, and at about 2 R_{Earth} and that high-altitude aerosols may extinct the light at the transit radius.

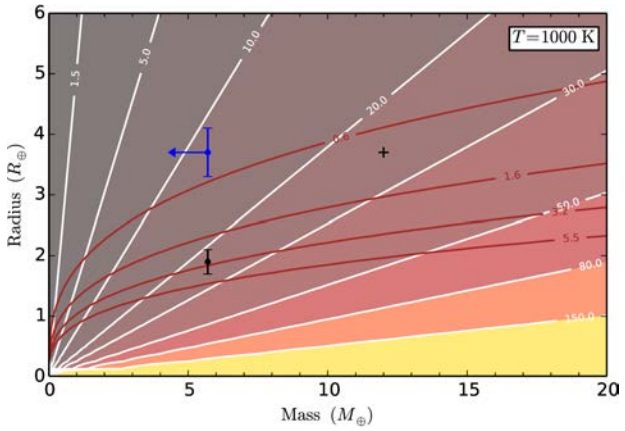

Fig. 38: Color-scaled value of Λ as a function of planetary mass and radius for T_{eq}=1000 K. The white straight lines indicate equal Λ values given in the plot. The red solid lines indicate lines of equal average densities of 0.6, 1.6, 3.2, and 5.5 g/cm^3. The symbols correspond to the observed (blue bar and arrow) and possible mass-radius combination (black points) for CoRoT-24b. Radial velocity measurements indicate that the high-mass solution is not possible.

New Insights in Stellar Physics with Kepler Photometry: The light curves of 1361 main sequence stars observed by the Kepler mission were analyzed with dedicated algorithms to study internal motions, so far inaccessible to astroseismology methods. The pattern of stellar surface activity was studied and global-scale Kolmogorov-type turbulence was found in the power spectra of the rotational variability of spotted stars. Extrapolation of this turbulent cascade to the scale of laminar convection gives a timescale analogous to the turnover time τ_{mlt} of the standard mixing length theory (Fig. 39 a). It has been shown, that with the measured timescales, one can obtain the classical relationship between stellar activity level and the Rossby number. Moreover, the lifetimes of spots in the photospheres of cold and fast-rotating stars have been measured. As a result, realistic values of the diffusivity of the magnetic elements in the photosphere were obtained for the broad interval of stellar effective temperatures from 3300 to 6600 K (Fig. 39 b).

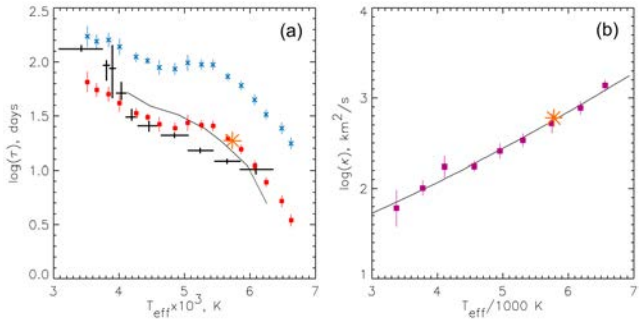

Fig. 39: (a) Averaged timescale τ (blue) of the first rotational harmonic and its reduction to the laminar convection scale (red) in comparison with the turnover time τ_{mlt} estimated on the basis of different models (black symbols and curve); (b) Average diffusivity κ versus stellar effective temperature T_{eff}. The asterisk stands for the solar values.

Long Period Oscillations of Solar Active Regions (ARs): An automated AR pattern detection method is used to investigate AR dynamics as well as the least-squares fitting an AR to an elliptical shape. Applying this to ARs 11327 and 11726 reveals oscillations of the ellipse's major axes with periods of 4.6 to 4.9 hours. These oscillations are interpreted as second harmonics of a standing kink mode on flux tubes connecting sunspots. The ARs are supposed to oscillate as a whole, so that the kink mode has a node in the apex above the solar surface. Comparing scenarios for fast and slow kink modes reveals that the characteristic depth of the wave turning point has to be at about 40 Mm below the solar surface, which is in agreement with the helioseismology predictions of the sunspot depth.

Modelling of the Interaction Between Stellar and Planetary Winds: The interaction of the escaping upper atmosphere of a non-magnetized analogue of HD209458b with the stellar wind (SW) of its host star at different orbital distances was simulated with a 2D multi-fluid hydrodynamic model. A realistic spectrum of XUV radiation, which ionizes and heats the planetary atmosphere, hydrogen photochemistry, and stellar-planetary tidal effects are included in the self-consistent model of the expanding planetary wind (PW). Two regimes of the PW and SW interaction were simulated (Fig. 40): 1) the "captured by the star" regime, when the tidal force and pressure gradient drive the planetary material towards the star, and 2) the "blown by the wind" regime, when sufficiently strong SW confines the escaping PW and channels it to the tail. The model also simulates production of energetic neutral atoms (ENAs) around a planet due to charge exchange between planetary atoms and stellar protons.

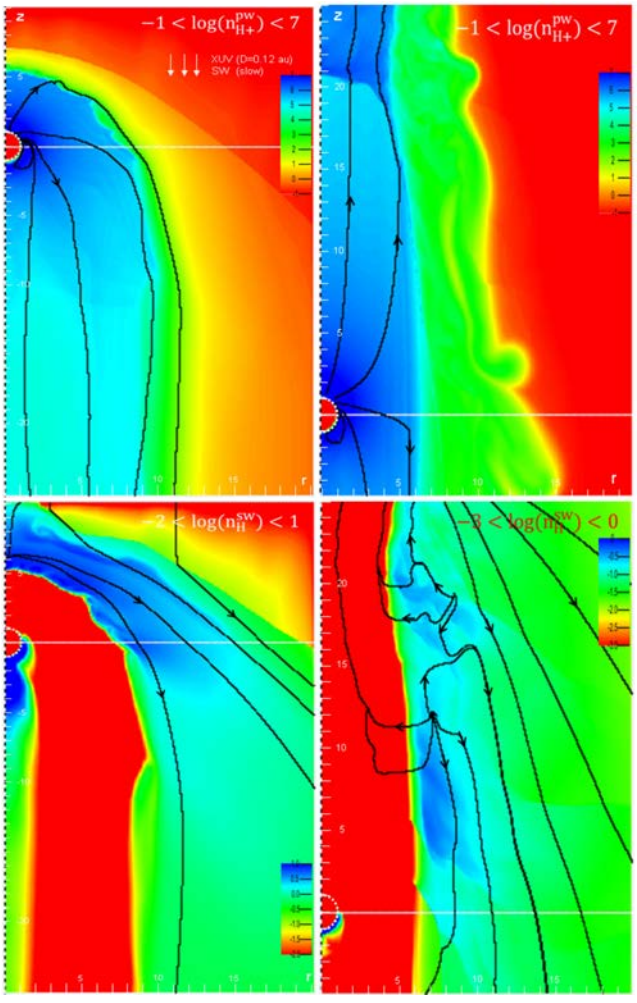

Fig. 40: Density distributions of planetary protons (top panels) and ENAs (bottom panels) in the "blown by the wind" (left) and "captured by the star" (right) regimes of SW and PW interaction.

OTHER TELESCOPES

Members of the institute obtained two nights of observing time with the FORS2 instrument at the Very Large Telescope (VLT, Fig. 41) at the Paranal site of the European Southern Observatory (ESO) in Chile and 16 nights with the Swiss Euler telescope located at the La Silla site of ESO.

The FORS2 observations, conducted during planetary transits, will be used to study the physical properties of the atmosphere of two close-in giant planets, while the Euler observations will be used to measure the mass of newly-detected planets.

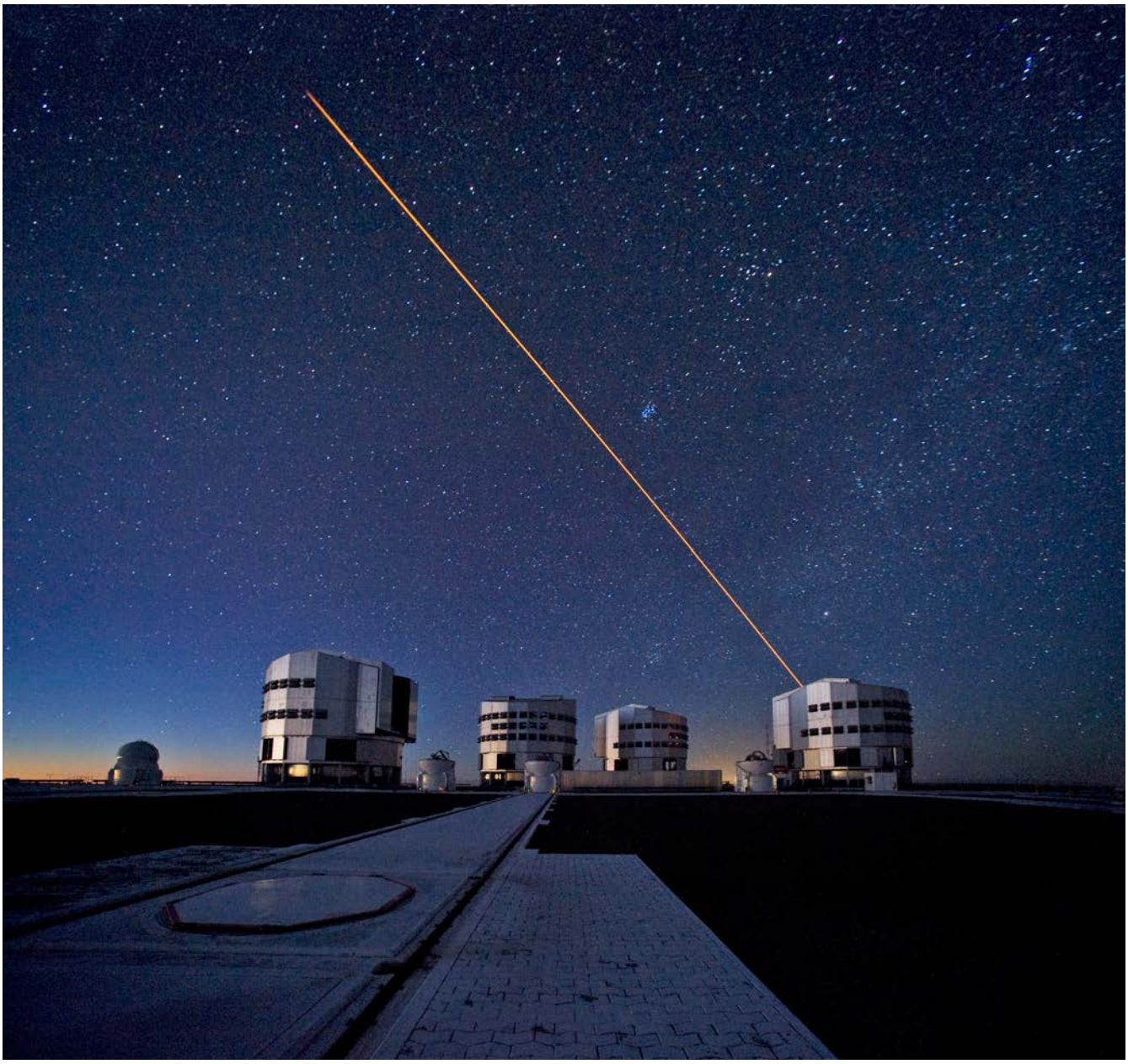

Fig. 41: The ESO Very Large Telescope (VLT) during observations (Credit: ESO/S. Brunier).

INFRASTRUCTURE

Instruments aboard spacecraft are exposed to harsh environments, e.g., vacuum, large temperature ranges, radiation, and high mechanical loads during launch. Furthermore, these instruments are expected to be highly reliable, providing full functionality over the entire mission time, which could last for more than a decade.

VACUUM CHAMBERS

The *Small Vacuum Chamber* is a manually controlled, cylindrical vacuum chamber (160 mm diameter, 300 mm length) for small electronic components or printed circuit boards. It features a turbo molecular pump and a rotary dry scroll forepump. A pressure level of 10^{-10} mbar can be achieved.

The *Medium Vacuum Chamber* has a cylindrical stainless steel body with the overall length of 850 mm and a diameter of 700 mm. A dry scroll forepump and a turbo molecular pump provide a pressure level of about 10^{-7} mbar. A target manipulator with two axes and an ion beam source are installed. This chamber mainly serves for functional tests of the ion mass spectrometer for *BepiColombo*.

The *Large Vacuum Chamber* has a horizontal cylindrical stainless steel body and door, a vision panel, two turbo molecular pumps and a dry scroll forepump. A pressure of 10^{-7} mbar can be achieved. The cylinder has a diameter of 650 mm and a length of 1650 mm. During shutdown the chamber is vented with nitrogen. A target manipulator inside the chamber allows for computer-controlled rotation of the target around three mutually independent perpendicular axes. The vacuum chamber is enclosed by a permalloy layer for magnetic shielding. To enable the baking of structures and components (to outgas volatile products and unwanted contaminations), the chamber is equipped with a heater around the circumference.

The *Thermal Vacuum Chamber* is fitted with two turbo molecular pumps, a dry scroll forepump, and an ion getter pump, which together achieve a pressure level of 10^{-6} mbar and allow quick change of components or devices to be tested. A thermal plate installed in the chamber and liquid nitrogen are used for thermal cycling in a temperature range between -90 °C and +140 °C. The vertically oriented cylindrical chamber allows a maximum experiment diameter of 410 mm and a maximum height of 320 mm.

The *Surface Laboratory Chamber* is dedicated to surface science research. It has a diameter of 400 mm and a height of 400 mm, extendable up to 1200 mm. One rotary vane pump and one turbo-molecular pump achieve a minimum pressure of 10^{-5} mbar. With an external thermostat the chamber temperature can optionally be controlled between -90 °C and +50 °C.

The *Sample Chamber* contains an 8µ particle filter and allows measurements of grain sample electrical permittivity. One rotary vane pump achieves a minimum pressure of 10^{-3} mbar.

HIGH-PERFORMANCE COMPUTER

IWF invested in extending the hardware and computing capabilities of the high-performance computer LEO. In particular, a highly efficient storage system was added, consisting of 64 TB of solid-state disk (SSD) space. This allows massive-parallel simulations to output large amounts of data from hundreds of processes, which plasma-kinetic particle codes would typically produce, simultaneously. Together with a doubling of the main working memory of the machine, now totaling a 4 TB of RAM, better statistics are now able to be performed in particle-based simulations.

Also a second long-term storage system with high reliability and 144 TB of raw capacity was added with regard to the currently arriving *MMS* mission data. For a fast access from the scientist's desktop computers to the new data storage servers, the network backbone within the building was upgraded to a 10 GBit/s glass fiber.

OTHER TEST FACILITIES

The *Temperature Test Chamber* allows verifying the resistance of electronic components and circuits to most temperatures that occur under natural conditions, i.e., -40 °C to +180 °C. The chamber has a test space of 190 l and is equipped with a 32-bit control and communication system.

The second *Temperature Test Chamber* is used for fast cycling electronic components and circuit. The temperature range is -70 °C to +180 °C. The chamber has a test space of 37 l and is equipped with similar interfaces for communication.

The *Penetrometry Test Stand* is designed to measure mechanical soil properties, like bearing strength. The UV Exposure Facility is capable to produce radiation between 200-400 nm (UV-A, UV-B, UV-C).

Magnetometer Calibration: A three-layer magnetic shielding made from mu-metal is used for all basic magnetometer performance and calibration tests. The remaining DC field in the shielded volume is <10 nT and the remaining field noise is <2 pT/√Hz at 1 Hz. A special Helmholtz coil system allows generating field vectors of up to ±30000 nT around the sensor under test.

The *Magnetometer Temperature Test Facility* is used to test magnetic field sensors between -170 °C and +220 °C in a low field and low noise environment. Liquid nitrogen is the base substance for the regulation, which is accurate to ±0.1 °C. A magnetic field of up to ±100000 nT can be applied to the sensor during the test cycles.

FLIGHT HARDWARE PRODUCTION

Clean Room: Class 10000 (according to U.S. Federal Standard 209e) certified laboratory with a total area of 30 m^2. The laboratory is used for flight hardware assembling and testing and accommodates up to six engineers (Fig. 42).

Clean Bench: The laminar flow clean bench has its own filtered air supply. It provides product protection by ensuring that the work piece in the bench is exposed only to HEPA-filtered air (HEPA = High Efficiency Particulate Air). The internal dimensions are 118 x 60 x 56 cm^3.

Vapor Phase and IR Soldering Machine: The vapor phase soldering machine is suitable for mid size volume production. The maximum board size is 340 x 300 x 80 mm^3. Vapor phase soldering is currently the most flexible, simplest and most reliable method of soldering. It is ideally suited for all types of surface mounted device (SMD) components and base materials. It allows processing of all components without the need of any complicated calculations or having to maintain temperature profiles. For placing of fine pitch parts and rework of electronic boards an infrared soldering and precision placing system is used.

The new DispenseMate 585 is a solder paste printer in a compact benchtop format. This machine allows a precise dosing of solder pastes on PCBs. As an option, a dispenser for precise glue application can be used. The range of motion is 525 x 525 mm.

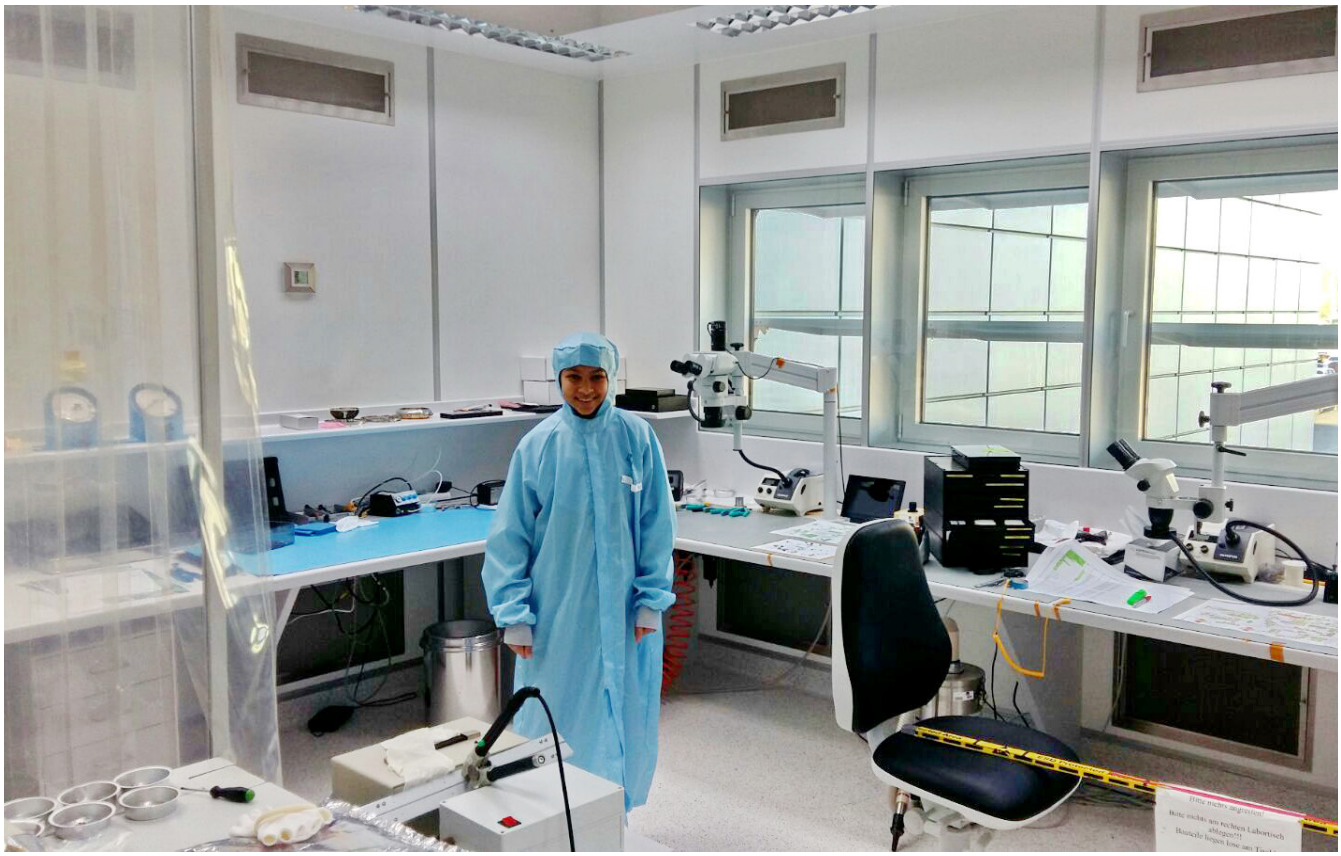

Fig. 42: 14 years old student Vanessa visiting the IWF clean room.

OUTREACH

PUBLIC OUTREACH

IWF is actively engaged in science education and public outreach. 2016's highlight was the "Rosetta Finale" on 30 September, followed by about 120 people, among them former ÖAW president Helmut Denk and Andreas Geisler, head of the Aeronautics and Space Agency (ALR) of FFG.

From February to October IWF was partner of the special exhibition "Weightless" at Welios Science Center in Wels.

On 14 March, numerous prominent guests from science and politics visited IWF for a preview of ORF's documentary "Weltraumhauptstadt Graz" by Günter Schilhan and Erhard Seidl.

During Yuri's Night on 12 April, Rumi Nakamura talked about space weather and its influence on life on Earth at TU Wien.

IWF Director Baumjohann was invited to a BMWFW panel discussion about life on Mars on 18 April in Vienna.

Fig. 43: Children playing with a plasma ball.

On 22 April, more than 1700 people visited IWF during the "Lange Nacht der Forschung" (Fig. 43). The program included experiments, talks, movie shows, guided tours through the labs, a remote controlled Mars Rover tour over a simulated surface of the Red Planet, and last but not least a demonstration of the laser at Lustbühel Observatory. This year's special guest was ESA's education mascot Paxi.

On the occasion of the Mercury transit, several IWF members reported about the planet and the *BepiColombo* mission during a URANIA symposium on 29 April.

During summer time, seven high-school students performed an internship at IWF under the "Talente-Praktika" program of FFG. They worked on aurora, hot Jupiters, stellar activity measurements, *BepiColombo's PICAM*, and VLF data analysis. In the framework of the "FEMtech" program of FFG, three young ladies from KFU Graz and TU Graz worked at IWF. Finally, IWF enabled the obligatory work experience week for two high-school students and one visually impaired student from the Odilien institute.

In August, the ÖAW Young Academics summer series portraited Kristina Kislyakova and her search for another Earth in the Milky Way.

From 8-9 September, the Summer University "Graz in Space" was held at IWF. The program concentrated on the atmospheres of exoplanets and the results of the Rosetta mission. Rudi Schmidt, ESA's Inspector General, gave a lecture about his long-year experience in space business.

From 12-14 September, IWF hosted the UN/Austria Symposium on "Integrated Space Technology Applications for Climate Change" with more than 50 participants from all over the world.

On 5 October, IWF presented itself for the third time during the "Grazer Weltraumtag" in downtown Graz. This year Federal Minister Jörg Leichtfried took the chance to try a remote controlled Mars Rover tour (Fig. 44).

On 15 November, Helmut Lammer talked about the search for habitable planets in the frame of the FWF series of lectures "Am Puls" in Vienna.

From 20-25 November, a "Post Alpbach" meeting was held at ESA's Redu Center in Belgium, where Günter Kargl served es tutor.

Throughout the rest of the year, many different groups and school classes visited the institute and were guided through the labs and the planetary garden.

Fig. 44: Federal Minister Leichtfried (1st f.l.) at the "Grazer Weltraumtag".

AWARDS & RECOGNITION

Christian Möstl received the Arne Richter Award for Outstanding Young Scientists during EGU 2016 General Assembly.

On 24 May, Wolfgang Baumjohann received the "Großes Ehrenzeichen des Landes Steiermark" from Styrian Governor Hermann Schützenhöfer in the aula of the "Alte Universität" (Fig. 45). On 22 September, he was elected into the presidium of the German National Academy of Sciences Leopoldina.

Fig. 46: Bettina Vollath, President of the Styrian Parliament, Wolfgang Baumjohann, Edith Hornig, and Styrian Governor Hermann Schützenhöfer (f.l.t.r.) during the Styrian award ceremony (© steiermark.at/Frankl).

MEETINGS

Helmut Lammer co-chaired the conference "The Astrophysics of Planetary Habitability", which was held at University of Vienna from 8-12 February.

Between 20 and 22 June, IWF hosted the "Rosetta Ground Observation Workshop" at Schloss Seggau, near Graz, as part of the Europlanet NA1 program and the international campaign of observations supporting the *Rosetta* mission.

Wolfgang Baumjohann served as Vice Director and chair of the Program Committee of the Summer School Alpbach, which took place from 12 to 21 July and was dedicated to "Satellite Observations of the Global Water Cycle". Every year, 60 students and about 25 lecturers and tutors from among ESA's member states are invited to this meeting.

The 8th International Workshop on Planetary, Solar and Heliospheric Radio Emissions (PRE 8), dealing with the most recent developments in the study of non-thermal radio emissions, was hosted by the institute at Schloss Seggau from 25-27 October with 50 participants from all over the world. The meeting was organized by Georg Fischer.

In addition, M.Y. Boudjada, G. Kargl, M.L. Khodachenko, G. Kirchner, H. Lammer, C. Lhotka, C. Möstl, R. Nakamura, M. Panchenko, M. Scherf, D. Schmid, and M. Volwerk were members of scientific program and/or organizing committees at six international conferences and/or workshops.

LECTURING

In summer 2016 and in winter term 2016/2017 IWF members gave lectures at the University of Graz, Graz University of Technology, University of Vienna, TU Braunschweig, FH Joanneum, and FH Wiener Neustadt.

THESES

Besides lecturing, members of the institute are supervising Bachelor, Diploma, Master and Doctoral Theses. In 2016, the following supervised theses have been completed:

Alexandrova, A.: Magnetic Reconnection in the Earth's Magnetotail: Temporal Evolution and Spatial Characteristics, Doctoral Thesis, Universität Graz, 120 pages (2016)

Chaghiashvili, T.: Flare-related Changes in Active Regions, Master Thesis, Tbilisi State University, 52 pages (2016)

Grassitelli, L.: Instabilities in the Envelope of Stars, Doctoral Thesis, Universität Bonn, 103 pages (2016)

Odert, P.: Activity of M-type Stars and its Influence on Planetary Atmospheres, Doctoral Thesis, Universität Graz, 254 pages (2016)

Perschke, C.: Dispersionseigenschaften magnetischer Fluktuationen auf ionenkinetischen Skalen in der Sonnenwindturbulenz, Doctoral Thesis, TU Braunschweig, 100 pages (2016)

Schmid, D.: Magnetotail Dipolarization Fronts, Doctoral Thesis, Universität Graz, 110 pages (2016)

Törmänen, O.: Laser Communication Concept for Space Weather Forecasting CubeSat Fleet Mission, Master Thesis, Aalto University, Espoo, Finland, 82 pages (2016)

Wang, G.Q.: Ultra-Low-Frequency Waves in the Magnetotail, Doctoral Thesis, University of Science and Technology of China, Hefei, China, 96 pages (2016)

PUBLICATIONS

REFEREED ARTICLES

Alexandrova, A., R. Nakamura, E.V. Panov, Y.L. Sasunov, T. Nakamura, Z. Vörös, A. Retinò, V.S. Semenov: Two interacting X lines in magnetotail: Evolution of collision between the counterstreaming jets, *Geophys. Res. Lett.*, **43**, 7795-7803 (2016)

Amerstorfer, T., C. Möstl, A. Isavnin, J.A. Davies, M. Kubicka, U.V. Amerstorfer, R.A. Harrison: Erratum: "ElEvoHI: A novel CME prediction tool for heliospheric imaging combining an elliptical front with drag-based model fitting", *Astrophys. J.*, **831**, 210 (2016)

Anderson, B.J., C.T. Russell, R.J. Strangeway, F. Plaschke, W. Magnes, D. Fischer, H. Korth, V.G. Merkin, R.J. Barnes, C.L. Waters, I.J. Cohen, J.H. Westlake, B.H. Mauk, H.K. Leinweber, D.J. Gershman, B.L. Giles, G. Le, R.B. Torbert, J.L. Burch: Electrodynamic context of magnetopause dynamics observed by magnetospheric multiscale, *Geophys. Res. Lett.*, **43**, 5988-5996 (2016)

André, M., W. Li, S. Toledo-Redondo, Yu.V. Khotyaintsev, A. Vaivads, D.B. Graham, C. Norgren, J. Burch, P.-A. Lindqvist, G. Marklund, R. Ergun, R. Torbert, W. Magnes, C.T. Russell, B. Giles, T.E. Moore, M.O. Chandler, C. Pollock, D.T. Young, L.A. Avanov, J.C. Dorelli, D.J. Gershman, W.R. Paterson, B. Lavraud, Y. Saito: Magnetic reconnection and modification of the Hall physics due to cold ions at the magnetopause, *Geophys. Res. Lett.*, **43**, 6705-6712 (2016)

Andriopoulou, M., R. Nakamura, K. Torkar, W. Baumjohann, R.B. Torbert, P.-A. Lindqvist, Y.V. Khotyaintsev, J. Dorelli, J.L. Burch, C.T. Russell: Study of the spacecraft potential under active control and plasma density estimates during the MMS commissioning phase, *Geophys. Res. Lett.*, **43**, 4858-4864 (2016)

Arkhypov, O.V., M.L. Khodachenko, H. Lammer, M. Güdel, T. Lüftinger, C.P. Johnstone: Deep mixing in stellar variability: Improved methods, statistics, and applications, *Astrophys. J.*, **826**, 35 (2016)

Arridge, C.S., J.P. Eastwood, C.M. Jackman, G.-K. Poh, J.A. Slavin, M.F. Thomsen, N. André, X. Jia, A. Kidder, L. Lamy, A. Radioti, D.B. Reisenfeld, N. Sergis, M. Volwerk, A.P. Walsh, P. Zarka, A.J. Coates, M.K. Dougherty: Cassini in situ observations of long-duration magnetic reconnection in Saturn's magnetotail, *Nat. Phys.*, **12**, 268-271 (2016)

Baker, D.N., A.N. Jaynes, D.L. Turner, R. Nakamura, D. Schmid, B.H. Mauk, I.J. Cohen, J.F. Fennell, J.B. Blake, R.J. Strangeway, C.T. Russell, R.B. Torbert, J.C. Dorelli, D.J. Gershman, B.L. Giles, J.L. Burch: A telescopic and microscopic examination of acceleration in the June 2015 geomagnetic storm: Magnetospheric Multiscale and Van Allen Probes study of substorm particle injection, *Geophys. Res. Lett.*, **43**, 6051-6059 (2016)

Barros, S.C.C., D.J.A. Brown, G. Hébrard, Y. Gómez Maqueo Chew3, D.R. Anderson, P. Boumis, L. Delrez, K.L. Hay, K.W.F. Lam, J. Llama, M. Lendl, J. McCormac, B. Skiff, B. Smalley, O. Turner, M. Vanhuysse, D.J. Armstrong, I. Boisse, F. Bouchy, A. Collier Cameron, F. Faedi, M. Gillon, C. Hellier, E. Jehin, A. Liakos, J. Meaburn, H.P. Osborn, F. Pepe, I. Plauchu-Frayn, D. Pollacco, D. Queloz, J. Rey, J. Spake, D. Ségransan, A.H.M. Triaud, S. Udry, S.R. Walker, C.A. Watson, R.G. West, P.J. Wheatley: WASP-113b and WASP-114b, two inflated hot Jupiters with contrasting densities, *Astron. Astrophys.*, **593**, A113 (2016)

Bentley, M.S., H. Arends, B. Butler, J. Gavira, H. Jeszenszky, T. Mannel, J. Romstedt, R. Schmied, K. Torkar: MIDAS: Lessons learned from the first spaceborne atomic force microscope, *Acta Astronaut.*, **125**, 11-21 (2016)

Bentley, M.S., R. Schmied, T. Mannel, K. Torkar, H. Jeszenszky, J. Romstedt, A.-C. Levasseur-Regourd, I. Weber, E.K. Jessberger, P. Ehrenfreund, C. Koeberl, O. Havnes: Aggregate dust particles at comet 67P/Churyumov-Gerasimenko, *Nature*, **537**, 73-76 (2016)

Bourdin, Ph.-A., S. Bingert, H. Peter: Scaling laws of coronal loops compared to a 3D MHD model of an active region, *Astron. Astrophys.*, **589**, A86 (2016)

Boyarchuk, A.A., B.M. Shustov, I.S. Savanov, M.E. Sachkov, D.V. Bisikalo, L.I. Mashonkina, D.Z. Wiebe, V.I. Shematovich, Yu.A. Shchekinov, T.A. Ryabchikova, N.N. Chugai, P.B. Ivanov, N.V. Voshchinnikov, A.I. Gomez de Castro, S.A. Lamzin, N. Piskunov, T. Ayres, K.G. Strassmeier, S. Jeffrey, S.K. Zwintz, D. Shulyak, J.-C. Gerard, B. Hubert, L. Fossati, H. Lammer, K. Werner, A.G. Zhilkin, P.V. Kaigorodov, S.G. Sichevskii, S. Ustamuich, E.N. Kanev, E.Yu. Kilpio: Scientific Problems Addressed by the Spektr-UV Space Project (World Space Observatory-Ultraviolet), *Astron. Rep.*, **60**, 1-42 (2016)

Breuillard, H., O. Le Contel, A. Retino, A. Chasapis, T. Chust, L. Mirioni, D.B. Graham, F.D. Wilder, I. Cohen, A. Vaivads, Yu.V. Khotyaintsev, P.-A. Lindqvist, G.T. Marklund, J.L. Burch, R.B. Torbert, R.E. Ergun, K.A. Goodrich, J. Macri, J. Needell, M. Chutter, D. Rau, I. Dors, C.T. Russell, W. Magnes, R.J. Strangeway, K.R. Bromund, F. Plaschke, D. Fischer, H.K. Leinweber, B.J. Anderson, G. Le, J.A. Slavin, E.L. Kepko, W. Baumjohann, B. Mauk, S.A. Fuselier, R. Nakamura: Multispacecraft analysis of dipolarization fronts and associated whistler wave emissions using MMS data, *Geophys. Res. Lett.*, **43**, 7279-7286 (2016)

Burch, J.L., R.B. Torbert, T.D. Phan, L.-J. Chen, T.E. Moore, R.E. Ergun, J.P. Eastwood, D.J. Gershman, P.A. Cassak, M.R. Argall, S. Wang, M. Hesse, C.J. Pollock, B.L. Giles, R. Nakamura, B.H. Mauk, S.A. Fuselier, C.T. Russell, R.J. Strangeway, J.F. Drake, M.A. Shay, Yu.V. Khotyaintsev, P.-A. Lindqvist, G. Marklund, F.D. Wilder, D.T. Young, K. Torkar, J. Goldstein, J.C. Dorelli, L.A. Avanov, M. Oka,

D.N. Baker, A.N. Jaynes, K.A. Goodrich, I.J. Cohen, D.L. Turner, J.F. Fennell, J.B. Blake, J. Clemmons, M. Goldman, D. Newman, S.M. Petrinec, K.J. Trattner, B. Lavraud, P.H. Reiff, W. Baumjohann, W. Magnes, M. Steller, W. Lewis, Y. Saito, V. Coffey, M. Chandler: Electron-scale measurements of magnetic reconnection in space, *Science*, **352**, 1189-1199 (2016)

Caporalia, A., C. Bruyninx, R. Fernandes, A. Ganas, A. Kenyeres, M. Lidberg, G. Stangl, H. Steffen, J. Zurutuz: Stress drop at the Kephalonia transform zone estimated from the 2014 seismic sequence, *Tectonophys.*, **666**, 164-172 (2016)

Chai, L., Y. Wei, W. Wan, T. Zhang, Z. Rong, M. Fraenz, E. Dubinin, H. Zhang, J. Zhong, X. Han, S. Barabash: An induced global magnetic field looping around the magnetotail of Venus, *J. Geophys. Res.*, **121**, 688-698 (2016)

Ciceri, S., L. Mancini, J. Southworth, M. Lendl, J. Tregloan-Reed, R. Brahm, G. Chen, G. D'Ago, M. Dominik, R. Figuera Jaimes, P. Galianni, K. Harpsoe, T.C. Hinse, U.G. Jorgensen, D. Juncher, H. Korhonen, C. Liebig, M. Rabus, A.S. Bonomo, K. Bott, Th. Henning, A. Jordan, A. Sozzetti, K.A. Alsubai, J.M. Andersen, D. Bajek, V. Bozza, D.M. Bramich, P. Browne, S. Calchi Novati, Y. Damerdji, C. Diehl, A. Elyiv, E. Giannini, S-H. Gu, M. Hundertmark, N. Kains, M. Penny, A. Popovas, S. Rahvar, G. Scarpetta, R.W. Schmidt, J. Skottfelt, C. Snodgrass, J. Surdej, C. Vilela, X.-B. Wang, O. Wertz: Physical properties of the planetary systems WASP-45 and WASP-46 from simultaneous multiband photometry, *MNRAS*, **456**, 990-1002 (2016)

Cockell, C.S., T. Bush, C. Bryce, S. Direito, M. Fox-Powell, J.P. Harrison, H. Lammer, H. Landenmark, J. Martin-Torres, N. Nicholson, L. Noack, J. O'Malley-James, S.J. Payler, A. Rushby, T. Samuels, P. Schwendner, J. Wadsworth, M.P. Zorzano: Habitability: A review, *Astrobiol.*, **16**, 89-117 (2016)

Cohen, I.J., B.H. Mauk, B.J. Anderson, J.H. Westlake, D.G. Sibeck, B.L. Giles, C.J. Pollock, D.L. Turner, J.F. Fennell, J.B. Blake, J.H. Clemmons, A.N. Jaynes, D.N. Baker, J.V. Craft, H.E. Spence, J.T. Niehof, G.D. Reeves, R.B. Torbert, C.T. Russell, R.J. Strangeway, W. Magnes, K.J. Trattner, S.A. Fuselier, J.L. Burch: Observations of energetic particle escape at the magnetopause: Early results from the MMS Energetic Ion Spectrometer (EIS), *Geophys. Res. Lett.*, **43**, 5960-5968 (2016)

Collinson, G.A., R.A. Frahm, A. Glocer, A.J. Coates, J.M. Grebowsky, S. Barabash, S.D. Domagal-Goldman, A. Fedorov, Y. Futaana, L.K. Gilbert, G. Khazanov, T.A. Nordheim, D. Mitchell, T.E. Moore, W.K. Peterson, J.D. Winningham, T.L. Zhang: The electric wind of Venus: A global and persistent "polar wind"-like ambipolar electric field sufficient for the direct escape of heavy ionospheric ions, *Geophys. Res. Lett.*, **43**, 5926-5934 (2016)

Comisel, H., Y. Nariyuki, Y. Narita, U. Motschmann: On the role of ion-scale whistler waves in space and astrophysical plasma turbulence, *Ann. Geophys.*, **34**, 975-984 (2016)

Consolini, G., F. Giannattasio, E. Yordanova, Z. Vörös, M.F. Marcucci, M. Echim, T. Chang: On the scaling features of magnetic field fluctuations at non-MHD scales in turbulent space plasmas, *J. Phys. Conf. Ser.*, **767**, 012003 (2016)

Delrez, L., A. Santerne, J.-M. Almenara, D.R. Anderson, A. Collier-Cameron, R.F. Diaz, M. Gillon, C. Hellier, E. Jehin, M. Lendl, P.F.L. Maxted, M. Neveu-VanMalle, F. Pepe, D. Pollacco, D. Queloz, D. Segransan, B. Smalley, A.M.S. Smith, A.H.M.J. Triaud, S. Udry, V. Van Grootel, R.G. West: WASP-121 b: a hot Jupiter close to tidal disruption transiting an active F star, *MNRAS*, **458**, 4025-4043 (2016)

Divin, A., V. Semenov, D. Korovinskiy, S. Markidis, J. Deca, V. Olshevsky, G. Lapenta: A new model for the electron pressure nongyrotropy in the outer electron diffusion region, *Geophys. Res. Lett.*, **43**, 10565-10573 (2016)

Dunn, W.R., G. Branduardi-Raymont, R.F. Elsner, M.F. Vogt, L. Lamy, P.G. Ford, A.J. Coates, G.R. Gladstone, C.M. Jackman, J.D. Nichols, I.J. Rae, A. Varsani, T. Kimura, K.C. Hansen, J.M. Jasinski: The impact of an ICME on the Jovian X-ray aurora, *J. Geophys. Res.*, **121**, 2274-2307 (2016)

Eastwood, J.P., T.D. Phan, P.A. Cassak, D.J. Gershman, C. Haggerty, K. Malakit, M.A. Shay, R. Mistry, M. Øieroset, C.T. Russell, J.A. Slavin, M.R. Argall, L.A. Avanov, J.L. Burch, L.J. Chen, J.C. Dorelli, R.E. Ergun, B.L. Giles, Y. Khotyaintsev, B. Lavraud, P.A. Lindqvist, T.E. Moore, R. Nakamura, W. Paterson, C. Pollock, R.J. Strangeway, R.B. Torbert, S. Wang: Ion-scale secondary flux ropes generated by magnetopause reconnection as resolved by MMS, *Geophys. Res. Lett.*, **43**, 4716-4724 (2016)

Edberg, N.J.T., M. Alho, M. Andre, D.J. Andrews, E. Behar, J.L. Burch, C.M. Carr, E. Cupido, I.A.D. Engelhardt, A.I. Eriksson, K.-H. Glassmeier, C. Goetz, R. Goldstein, P. Henri, F.L. Johansson, C. Koenders, K. Mandt, C. Möstl, H. Nilsson, E. Odelstad, I. Richter, C. Simon Wedlund, G. Stenberg Wieser, K. Szego, E. Vigren, M. Volwerk: CME impact on comet 67P/Churyumov-Gerasimenko, *MNRAS*, **462**, S45-S56 (2016)

Ergun, R.E., J.C. Holmes, K.A. Goodrich, F.D. Wilder, J.E. Stawarz, S. Eriksson, D.L. Newman, S.J. Schwartz, M.V. Goldman, A.P. Sturner, D.M. Malaspina, M.E. Usanova, R.B. Torbert, M. Argall, P.-A. Lindqvist, Y. Khotyaintsev, J.L. Burch, R.J. Strangeway, C.T. Russell, C.J. Pollock, B.L. Giles, J.J.C. Dorelli, L. Avanov, M. Hesse, L.J. Chen, B. Lavraud, O. Le Contel, A. Retino, T.D. Phan, J.P. Eastwood, M. Oieroset, J. Drake, M.A. Shay, P.A. Cassak, R. Nakamura, M. Zhou, M. Ashour-Abdalla, M. André: Magnetospheric Multiscale observations of large-amplitude, parallel, electrostatic waves associated with magnetic reconnection at the magnetopause, *Geophys. Res. Lett.*, **43**, 5626-5634 (2016)

Ergun, R.E., K.A. Goodrich, F.D. Wilder, J.C. Holmes, J.E. Stawarz, S. Eriksson, A.P. Sturner, D.M. Malaspina, M.E. Usanova, R.B. Torbert, P.-A. Lindqvist, Y. Khotyaintsev, J.L. Burch, R.J. Strangeway, C.T. Russell, C.J. Pollock, B.L. Giles, M. Hesse, L.J. Chen, G. Lapenta, M.V. Goldman, D.L. Newman, S.J. Schwartz, J.P. Eastwood, T.D. Phan, F.S. Mozer, J. Drake, M.A. Shay, P.A. Cassak, R. Nakamura, G. Marklund: Magnetospheric Multiscale Satellites observations of parallel electric fields associated with magnetic reconnection, *Phys. Rev. Lett.*, **116**, 235102 (2016)

Erickson, P.J., H. Matsui, J.C. Foster, R.B. Torbert, R.E. Ergun, Yu.V. Khotyaintsev, P.-A. Lindqvist, M.R. Argall, C.J. Farrugia, K.W. Paulson, R.J. Strangeway, W. Magnes: Multipoint MMS observations of fine-scale SAPS structure in the inner magnetosphere, *Geophys. Res. Lett.*, **43**, 7294-7300 (2016)

Eriksson, E., A. Vaivads, D.B. Graham, Yu.V. Khotyaintsev, E. Yordanova, H. Hietala, M. André, L.A. Avanov, J.C. Dorelli, D.J. Gershman, B.L. Giles, B. Lavraud, W.R. Paterson, C.J. Pollock, Y. Saito, W. Magnes, C. Russell, R. Torbert, R. Ergun, P.-A. Lindqvist, J. Burch: Strong current sheet at a magnetosheath jet: Kinetic structure and electron acceleration, *J. Geophys. Res.*, **121**, 9608-9618 (2016)

Eriksson, S., B. Lavraud, F.D. Wilder, J.E. Stawarz, B.L. Giles, J.L. Burch, W. Baumjohann, R.E. Ergun, P.-A. Lindqvist, W. Magnes, C.J. Pollock, C.T. Russell, Y. Saito, R.J. Strangeway, R.B. Torbert, D.J. Gershman, Yu.V. Khotyaintsev, J.C. Dorelli, S.J. Schwartz, L. Avanov, E. Grimes, Y. Vernisse, A.P. Sturner, T.D. Phan, G.T. Marklund, T.E. Moore, W.R. Paterson, K.A. Goodrich: Magnetospheric Multiscale observations of magnetic reconnection associated with Kelvin-Helmholtz waves, *Geophys. Res. Lett.*, **43**, 5606-5615 (2016)

Eriksson, S., F.D. Wilder, R.E. Ergun, S.J. Schwartz, P.A. Cassak, J.L. Burch, L.-J. Chen, R.B. Torbert, T.D. Phan, B. Lavraud, K.A. Goodrich, J.C. Holmes, J.E. Stawarz, A.P. Sturner, D.M. Malaspina, M.E. Usanova, K.J. Trattner, R.J. Strangeway, C.T. Russell, C.J. Pollock, B.L. Giles, M. Hesse, P.-A. Lindqvist, J.F. Drake, M.A. Shay, R. Nakamura, G.T. Marklund: Magnetospheric Multiscale observations of the electron diffusion region of large guide field magnetic reconnection, *Phys. Rev. Lett.*, **117**, 015001 (2016)

Erkaev, N.V., H. Lammer, P. Odert, K.G. Kislyakova, C.P. Johnstone, M. Güdel, M.L. Khodachenko: EUV-driven mass-loss of protoplanetary cores with hydrogen-dominated atmospheres: the influences of ionization and orbital distance, *MNRAS*, **460**, 1300-1309 (2016)

Fischer, D., W. Magnes, C. Hagen, I. Dors, M.W. Chutter, J. Needell, R.B. Torbert, O. Le Contel, R.J. Strangeway, G. Kubin, A. Valavanoglou, F. Plaschke, R. Nakamura, L. Mirioni, C.T. Russell, H.K. Leinweber, K.R. Bromund, G. Le, L. Kepko, B.J. Anderson, J.A. Slavin, W. Baumjohann: Optimized merging of search coil and fluxgate data for MMS, *Geosci. Instrum. Method. Data Syst.*, **5**, 521-530 (2016)

Fossati, L., F.R.N. Schneider, N. Castro, N. Langer, S. Simón-Díaz, A. Müller, A. de Koter, T. Morel, V. Petit, H. Sana, G.A. Wade: Evidence of magnetic field decay in massive main-sequence stars, *Astron. Astrophys.*, **592**, A84 (2016)

Fray, N., A. Bardyn, H. Cottin, K. Altwegg, D. Baklouti, C. Briois, L. Colangeli, C. Engrand, H. Fischer, A. Glasmachers, E. Grün, G. Haerendel, H. Henkel, H. Höfner, K. Hornung, E.K. Jessberger, A. Koch, H. Krüger, Y. Langevin, H. Lehto, K. Lehto, L. Le Roy, S. Merouane, P. Modica, F.-R. Orthous-Daunay, J. Paquette, F. Raulin, J. Rynö, R. Schulz, J. Silén, S. Siljeström, W. Steiger, O. Stenzel, T. Stephan, L. Thirkell, R. Thomas, K. Torkar, K. Varmuza, K.-P. Wanczek, B. Zaprudin, J. Kissel, M. Hilchenbach: High-molecular-weight organic matter in the particles of comet 67P/Churyumov-Gerasimenko, *Nature*, **538**, 72-74 (2016)

Fuselier, S.A., J.L. Burch, P.A. Cassak, J. Goldstein, R.G. Gomez, K. Goodrich, W.S. Lewis, D. Malaspina, J. Mukherjee, R. Nakamura, S.M. Petrinec, C.T. Russell, R.J. Strangeway, R.B. Torbert, K.J. Trattner, P. Valek: Magnetospheric ion influence on magnetic reconnection at the duskside magnetopause, *Geophys. Res. Lett.*, **43**, 1435-1442 (2016)

Galopeau, P.H.M., M.Y. Boudjada: An oblate beaming cone for Io-controlled Jovian decameter emission, *J. Geophys. Res.*, **121**, 3120-3138 (2016)

Goetz, C., C. Koenders, I. Richter, K. Altwegg, J. Burch, C. Carr, E. Cupido, A. Eriksson, C. Güttler, P. Henri, P. Mokashi, Z. Nemeth, H. Nilsson, M. Rubin, H. Sierks, B. Tsurutani, C. Vallat, M. Volwerk, K.-H. Glassmeier: First detection of a diamagnetic cavity at comet 67P/Churyumov-Gerasimenko, *Astron. Astrophys.*, **588**, A24 (2016)

Goetz, C., C. Koenders, K.C. Hansen, J. Burch, C. Carr, A. Eriksson, D. Frühauff, C. Güttler, P. Henri, H. Nilsson, I. Richter, M. Rubin, H. Sierks, B. Tsurutani, M. Volwerk, K.H. Glassmeier: Structure and evolution of the diamagnetic cavity at comet 67P/Churyumov-Gerasimenko, *MNRAS*, **463**, S459-S467 (2016)

Goodrich, K.A., R.E. Ergun, F.D. Wilder, J. Burch, R. Torbert, Yu. Khotyaintsev, P.-A. Lindqvist, C.T. Russell, R.J. Strangeway, W. Magnes, D. Gershman, B. Giles, R. Nakamura, J. Stawarz, J. Holmes, A. Sturner, D.M. Malaspina: MMS Multipoint electric field observations of small-scale magnetic holes, *Geophys. Res. Lett.*, **43**, 5953-5959 (2016)

Graham, D.B., Yu.V. Khotyaintsev, C. Norgren, A. Vaivads, M. André, P.-A. Lindqvist, G.T. Marklund, R.E. Ergun, W.R. Paterson, D.J. Gershman, B.L. Giles, C.J. Pollock, J.C. Dorelli, L.A. Avanov, B. Lavraud, Y. Saito, W. Magnes, C.T. Russell, R.J. Strangeway, R.B. Torbert, J.L. Burch: Electron currents and heating in the ion diffusion region of asymmetric reconnection, *Geophys. Res. Lett.*, **43**, 4691-4700 (2016)

Grassitelli, L., A.-N. Chene, D. Sanyal, N. Langer, N. St-Louis, J.M. Bestenlehner, L. Fossati: Diagnostics of the unstable envelopes of Wolf-Rayet stars, *Astron. Astrophys.*, **590**, A12 (2016)

Grassitelli, L., L. Fossati, N. Langer, S. Simón.-Díaz, N. Castro, D. Sanyal: Metallicity dependence of turbulent pressure and macroturbulence in stellar envelopes, *Astron. Astrophys.*, **593**, A14 (2016)

Grün, E., J. Agarwal, N. Altobelli, K. Altwegg, M.S. Bentley, N. Biver, V. Della Corte, N. Edberg, P.D. Feldman, M. Galand, B. Geiger, C. Götz, B. Grieger, C. Güttler, P. Henri, M. Hofstadter, M. Horanyi, E. Jehin, H. Krüger, S. Lee, T. Mannel, E. Morales, O. Mousis, M. Müller, C. Opitom, A. Rotundi, R. Schmied, F. Schmidt, H. Sierks, C. Snodgrass, R.H. Soja, M. Sommer, R. Srama, C.-Y. Tzou, J.-B. Vincent, P. Yanamandra-Fisher, M.F. A'Hearn, A.I. Erikson, C. Barbieri, M.A. Barucci, J.-L. Bertaux, I. Bertini, J. Burch, L. Colangeli, G. Cremonese, V. Da Deppo, B. Davidsson, S. Debei, M. De Cecco, J. Deller, L.M. Feaga, M. Ferrari, S. Fornasier, M. Fulle, A. Gicquel, M. Gillon, S.F. Green, O.

Groussin, P.J. Gutiérrez, M. Hofmann, S.F. Hviid, W.-H. Ip, S. Ivanovski, L. Jorda, H.U. Keller, M.M. Knight, J. Knollenberg, D. Koschny, J.-R. Kramm, E. Kührt, M. Küppers, P.L. Lamy, L.M. Lara, M. Lazzarin, J.J. Lòpez-Moreno, J. Manfroid, E. Mazzotta Epifani, F. Marzari, G. Naletto, N. Oklay, P. Palumbo, J.Wm. Parker, H. Rickman, R. Rodrigo, J. Rodrìguez, E. Schindhelm, X. Shi, R. Sordini, A.J. Steffl, S.A. Stern, N. Thomas, C. Tubiana, H.A. Weaver, P. Weissman, V.V. Zakharov, M.G.G.T. Taylor: The 2016 Feb 19 outburst of comet 67P/CG: An ESA Rosetta multi-instrument study, *MNRAS*, **462**, S220-S234 (2016)

Gurgenashvili, E., T.V. Zaqarashvili, V. Kukhianidze, R. Oliver, J.L. Ballester, G. Ramishvili, B. Shergelashvili, A. Hanslmeier, S. Poedts: Rieger-type periodicity during solar cycles 14-24: Estimation of dynamo magnetic field strength in the solar interior, *Astrophys. J.*, **826**, 55 (2016)

Hamelin, M., A. Lethuillier, A. Le Gall, R. Grard, C. Beghin, K. Schwingenschuh, I. Jernej, J.-J. Lopez-Moreno, V. Brown, R.D. Lorenz, F. Ferri, V. Ciarletti: The electrical properties of Titan's surface at the Huygens landing site measured with the PWA-HASI Mutual Impedance Probe. New approach and new findings, *Icarus*, **270**, 272-290 (2016)

Hay, K.L., A. Collier-Cameron, A.P. Doyle, G. Hebrard, I. Skillen, D.R. Anderson, S.C.C. Barros, D.J.A. Brown, F. Bouchy, R. Busuttil, P. Delorme, L. Delrez, O. Demangeon, R.F. Diaz, M. Gillon, Y. Gomez Maqueo Chew, E. Gonzalez, C. Hellier, S. Holmes, J.F. Jarvis, E. Jehin, Y.C. Joshi, U. Kolb, M. Lendl, P.F.L. Maxted, J. McCormac, G.R.M. Miller, A. Mortier, E. Palle, D. Pollacco, J. Prieto-Arranz, D. Queloz, D. Segransan, E.K. Simpson, B. Smalley, J. Southworth, A.H.M.J. Triaud, O.D. Turner, S. Udry, M. Vanhuysse, R.G. West, P.A. Wilson: WASP-92b,WASP-93b and WASP-118b: Three new transiting close-in giant planets, *MNRAS*, **463**, 3276-3289 (2016)

He, M., J. Vogt, T.-L. Zhang, Z. Rong: EMVIM: An empirical model for the magnetic field configuration near Venus, *J. Geophys. Res.*, **121**, 3362-3380 (2016)

Hilchenbach, M., J. Kissel, Y. Langevin, C. Briois, H. von Hoerner, A. Koch, R. Schulz, J. Silén, K. Altwegg, L. Colangeli, H. Cottin, C. Engrand, H. Fischer, A. Glasmachers, E. Grün, G. Haerendel, H. Henkel, H. Höfner, K. Hornung, E.K. Jessberger, H. Lehto, K. Lehto, F. Raulin, L. Le Roy, J. Rynö, W. Steiger, T. Stephan, L. Thirkell, R. Thomas, K. Torkar, K. Varmuza, K.-P. Wanczek, N. Altobelli, D. Baklouti, A. Bardyn, N. Fray, H. Krüger, N. Ligier, Z. Lin, P. Martin, S. Merouane, F. R. Orthous-Daunay, J. Paquette, C. Revillet, S. Siljeström, O. Stenzel, B. Zaprudin: Comet 67P/Churyumov-Gerasimenko: Close-up on dust particle fragments, *Astrophys. J. Lett.*, **816**, L32 (2016)

Hu, H., Y.D. Liu, R. Wang, C. Möstl, Z. Yang: Sun-to-Earth characteristics of the 2012 July 12 Coronal Mass Ejection and associatedgeo-effectiveness, *Astrophys. J.*, **829**, 97 (2016)

Huang, S.Y., F. Sahraoui, A. Retino, O. Le Contel, Z.G. Yuan, A. Chasapis, N. Aunai, H. Breuillard, X.H. Deng, M. Zhou, H.S. Fu, Y. Pang, D.D. Wang, R.B. Torbert, K.A. Goodrich, R.E. Ergun, Y.V. Khotyaintsev, P.-A. Lindqvist, C.T. Russell, R.J. Strangeway, W. Magnes, K. Bromund, H. Leinweber, F. Plaschke, B.J. Anderson, C.J. Pollock, B.L. Giles, T.E. Moore, J.L. Burch: MMS observations of ion-scale magnetic island in the magnetosheath turbulent plasma, *Geophys. Res. Lett.*, **43**, 7850-7858 (2016)

Imai, M., A. Lecacheux, T.E. Clarke, C.A. Higgins, M. Panchenko, J. Dowell, K. Imai, A.I. Brazhenko, A.V. Frantsuzenko, A.A. Konovalenko: The beaming structures of Jupiter's decametric common S-bursts observed from the LWA1, NDA, and URAN2 radio telescopes, *Astrophys. J.*, **826**, 176 (2016)

Johlander, A., S.J. Schwartz, A. Vaivads, Yu.V. Khotyaintsev, I. Gingell, I.B. Peng, S. Markidis, P.-A. Lindqvist, R.E. Ergun, G.T. Marklund, F. Plaschke, W. Magnes, R.J. Strangeway, C.T. Russell, H. Wei, R.B. Torbert, W.R. Paterson, D.J. Gershman, J.C. Dorelli, L.A. Avanov, B. Lavraud, Y. Saito, B.L. Giles, C.J. Pollock, J.L. Burch: Rippled quasiperpendicular shock observed by the Magnetospheric Multiscale Spacecraft, *Phys. Rev. Lett.*, **117**, 165101 (2016)

Khotyaintsev, Yu.V., D.B. Graham, C. Norgren, E. Eriksson, W. Li, A. Johlander, A. Vaivads, M. André, P.L. Pritchett, A. Retinò, T.D. Phan, R.E. Ergun, K. Goodrich, P.-A. Lindqvist, G.T. Marklund, O. Le Contel, F. Plaschke, W. Magnes, R.J. Strangeway, C.T. Russell, H. Vaith, M.R. Argall, C.A. Kletzing, R. Nakamura, R.B. Torbert, W.R. Paterson, D.J. Gershman, J.C. Dorelli, L.A. Avanov, B. Lavraud, Y. Saito, B.L. Giles, C.J. Pollock, D.L. Turner, J.D. Blake, J.F. Fennell, A. Jaynes, B.H. Mauk, J.L. Burch: Electron jet of asymmetric reconnection, *Geophys. Res. Lett.*, **43**, 5571-5580 (2016)

Kislyakova, K.G., E. Pilat-Lohinger, B. Funk, H. Lammer, L. Fossati, S. Eggl, R. Schwarz, M.Y. Boudjada, N.V. Erkaev: On the ultraviolet anomalies of the WASP-12 and HD 189733 systems: Trojan satellites as a plasma source, *MNRAS*, **461**, 988-999 (2016)

Kollmann, P., P.C. Brandt, G. Collinson, Z.J. Rong, Y. Futaana, T.L. Zhang: Properties of planetward ion flows in Venus' magnetotail, *Icarus*, **274**, 73-82 (2016)

Konovalenko, A., L. Sodin, V. Zakharenko, P. Zarka, O. Ulyanov, M. Sidorchuk, S. Stepkin, P. Tokarsky, V. Melnik, N. Kalinichenko, A. Stanislavsky, V. Koliadin, V. Shepelev, V. Dorovskyy, V. Ryabov, A. Koval, I. Bubnov, S. Yerin, A. Gridin, V. Kulishenko, A. Reznichenko, V. Bortsov, V. Lisachenko, A. Reznik, G. Kvasov, D. Mukha, G. Litvinenko, A. Khristenko, V.V. Shevchenko, V.A. Shevchenko, A. Belov, E. Rudavin, I. Vasylieva, A. Miroshnichenko, N. Vasilenko, M. Olyak, K. Mylostna, A. Skoryk, A. Shevtsova, M. Plakhov, I. Kravtsov, Y. Volvach, O. Lytvinenko, N. Shevchuk, I. Zhouk, V. Bovkun, A. Antonov, D. Vavriv, V. Vinogradov, R. Kozhin, A. Kravtsov, E. Bulakh, A. Kuzin, A. Vasilyev, A. Brazhenko, R. Vashchishin, O. Pylaev, V. Koshovyy, A. Lozinsky, O. Ivantyshin, H.O. Rucker, M. Panchenko, G. Fischer, A. Lecacheux, L. Denis, A. Coffre, J.-M. Grießmeier, M. Tagger, J. Girard, D. Charrier, C. Briand, G. Mann: The modern radio astronomy network in Ukraine: UTR-2, URAN and GURT, *Exp. Astron.*, **42**, 11-48 (2016)

Korovinskiy, D.B., I.B. Ivanov, V.S. Semenov, N.V. Erkaev, S.A. Kiehas: Numerical linearized MHD model of flapping

oscillations, *Phys. Plasmas*, **23**, 062905 (2016)

Korovinskiy, D.B., S.A. Kiehas: Generalized double-gradient model of flapping oscillations: Oblique waves, *Phys. Plasmas*, **23**, 092902 (2016)

Kubicka, M., C. Möstl, T. Amerstorfer, P.D. Boakes, L. Feng, J.P. Eastwood, O. Törmänen: Prediction of geomagnetic storm strength from inner heliospheric in situ observations, *Astrophys. J.*, **833**, 255 (2016)

Kucharski, D., G. Kirchner, T. Otsubo, H.-C. Lim, J. Bennett, F. Koidl, Y.-R. Kim, J.-Y. Hwang: Confirmation of gravitationally induced attitude drift of spinning satellite Ajisai with Graz high repetition rate SLR data, *Adv. Space Res.*, **57**, 983-990 (2016)

Kuridze, D., T.V. Zaqarashvili, V. Henriques, M. Mathioudakis, F.P. Keenan, A. Hanslmeier: Kelvin–Helmholtz instability in solar chromospheric jets: Theory and observation, *Astrophys. J.*, **830**, 133 (2016)

Kuznetsov, V.D., L.M. Zelenyi, I.V. Zimovets, K. Anufreychik, V. Bezrukikh, I.V. Chulkov, A.A. Konovalov, G.A. Kotova, R.A. Kovrazhkin, D. Moiseenko, A.A. Petrukovich, A. Remizov, A. Shestakov, A. Skalsky, O.L. Vaisberg, M.I. Verigin, R.N. Zhuravlev, S.E. Andreevskyi, V.S. Dokukin, V.V. Fomichev, N.I. Lebedev, V.N. Obridko, V.P. Polyanskyi, V.A. Styazhkin, E.A. Rudenchik, V.M. Sinelnikov, Yu.D. Zhugzhda, A.P. Ryzhenko, A.V. Ivanov, A.V. Simonov, V.S. Dobrovolskyi, M.S. Konstantinov, S.V. Kuzin, S.A. Bogachev, A.A. Kholodilov, A.S. Kirichenko, E.N. Lavrentiev, A.A. Pertsov, A.A. Reva, S.V. Shestov, A.S. Ulyanov, M.I. Panasyuk, A.F. Iyudin, S.I. Svertilov, V.V. Bogomolov, V.I. Galkin, B.V. Marjin, O.V. Morozov, V.I. Osedlo, I.A. Rubinshtein, B.Ya. Scherbovsky, V.I. Tulupov, Yu.D. Kotov, V.N. Yurov, A.S. Glyanenko, A.V. Kochemasov, E.E. Lupar, I.V. Rubtsov, Yu.A. Trofimov, V.G. Tyshkevich, S.E. Ulin, A.S. Novikov, V.V. Dmitrenko, V.M. Grachev, V.N. Stekhanov, K.F. Vlasik, Z.M. Uteshev, I.V. Chernysheva, A.E. Shustov, D.V. Petrenko, R.L. Aptekar, V.A. Dergachev, S.V. Golenetskii, K.S. Gribovskyi, D.D. Frederiks, E.M. Kruglov, V.P. Lazutkov, V.V. Levedev, F.P. Oleinik, V.D. Palshin, A.I. Repin, M.I. Savchenko, D.V. Skorodumov, D.S. Svinkin, A.S. Tsvetkova, M.V. Ulanov, I.E. Kozhevatov, J. Sylwester, M. Siarkowski, J. Bąkala, Ż. Szaforz, M. Kowaliński, O.V. Dudnik, B. Lavraud, F. Hruška, I. Kolmasova, O. Santolik, J. Šimunek, V. Truhlík, H.-U. Auster, M. Hilchenbach, Yu. Venedictov, G. Berghofer: The Sun and Heliosphere Explorer - The Interhelioprobe Mission, *Geomagn. Aeron.*, **56**, 781-841 (2016)

Lammer, H., N.V. Erkaev, L. Fossati, I. Juvan, P. Odert, P.E. Cubillos, E. Guenther, K.G. Kislyakova, C.P. Johnstone, T. Lüftinger, M. Güdel: Identifying the 'true' radius of the hot sub-Neptune CoRoT-24b by mass-loss modelling, *MNRAS*, **461**, L62-L66 (2016)

Lavraud, B., Y.C. Zhang, Y. Vernisse, D.J. Gershman, J. Dorelli, P.A. Cassak, J. Dargent, C. Pollock, B. Giles, N. Aunai, M. Argall, L. Avanov, A. Barrie, J. Burch, M. Chandler, L.-J. Chen, G. Clark, I. Cohen, V. Coffey, J.P. Eastwood, J. Egedal, S. Eriksson, R. Ergun, C.J. Farrugia, S.A. Fuselier, V. Genot, D. Graham, E. Grigorenko, H. Hasegawa, C. Jacquey, I. Kacem, Y. Khotyaintsev, E. MacDonald, W. Magnes, A. Marchaudon, B. Mauk, T.E. Moore, T. Mukai, R. Nakamura, W. Paterson, E. Penou, T.D. Phan, A. Rager, A. Retino, Z.J. Rong, C.T. Russell, Y. Saito, J.-A. Sauvaud, S.J. Schwartz, C. Shen, S. Smith, R. Strangeway, S. Toledo-Redondo, R. Torbert, D.L. Turner, S. Wang, S. Yokota: Currents and associated electron scattering and bouncing near the diffusion region at Earth's magnetopause, *Geophys. Res. Lett.*, **43**, 3042-3050 (2016)

Le Contel, O., A. Retinò, H. Breuillard, L. Mirioni, P. Robert, A. Chasapis, B. Lavraud, T. Chust, L. Rezeau, F.D. Wilder, D.B. Graham, M.R. Argall, D.J. Gershman, P.-A. Lindqvist, Y.V. Khotyaintsev, G. Marklund, R.E. Ergun, K.A. Goodrich, J.L. Burch, R.B. Torbert, J. Needell, M. Chutter, D. Rau, I. Dors, C.T. Russell, W. Magnes, R.J. Strangeway, K.R. Bromund, H.K. Leinweber, F. Plaschke, D. Fischer, B.J. Anderson, G. Le, T.E. Moore, C.J. Pollock, B.L. Giles, J.C. Dorelli, L. Avanov, Y. Saito: Whistler mode waves and Hall fields detected by MMS during a dayside magnetopause crossing, *Geophys. Res. Lett.*, **43**, 5943-5952 (2016)

Le Contel, O., P. Leroy, A. Roux, C. Coillot, D. Alison, A. Bouabdellah, L. Mirioni, L. Meslier, A. Galic, M.C. Vassal, R.B. Torbert, J. Needell, D. Rau, I. Dors, R.E. Ergun, J. Westfall, D. Summers, J. Wallace, W. Magnes, A. Valavanoglou, G. Olsson, M. Chutter, J. Macri, S. Myers, S. Turco, J. Nolin, D. Bodet, K. Rowe, M. Tanguy, B. de la Porte: The search-coil magnetometer for MMS, *Space Sci. Rev.*, **199**, 257-282 (2016)

Le, G., H. Lühr, B.J. Anderson, R.J. Strangeway, C.T. Russell, H. Singer, J.A. Slavin, Y. Zhang, T. Huang, K. Bromund, P.J. Chi, G. Lu, D. Fischer, E.L. Kepko, H.K. Leinweber, W. Magnes, R. Nakamura, F. Plaschke, J. Park, J. Rauberg, C. Stolle, R.B. Torbert: Magnetopause erosion during the 17 March 2015 magnetic storm: Combined field-aligned currents, auroral oval, and magnetopause observations, *Geophys. Res. Lett.*, **43**, 2396-2404 (2016)

Leitzinger, M., P. Odert, T.V. Zaqarashvili, R. Greimel, A. Hanslmeier, H. Lammer: Indications of stellar prominence oscillations on fast rotating stars: The cases of HK Aqr and PZ Tel, *MNRAS*, **463**, 965-979 (2016)

Lendl, M., L. Delrez, M. Gillon, N. Madhusudhan, E. Jehin, D. Queloz, D.R. Anderson, B.-O. Demory, C. Hellier: FORS2 observes a multi-epoch transmission spectrum of the hot Saturn-mass exoplanet WASP-49b, *Astron. Astrophys.*, **587**, A67 (2016)

Lhotka, C., A. Celletti, C. Gales: Poynting-Robertson drag and solar wind in the space debris problem, *MNRAS*, **460**, 802-815 (2016)

Lhotka, C., P. Bourdin, Y. Narita: Charged dust grain dynamics subject to solar wind, Poynting-Robertson drag, and the interplanetary magnetic field, *Astrophys. J.*, **828**, 10 (2016)

Lhotka, Ch., S. Reimond, J. Souchay, O. Baur: Gravity field and solar component of the precession rate and nutation coefficients of Comet 67P/Churyumov-Gerasimenko, *MNRAS*, **455**, 3588-3596 (2016)

Li, W., M. André, Yu.V. Khotyaintsev, A. Vaivads, D.B. Graham, S. Toledo-Redondo, C. Norgren, P. Henri, C. Wang,

B.B. Tang, B. Lavraud, Y. Vernisse, D.L. Turner, J. Burch, R. Torbert, W. Magnes, C.T. Russell, J.B. Blake, B. Mauk, B. Giles, C. Pollock, J. Fennell, A. Jaynes, L.A. Avanov, J.C. Dorelli, D.J. Gershman, W.R. Paterson, Y. Saito, R.J. Strangeway: Kinetic evidence of magnetic reconnection due to Kelvin-Helmholtz waves, *Geophys. Res. Lett.*, **43**, 5635-5643 (2016)

Lichtenegger, H.I.M., K.G. Kislyakova, P. Odert, N.V. Erkaev, H. Lammer, H. Gröller, C.P. Johnstone, L. Elkins-Tanton, L. Tu, M. Güdel, M. Holmström: Solar XUV and ENA-driven water loss from early Venus' steam atmosphere, *J. Geophys. Res.*, **121**, 4718-4732 (2016)

Litvinenko, G.V., V.E. Shaposhnikov, A.A. Konovalenko, V.V. Zakharenko, M. Panchenko, V.V. Dorovsky, A.I. Brazhenko, H.O. Rucker, V.V. Vinogradov, V.N. Melnik: Quasi-similar decameter emission features appearing in the solar and jovian dynamic spectra, *Icarus*, **272**, 80-87 (2016)

Maier, A., O. Baur: Orbit determination and gravity field recovery from Doppler tracking data to the Lunar Reconnaissance Orbiter, *Planet. Space Sci.*, **122**, 94-100 (2016)

Mandt, K.E., A. Eriksson, N.J.T. Edberg, C. Koenders, T. Broiles, S.A. Fuselier, P. Henri, Z. Nemeth, M. Alho, N. Biver, A. Beth, J. Burch, C. Carr, K. Chae, A.J. Coates, E. Cupido, M. Galand, K.-H. Glassmeier, C. Goetz, R. Goldstein, K.C. Hansen, J. Haiducek, E. Kallio, J.-P. Lebreton, A. Luspay-Kuti, P. Mokashi, H. Nilsson, A. Opitz, I. Richter, M. Samara, K. Szego, C.-Y. Tzou, M. Volwerk, C. Simon Wedlund, G. Stenberg Wieser: RPC observation of the development and evolution of plasma interaction boundaries at 67P/Churyumov-Gerasimenko, *MNRAS*, **462**, S9-S22 (2016)

Mannel, T., M.S. Bentley, R. Schmied, H. Jeszenszky, A.C. Levasseur-Regourd, J. Romstedt, K. Torkar: Fractal cometary dust - a window into the early Solar system, MNRAS, 462, S304-S311 (2016)

Marsch, E., Y. Narita: Fundamental Fermion interactions via vector bosons of unified SU(2)\otimesSU(4) gauge fields, *Front. Physics*, **4**, 5 (2016)

Massol, H., K. Hamano, F. Tian, M. Ikoma, Y. Abe, E. Chassefière, A. Davaille, H. Genda, M. Güdel, Y. Hori, F. Leblanc, E. Marcq, P. Sarda, V.I. Shematovich, A. Stök, H. Lammer: Formation and evolution of protoatmospheres, *Space Sci. Rev.*, **205**, 153-211 (2016)

Matsui, H., P.J. Erickson, J.C. Foster, R.B. Torbert, M.R. Argall, B.J. Anderson, J.B. Blake, I.J. Cohen, R.E. Ergun, C.J. Farrugia, Yu.V. Khotyaintsev, H. Korth, P.-A. Lindqvist, W. Magnes, G.T. Marklund, B.H. Mauk, K.W. Paulson, C.T. Russell, R.J. Strangeway, D.L. Turner: Dipolarization in the inner magnetosphere during a geomagnetic storm on 7 October 2015, *Geophys. Res. Lett.*, **43**, 9397-9405 (2016)

Maxted, P.F.L., D.R. Anderson, A. Collier Cameron, L. Delrez, M. Gillon, C. Hellier, E. Jehin, M. Lendl, M. Neveu-VanMalle, F. Pepe, D. Pollacco, D. Queloz, D. Ségransan, B. Smalley, A.M.S. Smith, J. Southworth, A.H.M.J. Triaud, S. Udry, T. Wagg, R.G. West: Five transiting hot Jupiters discovered using WASP-South, Euler, and TRAPPIST: WASP-119 b, WASP-124 b, WASP-126 b, WASP-129 b, and WASP-133 b, *Astron. Astrophys.*, **591**, A55 (2016)

Močnik, T., D.R. Anderson, D.J.A. Brown, A. Collier Cameron, L. Delrez, M. Gillon, C. Hellier, E. Jehin, M. Lendl, P.F.L. Maxted, M. Neveu-VanMalle, F. Pepe, D. Pollacco, D. Queloz, D. Ségransan, B. Smalley, J. Southworth, A.H.M.J. Triaud, S. Udry, R.G. West: WASP-157b, a transiting Hot Jupiter observed with K2, *Publ. Astron. Soc. Pac.*, **128**, 124403 (2016)

Mousis, O., D.H. Atkinson, T. Spilker, E. Venkatapathy, J. Poncy, R. Frampton, A. Coustenis, K. Reh, J.-P. Lebreton, L.N. Fletcher, R. Hueso, M.J. Amato, A. Colaprete, F. Ferri, D. Stam, P. Wurz, S. Atreya, S. Aslam, D.J. Banfield, S. Calcutt, G. Fischer, A. Holland, C. Keller, E. Kessler, M. Leese, P. Levacher, A. Morse, O. Muñoz, J.-B. Renard, S. Sheridan, F.-X. Schmider, F. Snik, J.H. Waite, M. Bird, T. Cavalié, M. Deleuil, J. Fortney, D. Gautier, T. Guillot, J.I. Lunine, B. Marty, C. Nixon, G.S. Orton, A. Sánchez-Lavega: The Hera Saturn entry probe mission, *Planet. Space Sci.*, **130**, 80-130 (2016)

Murawski, K., P. Chmielewski, T.V. Zaqarashvili, E. Khomenko: Numerical simulations of magnetic Kelvin-Helmholtz instability at a twisted solar flux tube, *MNRAS*, **459**, 2566-2572 (2016)

Murphy, S.J., L. Fossati, T.R. Bedding, H. Saio, D.W. Kurtz, L. Grassitelli, E.S. Wang: Near-uniform internal rotation of the main-sequence γ Doradus pulsator KIC 7661054, *MNRAS*, **459**, 1201-1212 (2016)

Nagai, T., N. Kitamura, H. Hasegawa, I. Shinohara, S. Yokota, Y. Saito, R. Nakamura, B.L. Giles, C. Pollock, T.E. Moore, J.C. Dorelli, D.J. Gershman, W.R. Paterson, L.A. Avanov, M.O. Chandler, V. Coffey, J.A. Sauvaud, B. Lavraud, C.T. Russell, R.J. Strangeway, M. Oka, K.J. Genestreti, J.L. Burch: Thick escaping magnetospheric ion layer in magnetopause reconnection with MMS observations, *Geophys. Res. Lett.*, **43**, 6028-6035 (2016)

Nakamura, R., V.A. Sergeev, W. Baumjohann, F. Plaschke, W. Magnes, D. Fischer, A. Varsani, D. Schmid, T.K.M. Nakamura, C.T. Russell, R.J. Strangeway, H.K. Leinweber, G. Le, K.R. Bromund, C.J. Pollock, B.L. Giles, J.C. Dorelli, D.J. Gershman, W. Paterson, L.A. Avanov, S.A. Fuselier, K. Genestreti, J.L. Burch, R.B. Torbert, M. Chutter, M.R. Argall, B.J. Anderson, P.-A. Lindqvist, G.T. Marklund, Y.V. Khotyaintsev, B.H. Mauk, I.J. Cohen, D.N. Baker, A.N. Jaynes, R.E. Ergun, H.J. Singer, J.A. Slavin, E.L. Kepko, T.E. Moore, B. Lavraud, V. Coffey, Y. Saito: Transient, small-scale field-aligned currents in the plasma sheet boundary layer during storm time substorms, *Geophys. Res. Lett.*, **43**, 4841-4849 (2016)

Nakamura, T.K.M., R. Nakamura, H. Hasegawa: Spatial dimensions of the electron diffusion region in anti-parallel magnetic reconnection, *Ann. Geophys.*, **34**, 357-367 (2016)

Nakamura, T.K.M., R. Nakamura, W. Baumjohann, T. Umeda, I. Shinohara: Three-dimensional development of front region of plasma jets generated by magnetic reconnection, *Geophys. Res. Lett.*, **43**, 8356-8364 (2016)

Nakamura, T.K.M., R. Nakamura, Y. Narita, W. Baumjo-

hann, W. Daughton: Multi-scale structures of turbulent magnetic reconnection, *Phys. Plasmas*, **23**, 052116 (2016)

Narita, Y.: Cluster observation of magnetohydrodynamic turbulence in the plasma sheet boundary layer, *Earth Planets Space*, **68**, 69 (2016)

Narita, Y.: Kinetic extension of critical balance to whistler turbulence, *Astrophys. J.*, **831**, 83 (2016)

Narita, Y., E. Marsch, C. Perschke, K.-H. Glassmeier, U. Motschmann, H. Comisel: Corrigendum to "Wave-particle resonance condition test for ion-kinetic waves in the solar wind" published in Ann. Geophys., 34, 393-398, 2016, *Ann. Geophys.*, **34**, 2 p. (2016)

Narita, Y., E. Marsch, C. Perschke, K.-H. Glassmeier, U. Motschmann, H. Comisel: Wave-particle resonance condition test for ion-kinetic waves in the solar wind, *Ann. Geophys.*, **34**, 393-398 (2016)

Narita, Y., F. Plaschke, R. Nakamura, W. Baumjohann, W. Magnes, D. Fischer, Z. Vörös, R.B. Torbert, C.T. Russell, R.J. Strangeway, H.K. Leinweber, K.R. Bromund, B.J. Anderson, G. Le, M. Chutter, J.A. Slavin, E.L. Kepko, J.L. Burch, U. Motschmann, I. Richter, K.-H. Glassmeier: Wave telescope technique for MMS magnetometer, *Geophys. Res. Lett.*, **43**, 4774-4780 (2016)

Narita, Y., H. Comisel, U. Motschmann: Critical pitch angle for electron acceleration in a collisionless shock layer, *Ann. Geophys.*, **34**, 591-593 (2016)

Narita, Y., R. Nakamura, W. Baumjohann, K.-H. Glassmeier, U. Motschmann, B. Giles, W. Magnes, D. Fischer, R.B. Torbert, C.T. Russell, R.J. Strangeway, J.L. Burch, Y. Nariyuki, S. Saito, S.P. Gary: On electron-scale whistler turbulence in the solar wind, *Astrophys. J. Lett.*, **827**, L8 (2016)

Narita, Y., R. Nakamura, W. Baumjohann, K.-H. Glassmeier, U. Motschmann, H. Comisel: Ion Bernstein waves in the magnetic reconnection region, *Ann. Geophys.*, **34**, 85-89 (2016)

Noack, L., D. Höning, A. Rivoldini, C. Heistracher, N. Zimov, B. Journaux, H. Lammer, T. Van Hoolst, J.H. Bredehöft: Water-rich planets: How habitable is a water layer deeper than on Earth?, *Icarus*, **277**, 215-236 (2016)

Norgren, C., D.B. Graham, Yu.V. Khotyaintsev, M. André, A. Vaivads, L.-J. Chen, P.-A. Lindqvist, G.T. Marklund, R.E. Ergun, W. Magnes, R.J. Strangeway, C.T. Russell, R.B. Torbert, W.R. Paterson, D.J. Gershman, J.C. Dorelli, L.A. Avanov, B. Lavraud, Y. Saito, B.L. Giles, C.J. Pollock, J.L. Burch: Finite gyroradius effects in the electron outflow of asymmetric magnetic reconnection, *Geophys. Res. Lett.*, **43**, 6724-6733 (2016)

Oliver, R., R. Soler, J. Terradas, T.V. Zaqarashvili: Dynamics of coronal rain and descending plasma blobs in solar prominences. II. Partially ionized case, *Astrophys. J.*, **818**, 128 (2016)

Palin, L., H.J. Opgenoorth, K. Agren, T. Zivkovic, V.A. Sergeev, M.V. Kubyshkina, A. Nikolaev, K. Kauristie, M. van de Kamp, O. Amm, S.E. Milan, S.M. Imber, G. Facsko, M. Palmroth, R. Nakamura: Modulation of the substorm current wedge by bursty bulk flows: 8 September 2002—Revisited, *J. Geophys. Res.*, **121**, 4466-4482 (2016)

Panchenko, M., H.O. Rucker: Estimation of emission cone wall thickness of Jupiter's decametric radio emission using stereoscopic STEREO/WAVES observations, *Astron. Astrophys.*, **596**, A18 (2016)

Panov, E.V., W. Baumjohann, R.A. Wolf, R. Nakamura, V. Angelopoulos, J.M. Weygand, M.V. Kubyshkina: Magnetotail energy dissipation during an auroral substorm, *Nat. Phys.*, **12**, 1158-1163 (2016)

Paranicas, C., M.F. Thomsen, N. Achilleos, M. Andriopoulou, S.V. Badman, G. Hospodarsky, C.M. Jackman, X. Jia, T. Kennelly, K. Khurana, P. Kollmann, N. Krupp, P. Louarn, E. Roussos, N. Sergis: Effects of radial motion on interchange injections at Saturn, *Icarus*, **264**, 342-351 (2016)

Perschke, C., Y. Narita, U. Motschmann, K.H. Glassmeier: Observational test for a random sweeping model in solar wind turbulence, *Phys. Rev. Lett.*, **116**, 125101 (2016)

Pitcher, C., N. Kömle, O. Leibniz, O. Morales-Calderon, Y. Gao, L. Richter: Investigation of the properties of icy lunar polar regolith simulants, *Adv. Space Res.*, **57**, 1197-1208 (2016)

Plainaki, C., J. Lilensten, A. Radioti, M. Andriopoulou, A. Milillo, T.A. Nordheim, I. Dandouras, A. Coustenis, D. Grassi, V. Mangano, S. Massetti, S. Orsini, A. Lucchetti: Planetary space weather: Scientific aspects and future perspectives, *J Space Weather Space Clim*, **6**, A31 (2016)

Plainaki, C., P. Paschalis, D. Grassi, H. Mavromichalaki, M. Andriopoulou: Solar energetic particle interactions with the Venusian atmosphere, *Ann. Geophys.*, **34**, 595-608 (2016)

Plaschke, F., H. Hietala, V. Angelopoulos, R. Nakamura: Geoeffective jets impacting the magnetopause are very common, *J. Geophys. Res.*, **121**, 3240-3253 (2016)

Plaschke, F., N. Kahr, D. Fischer, R. Nakamura, W. Baumjohann, W. Magnes, J.L. Burch, R.B. Torbert, C.T. Russell, B.L. Giles, R.J. Strangeway, H.K. Leinweber, K.R. Bromund, B.J. Anderson, G. Le, M. Chutter, J.A. Slavin, E.L. Kepko: Steepening of waves at the duskside magnetopause, *Geophys. Res. Lett.*, **43**, 7373-7380 (2016)

Plaschke, F., Y. Narita: On determining fluxgate magnetometer spin axis offsets from mirror mode observations, Ann. Geophys., 34, 759-766 (2016)

Plotnikov, I., A.P. Rouillard, J.A. Davies, V. Bothmer, J.P. Eastwood, P. Gallagher, R.A. Harrison, E. Kilpua, C. Möstl, C.H. Perry, L. Rodriguez, B. Lavraud, V. Génot, R.F. Pinto, E. Sanchez-Diaz: Long-term tracking of corotating density structures using heliospheric imaging, *Solar Phys.*, **291**, 1853-1875 (2016)

Przybilla, N., L. Fossati, S. Hubrig, M.-F. Nieva, S.P. Järvinen, N. Castro, M. Schöller, I. Ilyin, K. Butler, F.R.N. Schneider, L.M. Oskinova, T. Morel, N. Langer, A. de Koter, BOB collaboration: B fields in OB stars (BOB): Detection of a magnetic field in the He-strong star CPD−57° 3509, *Astron. Astrophys.*, **587**, A7 (2016)

Reiff, P.H., A.G. Daou, S.Y. Sazykin, R. Nakamura, M.R. Hairston, V. Coffey, M.O. Chandler, B.J. Anderson, C.T.

Russell, D. Welling, S.A. Fuselier, K.J. Genestreti: Multispacecraft observations and modeling of the 22/23 June 2015 geomagnetic storm, *Geophys. Res. Lett.*, **43**, 7311-7318 (2016)

Reimond, S., O. Baur: Spheroidal and ellipsoidal harmonic expansions of the gravitational potential of small Solar System bodies. Case study: Comet 67P/Churyumov-Gerasimenko, *J. Geophys. Res.*, **121**, 497-515 (2016)

Richter, I., H.-U. Auster, G. Berghofer, C. Carr, E. Cupido, K.-H. Fornacon, C. Goetz, P. Heinisch, C. Koenders, B. Stoll, B.T. Tsurutani, C. Vallat, M. Volwerk, K.-H. Glassmeier: Two-point observations of low-frequency waves at 67P/Churyumov-Gerasimenko during the descent of PHILAE: Comparison of RPCMAG and ROMAP, *Ann. Geophys.*, **34**, 609-622 (2016)

Rollett, T., C. Möstl, A. Isavnin, J.A. Davies, M. Kubicka, U.V. Amerstorfer, R.A. Harrison: ElEvoHI: A Novel CME prediction tool for heliospheric imaging combining an elliptical front with drag-based model fitting, *Astrophys. J.*, **824**, 131 (2016)

Roussos, E., N. Krupp, D.G. Mitchell, C. Paranicas, S.M. Krimigis, M. Andriopoulou, B. Palmaerts, W.S. Kurth, S.V. Badman, A. Masters, M.K. Dougherty: Quasi-periodic injections of relativistic electrons in Saturn's outer magnetosphere, *Icarus*, **263**, 101-116 (2016)

Roussos, E., N. Krupp, P. Kollmann, C. Paranicas, D.G. Mitchell, S.M. Krimigis, M. Andriopoulou: Evidence for dust-driven, radial plasma transport in Saturn's inner radiation belts, *Icarus*, **274**, 272-283 (2016)

Russell, C.T., B.J. Anderson, W. Baumjohann, K.R. Bromund, D. Dearborn, D. Fischer, G. Le, H.K. Leinweber, D. Leneman, W. Magnes, J.D. Means, M.B. Moldwin, R. Nakamura, D. Pierce, F. Plaschke, K.M. Rowe, J.A. Slavin, R.J. Strangeway, R. Torbert, C. Hagen, I. Jernej, A. Valavanoglou, I. Richter: The magnetospheric multiscale magnetometers, *Space Sci. Rev.*, **199**, 189-256 (2016)

Ryabchikova, T., N. Piskunov, Yu. Pakhomov, V. Tsymbal, A. Titarenko, T. Sitnova, S. Alexeeva, L. Fossati, L. Mashonkina: Accuracy of atmospheric parameters of FGK dwarfs determined by spectrum fitting, *MNRAS*, **456**, 1221-1234 (2016)

Sampl, M., W. Macher, T. Oswald, D. Plettemeier, H.O. Rucker, W.S. Kurth: Juno model rheometry and simulation, *Radio Sci.*, **51**, 1627-1635 (2016)

Schmid, D., R. Nakamura, M. Volwerk, F. Plaschke, Y. Narita, W. Baumjohann, W. Magnes, D. Fischer, H.U. Eichelberger, R.B. Torbert, C.T. Russell, R.J. Strangeway, H.K. Leinweber, G. Le, K.R. Bromund, B.J. Anderson, J.A. Slavin, E.L. Kepko: A comparative study of dipolarization fronts at MMS and Cluster, *Geophys. Res. Lett.*, **43**, 6012-6019 (2016)

Schneider, F.R.N., Ph. Podsiadlowski, N. Langer, N. Castro, L. Fossati: Rejuvenation of stellar mergers and the origin of magnetic fields in massive stars, *MNRAS*, **457**, 2355-2365 (2016)

Shaikhislamov, I.F., M.L. Khodachenko, H. Lammer, K.G. Kislyakova, L. Fossati, C.P. Johnstone, P.A. Prokopov, A.G. Berezutsky, Yu.P. Zakharov, V.G. Posukh: Two regimes of interaction of a hot Jupiter's escaping atmosphere with the stellar wind and generation of energized atomic hydrogen corona, *Astrophys. J.*, **832**, 173 (2016)

Shan, L., C. Mazelle, K. Meziane, M. Delva, Q. Lu, Y.S. Ge, A. Du, T.L. Zhang: Characteristics of quasi-monochromatic ULF waves in the Venusian foreshock, *J. Geophys. Res.*, **121**, 7385-7397 (2016)

Shevchuk, N.V., V.N. Melnik, S. Poedts, V.V. Dorovskyy, J. Magdalenic, A.A. Konovalenko, A.I. Brazhenko, C. Briand, A.V. Frantsuzenko, H.O. Rucker, P. Zarka: The storm of decameter spikes during the event of 14 June 2012, *Solar Phys.*, **291**, 211-228 (2016)

Solovieva, M.S., A.A. Rozhnoi, V. Fedun, K. Schwingenschuh: Effect of the total solar eclipse of March 20, 2015, on VLF/LF propagation, *Geomagn. Aeron.*, **56**, 323-330 (2016)

Sonnerup, B.U.Ö., H. Hasegawa, R.E. Denton, T.K.M. Nakamura: Reconstruction of the electron diffusion region, *J. Geophys. Res.*, **121**, 4279-4290 (2016)

Stancliffe, R.J., L. Fossati, J.-C. Passy, F.R.N. Schneider: Confronting uncertainties in stellar physics II. Exploring differences in main-sequence stellar evolution tracks, *Astron. Astrophys.*, **586**, A119 (2016)

Stawarz, J.E., S. Eriksson, F.D. Wilder, R.E. Ergun, S.J. Schwartz, A. Pouquet, J.L. Burch, B.L. Giles, Y. Khotyaintsev, O. Le Contel, P.-A. Lindqvist, W. Magnes, C.J. Pollock, C.T. Russell, R.J. Strangeway, R.B. Torbert, L.A. Avanov, J.C. Dorelli, J.P. Eastwood, D.J. Gershman, K.A. Goodrich, D.M. Malaspina, G.T. Marklund, L. Mirioni, A.P. Sturner: Observations of turbulence in a Kelvin-Helmholtz event on 8 September 2015 by the Magnetospheric Multiscale mission, *J. Geophys. Res.*, **121**, 11021-11034 (2016)

Stevenson, K.B., N.K. Lewis, J.L. Bean, C. Beichman, J. Fraine, B.M. Kilpatrick, J.E. Krick, J.D. Lothringer, A.M. Mandell, J.A. Valenti, E. Agol, D. Angerhausen, J.K. Barstow, S.M. Birkmann, A. Burrows, D. Charbonneau, N.B. Cowan, N. Crouzet, P.E. Cubillos, S.M. Curry, P.A. Dalba, J. de Wit, D. Deming, J.-M. Désert, R. Doyon, D. Dragomir, D. Ehrenreich, J.J. Fortney, A. Garcia Muñoz, N.P. Gibson, J.E. Gizis, T.P. Greene, J. Harrington, K. Heng, T. Kataria, E.M.-R. Kempton, H. Knutson, L. Kreidberg, D. Lafrenière, P.-O. Lagage, M.R. Line, M. Lopez-Morales, N. Madhusudhan, C.V. Morley, M. Rocchetto, E. Schlawin, E.L. Shkolnik, A. Shporer, D.K. Sing, K.O. Todorov, G.S. Tucker, H.R. Wakeford: Transiting exoplanet studies and community targets for JWST's early release science program, Publ. Astron. Soc. Pac., 128, 094401 (2016)

Stökl, A., E.A. Dorfi, C.P. Johnstone, H. Lammer: Dynamical accretion of primordial atmospheres around planets with masses between 0.1 and 5 M_E in the habitable zone, *Astrophys. J.*, **825**, 86 (2016)

Tezari, A., H. Mavromichalaki, D. Katsinis, A. Kanellakopoulos, S. Kolovi, C. Plainaki, M. Andriopoulou: Latitudinal and longitudinal dependence of the cosmic ray diurnal anisotropy during 2001-2014, *Ann. Geophys.*, **34**, 1053-1068 (2016)

Threlfall, J., Ph.-A. Bourdin, T. Neukirch, C.E. Parnell: Particle dynamics in a non-flaring solar active region model, *Astron. Astrophys.*, **587**, A4 (2016)

Tiefenbacher, P., N.I. Kömle, W. Macher, G. Kargl: Influence of probe geometry on measurement results of non-ideal thermal conductivity sensors, *Geosci. Instrum. Method. Data Syst.*, **5**, 383-401 (2016)

Toledo-Redondo, S., A. Salinas, J. Fornieles, J. Portí, H.I.M. Lichtenegger: Full 3-D TLM simulations of the Earth-ionosphere cavity: Effect of conductivity on the Schumann resonances, *J. Geophys. Res.*, **121**, 5579-5593 (2016)

Torbert, R.B., C.T. Russell, W. Magnes, R.E. Ergun, P.-A. Lindqvist, O. Le Contel, H. Vaith, J. Macri, S. Myers, D. Rau, J. Needell, B. King, M. Granoff, M. Chutter, I. Dors, G. Olsson, Y.V. Khotyaintsev, A. Eriksson, C.A. Kletzing, S. Bounds, B. Anderson, W. Baumjohann, M. Steller, K. Bromund, G. Le, R. Nakamura, R.J. Strangeway, H.K. Leinweber, S. Tucker, J. Westfall, D. Fischer, F. Plaschke, J. Porter, K. Lappalainen: The FIELDS instrument suite on MMS: Scientific objectives, measurements, and data products, *Space Sci. Rev.*, **199**, 105-135 (2016)

Torbert, R.B., H. Vaith, M. Granoff, M. Widholm, J.A. Gaidos, B.H. Briggs, I.G. Dors, M.W. Chutter, J. Macri, M. Argall, D. Bodet, J. Needell, M.B. Steller, W. Baumjohann, R. Nakamura, F. Plaschke, H. Ottacher, J. Hasiba, K. Hofmann, C.A. Kletzing, S.R. Bounds, R.T. Dvorsky, K. Sigsbee, V. Kooi: Erratum to "The Electron Drift Instrument for MMS" [Space Sci. Rev. (2016) DOI 10.1007/s11214-015-0182-7], *Space Sci. Rev.*, **199**, 307-308 (2016)

Torbert, R.B., H. Vaith, M. Granoff, M. Widholm, J.A. Gaidos, B.H. Briggs, I.G. Dors, M.W. Chutter, J. Macri, M. Argall, D. Bodet, J. Needell, M.B. Steller, W. Baumjohann, R. Nakamura, F. Plaschke, H. Ottacher, J. Hasiba, K. Hofmann, C.A. Kletzing, S.R. Bounds, R.T. Dvorsky, K. Sigsbee, V. Kooi: The Electron Drift Instrument for MMS, *Space Sci. Rev.*, **199**, 283-305 (2016)

Torbert, R.B., J.L. Burch, B.L. Giles, D. Gershman, C.J. Pollock, J. Dorelli, L. Avanov, M.R. Argall, J. Shuster, R.J. Strangeway, C.T. Russell, R.E. Ergun, F.D. Wilder, K. Goodrich, H.A. Faith, C.J. Farrugia, P.-A. Lindqvist, T. Phan, Y. Khotyaintsev, T.E. Moore, G. Marklund, W. Daughton, W. Magnes, C.A. Kletzing, S. Bounds: Estimates of terms in Ohm's law during an encounter with an electron diffusion region, *Geophys. Res. Lett.*, **43**, 5918-5925 (2016)

Torkar, K., R. Nakamura, M. Tajmar, C. Scharlemann, H. Jeszenszky, G. Laky, G. Fremuth, C.P. Escoubet, K. Svenes: Active spacecraft potential control investigation, *Space Sci. Rev.*, **199**, 515-544 (2016)

Treumann, R.A., W. Baumjohann: Anisotropic Jüttner (relativistic Boltzmann) distribution, *Ann. Geophys.*, **34**, 737-738 (2016)

Treumann, R.A., W. Baumjohann: Critical temperature in relativistic Lorentzian thermodynamics of massive bosons, *EPL*, **116**, 10003 (2016)

Treumann, R.A., W. Baumjohann: Generalised partition functions: Inferences on phase space distributions, *Ann. Geophys.*, **34**, 557-564 (2016)

Treumann, R.A., W. Baumjohann, Y. Narita: Inverse scattering problem in turbulent magnetic fluctuations, *Ann. Geophys.*, **34**, 673-689 (2016)

Turner, D.L., J.F. Fennell, J.B. Blake, J.H. Clemmons, B.H. Mauk, I.J. Cohen, A.N. Jaynes, J.V. Craft, F.D. Wilder, D.N. Baker, G.D. Reeves, D.J. Gershman, L.A. Avanov, J.C. Dorelli, B.L. Giles, C.J. Pollock, D. Schmid, R. Nakamura, R.J. Strangeway, C.T. Russell, A.V. Artemyev, A. Runov, V. Angelopoulos, H.E. Spence, R.B. Torbert, J.L. Burch: Energy limits of electron acceleration in the plasma sheet during substorms: A case study with the Magnetospheric Multiscale (MMS) mission, *Geophys. Res. Lett.*, **43**, 7785-7794 (2016)

Turner, O.D., D.R. Anderson, A. Collier Cameron, L. Delrez, D.F. Evans, M. Gillon, C. Hellier, E. Jehin, M. Lendl, P.F.L. Maxted, F. Pepe, D. Pollacco, D. Queloz, D. Ségransan, B. Smalley, A.M.S. Smith, A.H.M.J. Triaud, S. Udry, R.G. West: WASP-120b, WASP-122b, and WASP-123b: Three newly discovered planets from the WASP-south survey, *Publ. Astron. Soc. Pac.*, **128**, 064401 (2016)

Vaisberg, O., J.-J. Berthellier, T. Moore, L. Avanov, F. Leblanc, F. Leblanc, P. Moiseev, D. Moiseenko, J. Becker, M. Collier, G. Laky, J. Keller, G. Koynash, H.I.M. Lichtennegger, A. Leibov, R. Zhuravlev, A. Shestakov, J. Burch, D. McComas, S. Shuvalov, D. Chornay, K. Torkar: The 2π charged particles analyzer: All-sky camera concept and development for space missions, *J. Geophys. Res.*, **121**, 11750–11765 (2016)

Vaivads, A., A. Retinò, J. Soucek, Yu.V. Khotyaintsev, F. Valentini, C.P. Escoubet, O. Alexandrova, M. André, S.D. Bale, M. Balikhin, D. Burgess, E. Camporeale, D. Caprioli, C.H.K. Chen, E. Clacey, C.M. Cully, J. De Keyser, J.P. Eastwood, A.N. Fazakerley, S. Eriksson, M.L. Goldstein, D.B. Graham, S. Haaland, M. Hoshino, H. Ji, H. Karimabadi, H. Kucharek, B. Lavraud, F. Marcucci, W.H. Matthaeus, T.E. Moore, R. Nakamura, Y. Narita, Z. Nemecek, C. Norgren, H. Opgenoorth, M. Palmroth, D. Perrone, J.-L. Pinçon, P. Rathsman, H. Rothkaehl, F. Sahraoui, S. Servidio, L. Sorriso-Valvo, R. Vainio, Z. Vörös, R.F. Wimmer-Schweingruber: Turbulence Heating ObserveR - satellite mission proposal, *J. Plasma Phys.*, **82**, 905820501 (2016)

Vech, D., G. Stenberg, H. Nilsson, N.J.T. Edberg, A. Opitz, K. Szegő, T. Zhang, Y. Futaana: Statistical features of the global polarity reversal of the Venusian induced magnetosphere in response to the polarity change in interplanetary magnetic field, *J. Geophys. Res.*, **121**, 3951-3962 (2016)

Vemareddy, P., C. Möstl, T. Amerstorfer, W. Mishra, C. Farrugia, M. Leitner: Comparison of magnetic properties in a magnetic cloud and its solar source on 2013 April 11–14, *Astrophys. J.*, **828**, 12 (2016)

Vernisse, Y., B. Lavraud, S. Eriksson, D.J. Gershman, J. Dorelli, C. Pollock, B. Giles, N. Aunai, L. Avanov, J. Burch, M. Chandler, V. Coffey, J. Dargent, R.E. Ergun, C.J. Farrugia, V. Génot, D.B. Graham, H. Hasegawa, C. Jacquey, I. Kacem, Y. Khotyaintsev, W. Li, W. Magnes, A. Marchaudon, T. Moore, W. Paterson, E. Penou, T.D. Phan, A. Retino, C.T. Russell, Y. Saito, J.-A. Sauvaud, R. Torbert, F.D. Wilder, S.

Yokota: Signatures of complex magnetic topologies from multiple reconnection sites induced by Kelvin-Helmholtz instability, *J. Geophys. Res.*, **121**, 9926-9939 (2016)

Vida, K., L. Kriskovics, K. Oláh, M. Leitzinger, P. Odert, Zs. Kövári, H. Korhonen, R. Greimel, R. Robb, B. Csák, J. Kovács: Investigating magnetic activity in very stable stellar magnetic fields. Long-term photometric and spectroscopic study of the fully convective M4 dwarf V374 Pegasi, *Astron. Astrophys.*, **590**, A11 (2016)

Volwerk, M., D. Schmid, B.T. Tsurutani, M. Delva, F. Plaschke, Y. Narita, T.L. Zhang, K.-H. Glassmeier: Mirror mode waves in Venus's magnetosheath: Solar minimum vs. solar maximum, *Ann. Geophys.*, **34**, 1099-1108 (2016)

Volwerk, M., I. Richter, B. Tsurutani, C. Götz, K. Altwegg, T. Broiles, J. Burch, C. Carr, E. Cupido, M. Delva, M. Dósa, N.J.T. Edberg, A. Eriksson, P. Henri, C. Koenders, J.-P. Lebreton, K.E. Mandt, H. Nilsson, A. Opitz, M. Rubin, K. Schwingenschuh, G. Stenberg Wieser, K. Szegö, C. Vallat, X. Vallieres, K.-H. Glassmeier: Mass-loading, pile-up, and mirror-mode waves at comet 67P/Churyumov-Gerasimenko, *Ann. Geophys.*, **34**, 1-15 (2016)

Vörös, Z., E. Yordanova, M.M. Echim, G. Consolini, Y. Narita: Turbulence-generated proton-scale structures in the terrestrial magnetosheath, Astrophys. J. Lett., 819, L15 (2016)

Wang, G.Q., T.L. Zhang, M. Volwerk: Statistical study on ultralow-frequency waves in the magnetotail lobe observed by Cluster, *J. Geophys. Res.*, **121**, 5319-5332 (2016)

Wang, G.Q., T.L. Zhang, M. Volwerk, D. Schmid, W. Baumjohann, R. Nakamura, Z.H. Pan: Mirror mode structures ahead of dipolarization front near the neutral sheet observed by Cluster, *Geophys. Res. Lett.*, **43**, 8853-8858 (2016)

Wang, R., Q. Lu, R. Nakamura, C. Huang, A. Du, F. Guo, W. Teh, M. Wu, S. Lu, S. Wang: Coalescence of magnetic flux ropes in the ion diffusion region of magnetic reconnection, *Nat. Phys.*, **12**, 263-267 (2016)

Wang, R., Q. Lu, R. Nakamura, C. Huang, X. Li, M. Wu, A. Du, X. Gao, S. Wang: Electrostatic and electromagnetic fluctuations detected inside magnetic flux ropes during magnetic reconnection, *J. Geophys. Res.*, **121**, 9473-9482 (2016)

West, R.G., C. Hellier, J.-M. Almenara, D.R. Anderson, S.C.C. Barros, F. Bouchy, D.J.A. Brown, A. Collier Cameron, M. Deleuil, L. Delrez, A.P. Doyle, F. Faedi, A. Fumel, M. Gillon, Y. Gómez Maqueo Chew, G. Hébrard, E. Jehin, M. Lendl, P.F.L. Maxted, F. Pepe, D. Pollacco, D. Queloz, D. Ségransan, B. Smalley, A.M.S. Smith, J. Southworth, A.H.M.J. Triaud, S. Udry: Three irradiated and bloated hot Jupiters: WASP-76b, WASP-82b, and WASP-90b, *Astron. Astrophys.*, **585**, A126 (2016)

Wilder, F.D., R.E. Ergun, K.A. Goodrich, M.V. Goldman, D.L. Newman, D.M. Malaspina, A.N. Jaynes, S.J. Schwartz, K.J. Trattner, J.L. Burch, M.R. Argall, R.B. Torbert, P.-A. Lindqvist, G. Marklund, O. Le Contel, L. Mirioni, Yu.V. Khotyaintsev, R.J. Strangeway, C.T. Russell, C.J. Pollock, B.L. Giles, F. Plaschke, W. Magnes, S. Eriksson, J.E. Stawarz, A.P. Sturner, J.C. Holmes: Observations of whistler mode waves with nonlinear parallel electric fields near the dayside magnetic reconnection separatrix by the Magnetospheric Multiscale mission, *Geophys. Res. Lett.*, **43**, 5909-5917 (2016)

Wilder, F.D., R.E. Ergun, S.J. Schwartz, D.L. Newman, S. Eriksson, J.E. Stawarz, M.V. Goldman, K.A. Goodrich, D.J. Gershman, D.M. Malaspina, J.C. Holmes, A.P. Sturner, J.L. Burch, R.B. Torbert, P.-A. Lindqvist, G.T. Marklund, Y. Khotyaintsev, R.J. Strangeway, C.T. Russell, C.J. Pollock, B.L. Giles, J.C. Dorrelli, L.A. Avanov, W.R. Patterson, F. Plaschke, W. Magnes: Observations of large-amplitude, parallel, electrostatic waves associated with the Kelvin-Helmholtz instability by the Magnetospheric Multiscale mission, *Geophys. Res. Lett.*, **43**, 8859-8866 (2016)

Wu, M., Q. Lu, M. Volwerk, Z. Vörös, X. Ma, S. Wang: Current sheet flapping motions in the tailward flow of magnetic reconnection, *J. Geophys. Res.*, **121**, 7817-7827 (2016)

Wu, Q., A.M. Du, M. Volwerk, G.Q. Wang: The distribution of spectral index of magnetic field and ion velocity in Pi2 frequency band in BBFs: THEMIS statistics, *Adv. Space Res.*, **58**, 847-855 (2016)

Xiao, S., T.L. Zhang, Y. Ge, G. Wang, W. Baumjohann, R. Nakamura: A statistical study on the shape and position of the magnetotail neutral sheet, *Ann. Geophys.*, **34**, 303-311 (2016)

Xiao, S.D., T.L. Zhang, W. Baumjohann: Hemispheric asymmetry in the near-Venusian magnetotail during solar maximum, *J. Geophys. Res.*, **121**, 4542-4547 (2016)

Yao, Z., A.N. Fazakerley, A. Varsani, I.J. Rae, C.J. Owen, D. Pokhotelov, C. Forsyth, R.L. Guo, S.C. Bai, S.T. Yao, N. Doss: Substructures within a dipolarization front revealed by high-temporal resolution Cluster observations, *J. Geophys. Res.*, **121**, 5185-5202 (2016)

Ye, S.-Y., G. Fischer, W.S. Kurth, J.D. Menietti, D.A. Gurnett: Rotational modulation of Saturn's radio emissions after equinox, *J. Geophys. Res.*, **121**, 11714-11728 (2016)

Yordanova, E., Z. Vörös, A. Varsani, D.B. Graham, C. Norgren, Yu.V. Khotyaintsev, A. Vaivads, E. Eriksson, R. Nakamura, P.-A. Lindqvist, G. Marklund, R.E. Ergun, W. Magnes, W. Baumjohann, D. Fischer, F. Plaschke, Y. Narita, C.T. Russell, R.J. Strangeway, O. Le Contel, C. Pollock, R.B. Torbert, B.J. Giles, J.L. Burch, L.A. Avanov, J.C. Dorelli, D.J. Gershman, W.R. Paterson, B. Lavraud, Y. Saito: Electron scale structures and magnetic reconnection signatures in the turbulent magnetosheath, *Geophys. Res. Lett.*, **43**, 5969-5978 (2016)

Yushkov, E.V., A.V. Artemyev, A.A. Petrukovich, R. Nakamura: Current sheet flapping in the near-Earth magnetotail: Peculiarities of propagation and parallel currents, *Ann. Geophys.*, **34**, 739-750 (2016)

Zakharenko, V., A. Konovalenko, P. Zarka, O. Ulyanov, M. Sidorchuk, S. Stepkin, V. Koliadin, N. Kalinichenko, A. Stanislavsky, V. Dorovskyy, V. Shepelev, I. Bubnov, S. Yerin, V. Melnik, A. Koval, N. Shevchuk, I. Vasylieva, K. Mylostna, A. Shevtsova, A. Skoryk, I. Kravtsov, Y. Volvach, M. Plakhov, N. Vasilenko, Y. Vasylkivskyi, D. Vavriv, V. Vino-

gradov, R. Kozhin, A. Kravtsov, E. Bulakh, A. Kuzin, A. Vasilyev, V. Ryabov, A. Reznichenko, V. Bortsov, V. Lisachenko, G. Kvasov, D. Mukha, G. Litvinenko, A. Brazhenko, R. Vashchishin, O. Pylaev, V. Koshovyy, A. Lozinsky, O. Ivantyshyn, H.O. Rucker, M. Panchenko, G. Fischer, A. Lecacheux, L. Denis, A. Coffre, J.-M. Grießmeier: Digital receivers for low-frequency radio telescopes UTR-2, URAN, GURT, *J. Astron. Instrum.*, **5**, 1641010 (2016)

Zelenyi, L.M., A.G. Frank, A.V. Artemyev, A.A. Petrukovich, R. Nakamura: Formation of sub-ion scale filamentary force-free structures in the vicinity of reconnection region, *Plasma Phys. Control. Fusion*, **58**, 054002 (2016)

Zhang, L., A.-M. Du, X. Lang, T.-L. Zhang, D.-M. Yang, X.-D. Zhao: Characteristics of geomagnetic regular diurnal variation before Wenchuan earthquake, *Chin. J. Geophys.*, **59**, 952-958 (2016)

Zhang, L.Q., L. Dai, W. Baumjohann, A.T.Y. Lui, C. Wang, H. Rème, M.W. Dunlop: Temporal evolutions of the solar wind conditions at 1 AU prior to the near-Earth X lines in the tail: Superposed epoch analysis, *J. Geophys. Res.*, **121**, 7488-7496 (2016)

Zhang, L.Q., W. Baumjohann, C. Wang, L. Dai, B.B. Tang: Bursty bulk flows at different magnetospheric activity levels: Dependence on IMF conditions, *J. Geophys. Res.*, **121**, 8773-8789 (2016)

Zhang, T.L., W. Baumjohann, C.T. Russell, J.G. Luhmann, S.D. Xiao: Weak, quiet magnetic fields seen in the Venus atmosphere, *Sci. Rep.*, **6**, 23537 (2016)

Zhao, C., C.T. Russell, R.J. Strangeway, S.M. Petrinec, W.R. Paterson, M. Zhou, B.J. Anderson, W. Baumjohann, K.R. Bromund, M. Chutter, D. Fischer, G. Le, R. Nakamura, F. Plaschke, J.A. Slavin, R.B. Torbert, H.Y. Wei: Force balance at the magnetopause determined with MMS: Application to flux transfer events, *Geophys. Res. Lett.*, **43**, 11941-11947 (2016)

PROCEEDINGS & BOOK CHAPTERS

Auster, U., W. Magnes, M. Delva, A. Valavanoglou, S. Leitner, O. Hillenmaier, C. Strauch, P. Brown, B. Whiteside, M. Bendyk, A. Hilgers, S. Kraft, J.P. Luntama, J. Seon: Space weather magnetometer set with automated AC spacecraft field correction for Geo-Kompsat-2A. In: *Proc. of the 2016 ESA Workshop on Aerospace EMC*, Ed. Ouwehand, L., IEEE, New York, NY, 1-6 (2016)

Eichelberger, H., G. Fremuth, G. Prattes, C. Kürbisch, G. Laky, F. Giner, S. Neukirchner, R. Wallner, H. Jeszenszky, M. Leichtfried, J.J. Berthelier, K. Torkar, H.I.M. Lichtenegger: BepiColombo-MPO-Serena-PICAM EMC measurements. In: *Proc. of the 2016 ESA Workshop on Aerospace EMC*, Ed. Ouwehand, L., IEEE, New York, NY, 1-4 (2016)

Ferrao, R.C., S.R. Augusto, C. Berni, F.R.F. dos Santos, V.C. Parro, P. Plasson, L. Gueguen, S. Finco, G. Peter, M. Steller: Multi-purpose simulator for Plato mission. In: *Proc. of the 7th International SpaceWire Conference*, IEEE, Bellingham, WA, 1-4, (2016)

Focardi, M., S. Pezzuto, R. Cosentino, G. Giusi, M. Pancrazzi, V. Noce, R. Ottensamer, M. Steller, A.M. Di Giorgio, E. Pace, P. Plasson, G. Peter, I. Pagano: The Instrument Control Unit of the ESA-PLATO 2.0 mission. In: *Space Telescopes and Instrumentation 2016: Optical, Infrared, and Millimeter Wave. Proc. of SPIE*, Vol. 9904, Ed. H.A. MacEwen, G.G. Fazio, M. Lystrup, SPIE, Bellingham, WA, 15 p. (2016)

Konovalenko, A., P. Zarka, V. Zakharenko, O. Ulyanov, M. Sydorchuk, S. Stepkin, P. Tokarskyy, A. Stanislavski, M. Kalinichenko, V. Kolyadin, V. Melnik, W. Dorovskyy, V. Shepelev, A. Koval, I. Bubnov, S. Yerin, K. Mylostna, J. Vasiliev, V. Bortsov, V. Kulishenko, V. Lisachenko, A. Reznichenko, G. Kvasov, A. Hristenko, G. Litvynenko, H.O. Rucker, M. Panchenko, G. Fischer, L. Denis, A. Coffre, J.-M. Grießmeier, M. Tagger, J.N. Girard, D. Charrier, V. Ryabov, G. Mann, A. Brazhenko V. Koshovyy: Current status of low frequency radio astronomy in Ukraine: Ground-based and ground-space investigations. In: *Space Research in Ukraine*, Ed. Fedorov, O.P., Akademperiodika, Kiew, 64-70 (2016)

Petrukovich, A., A. Artemyev, R. Nakamura: Magnetotail reconnection. In: *Magnetic Reconnection. Concepts and Applications*, Eds. Gonzalez, W., E. Parker, Springer, Switzerland, 277-313 (2016)

Plaschke, F.: ULF waves at the magnetopause. In: *Low-Frequency Waves in Space Plasmas (Geophysical Monograph 216)*, Eds. Keiling, A., D.-H. Lee, V. Nakariakov, American Geophysical Union, Washington, DC, 195-212 (2016)

Plattner, M., S. Albrecht, J. Bayer, S. Brandt, P. Drumm, O. Hälker, F. Kerschbaum, A. Koch, I. Kuvvetli, N. Meidinger, S. Ott, R. Ottensamer, J. Reiffers, T. Schanz, K. Skup, M. Steller, C. Tenzer, C. Thomas: WFI electronics and onboard data processing. In: *Proc of Spie Vol. 9905: Space Telescopes and Instrumentation 2016: Ultraviolet to Gamma Ray*, Eds. den Herder, J.-W.A., T. Takahashi, M. Bautz, SPIE, Bellingham, WA, 99052D (2016)

Soucek, J., L. Ahlen, S. Bale, J. Bonnell, N. Boudin, D. Brienza, C. Carr, F. Cipriani, C.P. Escoubet, A. Fazakerley, M. Gehler, V. Génot, A. Hilgers, B. Hanock, G. Jannet, A. Junge, Y. Khotyaintsev, J. De Keyser, H. Kucharek, R. Lan, B. Lavraud, F. Leblanc, W. Magnes, M. Mansour, M.F. Marcucci, R. Nakamura, Z. Nemecek, C. Owen, Y. Phal, A. Retino, D. Rodgers, J. Safrankova, F. Sahraoui, R. Vainio, R. Wimmer-Schweingruber, J. Steinhagen, A. Vaivads, A. Wielders, A. Zaslavsky: EMC aspects of turbulence heating observer (THOR) spacecraft. In: *Proc. of the 2016 ESA Workshop on Aerospace EMC*, Ed. Ouwehand, L., IEEE, New York, NY, 1-4, doi:10.1109/AeroEMC.2016.7504544 (2016)

Volwerk, M.: ULF wave modes in the Earth's magnetotail. In: *Low-Frequency Waves in Space Plasmas (Geophysical Monograph 216)*, Eds. Keiling, A., D.-H. Lee, V. Nakariakov, American Geophysical Union, Washington, DC, 141-160 (2016)

For oral presentations and posters please refer to the "Publications" menu on www.iwf.oeaw.ac.at.

PERSONNEL

Agú, Martin Alejandro, Dipl.-Ing.
Almer, Hannes
Al-Ubaidi, Tarek, Dipl.-Ing.
Amerstorfer, Tanja, Dr.
Amerstorfer, Ute, Dr.
Andriopoulou, Maria, Dr.
Arkhypov, Oleksiy, Dr.
Aydogar, Özer, Dipl.-Ing.
Baumjohann, Wolfgang, Prof.
Bentley, Mark, Dr.
Berghofer, Gerhard, Ing.
Besser, Bruno P., Dr.
Boudjada, Mohammed Y., Dr.
Bourdin, Philippe, Dr.
Cubillos, Patricio, Dr.
Delva, Magda, Dr.
Donnerer, Julia Maria, BSc
Eichelberger, Hans U., Dipl.-Ing.
Fischer, David, Dipl.-Ing.
Fischer, Georg, Dr.
Fossati, Luca, Dr.
Fremuth, Gerhard, Dipl.-Ing.
Genestreti, Kevin James, Dr.
Giner, Franz, Dipl.-Ing.
Graf, Christian, Ing.
Grill, Claudia
Gyurica, Mateja, Dipl.-Ing.
Hagen, Christian, Dipl.-Ing.
Hasiba, Johann, Dipl.-Ing.
Hofer, Bernhard, BSc
Hofmann, Karl, Dipl.-Ing.
Höck, Eduard, Dipl.-Ing.
Hradecky, Doris
Jernej, Irmgard, Ing.
Jeszenszky, Harald, Dipl.-Ing.
Juvan, Ines, Mag.
Kargl, Günter, Dr.
Khodachenko, Maxim L., Dr.
Kiehas, Stefan, Dr.
Kirchner, Georg, Dr.
Kislyakova, Kristina, Dr.
Koidl, Franz, Ing.
Kömle, Norbert I., Doz.
Korovinskiy, Daniil, Dr.
Krauss, Sandro, Dr.
Kubyshkina, Daria, Dr.
Kürbisch, Christoph, Ing.
Laky, Gunter, Dipl.-Ing.
Lammer, Helmut, Dr.
Leichtfried, Mario, Ing.
Leitner, Stefan, Dipl.-Ing.
Lendl, Monika, Dr.
Lhotka, Christoph, Dr.
Lichtenegger, Herbert I.M., Dr.
Macher, Wolfgang, Dr.
Magnes, Werner, Dr.
Mannel, Thurid, Msc
Močnik, Karl, Dr.
Möstl, Christian, Dr.
Muck, Cosima
Nakamura, Rumi, Doz.
Nakamura, Takuma, Dr.
Narita, Yasuhito, Doz.
Neukirchner, Sonja, Ing.
Nischelwitzer-Fennes, Ute, Ing.
Odert, Petra, Mag.
Ottacher, Harald, Dipl.-Ing.
Panchenko, Mykhaylo, Dr.
Panov, Evgeny, Dr.
Pitterle, Martin
Plaschke, Ferdinand, Dr.
Poganski, Joshua
Pollinger, Andreas, Dr.
Prattes, Gustav, Dipl.-Ing.
Reimond, Stefan, Dipl.-Ing.
Sasunov, Jury, Dr.
Scherf, Manuel, Mag.
Scherr, Alexandra, Mag.
Schmid, Daniel, Dipl.-Ing.
Schmied, Roland
Schwarzbauer, Gerald
Shergelashvili, Bidzina, Dr.
Stachel, Manfred, Dipl.-Ing.
Stangl, Günter, Dr. (BEV)
Steinberger, Michael, Dipl.-Ing.
Steindorfer, Michael, Dr.
Steller, Manfred B., Dr.
Stieninger, Reinhard, Ing.
Tiefenbacher, Patrick, Mag.
Tonfat Seclen, Jorge Lucio, Dr.
Tschachler, Elvira, Mag.
Valavanoglou, Aris, Dipl.-Ing.
Varsani, Ali, Dr.
Voller, Wolfgang G., Mag.
Volwerk, Martin, Dr.
Vörös, Zoltán, Dr.
Wallner, Robert, Ing.
Wang, Peiyuan, Dr.
Weber, Christof, Mag.
Wilfinger, Josef, BSc
Wirnsberger, Harald, Dipl.-Ing.
Zhang, Tie-Long, Prof.

As of 31 December 2016

BEV: Federal Office for Metrology and Surveying

IMPRESSUM

PUBLISHER

Wolfgang Baumjohann, Director
Institut für Weltraumforschung (IWF)
Österreichische Akademie der Wissenschaften (ÖAW)
Schmiedlstraße 6, 8042 Graz, Austria
www.iwf.oeaw.ac.at

EDITORS

Bruno Besser, Alexandra Scherr, Martin Volwerk

DESIGN

Alexandra Scherr
pr.iwf@oeaw.ac.at
Twitter: @IWF_Graz

PRINT

Servicebetrieb ÖH-Uni Graz GmbH


ÖAW IWF